TU Delft

Delft University of Technology

Isogeometric discrete differential forms: Non-uniform degrees, Bezier extraction, polar splines and flows on surfaces

Non-uniform degrees, Bézier extraction, polar splines and flows on surfaces

Toshniwal, Deepesh; Hughes, Thomas J.R.

DOI
10.1016/j.cma.2020.113576

Publication date
2021

Document Version
Final published version

Published in
Computer Methods in Applied Mechanics and Engineering

Citation (APA)
Toshniwal, D., & Hughes, T. J. R. (2021). Isogeometric discrete differential forms: Non-uniform degrees, Bezier extraction, polar splines and flows on surfaces: Non-uniform degrees, Bézier extraction, polar splines and flows on surfaces. *Computer Methods in Applied Mechanics and Engineering*, *376*, 1-44. Article 113576. https://doi.org/10.1016/j.cma.2020.113576

Important note
To cite this publication, please use the final published version (if applicable).
Please check the document version above.

Copyright
Other than for strictly personal use, it is not permitted to download, forward or distribute the text or part of it, without the consent of the author(s) and/or copyright holder(s), unless the work is under an open content license such as Creative Commons.

Takedown policy
Please contact us and provide details if you believe this document breaches copyrights.
We will remove access to the work immediately and investigate your claim.

This work is downloaded from Delft University of Technology.
For technical reasons the number of authors shown on this cover page is limited to a maximum of 10.

Available online at www.sciencedirect.com
ScienceDirect
Comput. Methods Appl. Mech. Engrg. 376 (2021) 113576
Computer methods in applied mechanics and engineering
www.elsevier.com/locate/cma

Isogeometric discrete differential forms: Non-uniform degrees, Bézier extraction, polar splines and flows on surfaces

Deepesh Toshniwal[a,*], Thomas J.R. Hughes[b]

[a] Delft Institute of Applied Mathematics, Delft University of Technology, Netherlands
[b] Oden Institute, The University of Texas at Austin, United States of America

Received 28 August 2020; received in revised form 10 November 2020; accepted 10 November 2020
Available online xxxx

Abstract

Spaces of discrete differential forms can be applied to numerically solve the partial differential equations that govern phenomena such as electromagnetics and fluid mechanics. Robustness of the resulting numerical methods is complemented by pointwise satisfaction of conservation laws (e.g., mass conservation) in the discrete setting. Here we present the construction of isogeometric discrete differential forms, i.e., differential form spaces built using smooth splines. We first present an algorithm for computing Bézier extraction operators for univariate spline differential forms that allow local degree elevation. Then, using tensor-products of the univariate splines, a complex of discrete differential forms is built on meshes that contain polar singularities, i.e., edges that are singularly mapped onto points. We prove that the spline complexes share the same cohomological structure as the de Rham complex. Several examples are presented to demonstrate the applicability of the proposed methodology. In particular, the splines spaces derived are used to simulate generalized Stokes flow on arbitrarily curved smooth surfaces and to numerically demonstrate (a) optimal approximation and inf–sup stability of the spline spaces; (b) pointwise incompressible flows; and (c) flows on deforming surfaces.
© 2020 The Author(s). Published by Elsevier B.V. This is an open access article under the CC BY license (http://creativecommons.org/licenses/by/4.0/).

Keywords: Smooth splines; Singularly parametrized surfaces; The de Rham complex; Surface flows; Optimal approximation; Pointwise incompressibility

1. Introduction

Partial differential equations (PDEs) describing physical phenomena are built on a rich differential and geometric foundation of conservation laws, topological constraints, symmetries and invariants. The reliability of numerical algorithms that are used to discretize and approximately solve these equations is of the utmost importance for countless scientific and engineering applications, and this is intimately connected to the differential and geometric structure underlying the PDEs. Specifically, for physical problems such as electromagnetism and incompressible fluid flows, consistent, stable and accurate numerical methods that ensure physical fidelity of the discrete solutions can be built by mimicking the structure underlying the continuous problem (e.g., the identities div–curl$= 0$ and curl-grad$= \mathbf{0}$) at the discrete level. The formulation of such numerical methods is our focus in this article, with a special attention towards high-order accurate discretizations of PDEs defined on surfaces in $\mathbb{R}^3$.

* Corresponding author.
E-mail addresses: d.toshniwal@tudelft.nl (D. Toshniwal), hughes@oden.utexas.edu (T.J.R. Hughes).

https://doi.org/10.1016/j.cma.2020.113576
0045-7825/© 2020 The Author(s). Published by Elsevier B.V. This is an open access article under the CC BY license (http://creativecommons.org/licenses/by/4.0/).

The development of discretization methods that aim to mimic symmetries and invariants at the continuous level is an active area of research. Some of the significant contributions in this area have come in the form of mimetic finite difference methods [1,2], mimetic spectral element methods [3,4], discrete exterior calculus [5,6], finite element exterior calculus [7,8], and physics-compatible or structure-preserving isogeometric analysis [9–12]. These methods have one thing in common: they are driven by geometric interpretations of the solution fields. In particular, the solution fields are interpreted as differential forms [13], which are objects that are naturally associated to geometric objects of different dimensions. For example, for fluid flow on an $\mathfrak{d}$-dimensional domain, velocities may be interpreted as fluxes that flow through codimension-1 geometries (i.e., as differential forms of order $\mathfrak{d}-1$) and their divergence as the mass being lost or produced in $\mathfrak{d}$-dimensional geometries (i.e., as differential forms of order $\mathfrak{d}$).

Differential forms provide a compact, clear and intuitive language for discussing both PDEs as well as their discretization. They are particularly helpful in identifying which parts of the PDE are conservation laws that do not depend on any notion of a metric, and which parts are constitutive laws — the discretizations are then constructed to exactly satisfy the former and accurately approximate the latter. The framework of finite element exterior calculus [7,8] is based on precisely this formalism. It has led to a unified approach for developing accurate finite element differential form spaces and analysing stability and well-posedness of the discrete problems. This article focuses on the methods that belong to the extension of finite element exterior calculus to isogeometric analysis.

Isogeometric analysis [14] relies on the use of smooth splines, i.e., smooth piecewise-polynomial functions, for building both the geometry on which the problem is defined, as well as the discrete finite element spaces used to solve the problem. The last decades have seen the extensive use of splines for numerical solutions of challenging problems such as the design and optimization of wind turbines [15], development of cardiac devices [16], and multiphase flows [17–19] and fracture dynamics [20,21] governed by high-order phase field theories. Several recent developments [22–24] have provided the theory supporting the large body of numerical evidence that smooth splines demonstrate better approximation behaviour per degree of freedom than less smooth or non-smooth spline spaces (e.g., traditional C^0 finite element spaces). The extensions of finite element exterior calculus to isogeometric analysis have come via the development of isogeometric discrete differential form spaces, i.e., discrete differential form spaces built using smooth splines. These isogeometric discrete differential forms are used to solve PDEs on domains that are also built using smooth splines. Examples include discrete differential forms on rectangular or cuboidal domains built using tensor-product splines [10,11,25,26] and adaptively-refined splines [12,27,28], with applications to electromagnetism and incompressible flows being common.

The above represents the state of the art on spline differential forms and the existing literature does not address the problem of simulating PDEs on arbitrary surfaces with smooth spline-based differential forms. While significant advances have been made in the understanding of spline differential forms on (locally refined) quadrilateral meshes, unstructured meshes are needed for building arbitrary surfaces. In particular, there are two types of unstructured meshes that need to be studied — ones where the number of quadrilaterals meeting at an interior vertex is not equal to 4 (excluding T-junctions), and ones where the quadrilaterals degenerate into triangles. One of the contributions of this article is taking the first steps that address the latter class of unstructured meshes; such meshes are called polar meshes and the splines built on them are called polar splines.

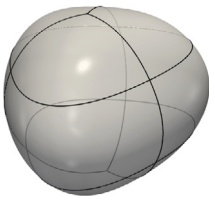

More broadly, the motivation for this article is construction of isogeometric discrete differential forms for numerical approximation of (scalar and vector) solutions to PDEs. We focus on discrete differential form spaces built using two particular classes of non-standard spline spaces — univariate multi-degree splines and bivariate polar splines. Multi-degree splines [29–31] are splines that allow local polynomial degree adaptivity, and polar splines [29,32] are non-tensor-product splines that allow the construction of singularly parametrized, genus 0 surfaces that are nevertheless C^k smooth. For instance, the geometry on the right is a C^1 polar spline surface that is singularly parametrized — it is built from a rectangular domain by collapsing a pair of opposite edges to points.

Solving PDEs on such surfaces has many applications; e.g., numerical weather prediction [33]. Of particular interest to us is the study of biological fluidic membranes such as lipid bilayers [34–36]. These membranes can

be thought of as the envelopes for eukaryotic cell contents. These are versatile structures that behave as in-plane viscous fluids and out-of-plane solids. Computationally studying the behaviour of such structures requires the ability to simulate two-dimensional viscous fluid flow on a curved, evolving surface. Several recent methods have been proposed to solve such problems; e.g., using discrete exterior calculus [37], trace finite elements [38,39] and surface finite elements [40–43]. These methods are built using functions of low-regularity that are either C^0 or discontinuous. The methods in [37–39] are low-order methods that use piecewise polynomials of degree at most 1, and the methods in [38,39] are for surfaces defined implicitly on a background mesh. The method in [41] is high-order accurate but needs Lagrange multipliers to impose tangentiality of the fluid velocity on a curved surface; penalties are used to approximately achieve the same or to enforce approximate conservation in [38,39,43].

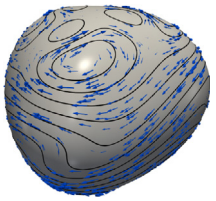

In this paper, we develop novel isogeometric discrete differential forms that, in particular, offer a high-order alternative to the above methods for simulation of flows on smooth surfaces without any recourse to Lagrange multipliers or penalties for enforcing tangentiality of the flow. Section 2 presents the mathematical preliminaries needed for our approach. We subsequently discuss the theoretical and algorithmic aspects behind the construction of multi-degree spline differential forms (Sections 4 and 3.2), and their application to building polar spline differential forms (Section 5). In particular, we show how this enables us to mimic the cohomological structure of the de Rham complex at the discrete level. We demonstrate the high-order accuracy, stability and applicability of the discrete differential form spaces by simulating, in particular, generalized Stokes flow on fixed and deforming smooth surfaces (Section 6). The spaces also allow us to simulate pointwise incompressible tangential flows on surfaces. See an example of such pointwise incompressible tangential flow on the right where streamfunction contours and tangential velocities are displayed; see Section 6.3 for details.

2. Mathematical preliminaries

Let us start by presenting some exterior calculus preliminaries and, in particular, introduce the L^2 de Rham complex. We follow the presentation of [8] in an abbreviated form. Moreover, since we are interested in building spline differential forms on smooth 2-manifolds, $\overline{\Omega}$, we restrict the following discussion to the two-dimensional setting. Note that we only present the most basic relations in this section; other necessary notation and material will be presented when needed.

2.1. Outlook

As mentioned in Section 1, the motivation for this article is the construction of stable and high-order accurate spline-based finite element methods for numerical approximation of (scalar and vector) solutions to PDEs on smooth 2-manifolds $\overline{\Omega}$. We do so within the conceptual framework of finite element exterior calculus [7,8] and its spline-based counterparts [10,11,26]. As shown in [8], for instance, well-posed problems can be formulated at the discrete level if the finite element spaces form a subcomplex (Section 2.2) of the de Rham complex of differential forms (Section 2.3). The scalar and vector fields that solve the desired PDEs can be thought of as proxies for differential forms, and well-posedness of the continuous problems is implied by properties of the de Rham complex. Then, a first step in the construction of stable methods is the construction of a finite element subcomplex that mimics the properties of the continuous de Rham complex. The next two subsections introduces Hilbert cochain complexes and the de Rham complex of differential forms.

2.2. Hilbert cochain complexes

Let V denote a sequence of Hilbert spaces $\left\{V^{(i)}\right\}_{i=0}^{2}$, and let d denote a sequence $\left\{d^{(i)}\right\}_{i=0}^{1}$ of connecting closed, linear maps of degree +1, $d^{(i)} : V^{(i)} \to V^{(i+1)}$. If $d^{(1)} \circ d^{(0)} = 0$, V and d together form a *Hilbert complex* $\mathfrak{V} := (V, d)$,

$$\mathfrak{V} : \qquad V^{(0)} \xrightarrow{d^{(0)}} V^{(1)} \xrightarrow{d^{(1)}} V^{(2)} . \tag{1}$$

The connecting maps $d^{(i)}$ are called the differentials of the complex $\mathfrak{V}$. Moreover, $\mathfrak{V}$ is called bounded if its differentials are bounded linear operators, and it is called closed if the image of $d^{(i)}$ is closed in $V^{(i+1)}$ for all i.

The composition property of the differentials implies that the following containment holds,

$$\operatorname{im} d^{(i-1)} \subseteq \ker d^{(i)} \ . \tag{2}$$

Members of $V^{(i)}$ in $\ker d^{(i)}$ are called i-cocycles or closed, and the members of $V^{(i)}$ in $\operatorname{im} d^{(i-1)}$ are called i-coboundaries or exact. The i-th cohomology space associated to the complex $\mathfrak{V}$, $H^i(\mathfrak{V})$, is defined as the following quotient,

$$H^i(\mathfrak{V}) = \ker d^{(i)} / \operatorname{im} d^{(i-1)} \ . \tag{3}$$

Note that, for defining $H^0(\mathfrak{V})$ and $H^1(\mathfrak{V})$, the beginning and the end of the complex are automatically augmented with zero maps $d^{(-1)} := 0 =: d^{(2)}$. The cohomology space $H^i(\mathfrak{V})$ measures the extent to which the equality in Eq. (2) fails to hold.

Given two complexes $\mathfrak{V} = (V, d_V)$ and $\mathfrak{W} = (W, d_W)$, linear maps $f^{(i)} : V^{(i)} \to W^{(i)}$ of degree 0 are called cochain maps if they commute with the differentials for all i,

$$d_W^{(i)} \circ f^{(i)} = f^{(i+1)} \circ d_V^{(i)} \ . \tag{4}$$

Cochain maps preserve closed and exact forms and, consequently, induce maps between cohomology spaces of the two complexes, $f^{*,(i)} : H^i(\mathfrak{V}) \to H^i(\mathfrak{W})$. Additionally, for $i = 0, 1, 2$, if $W^{(i)} \subseteq V^{(i)}$ and all differentials $d_W^{(i)}$ are obtained from $d_V^{(i)}$ by restriction, then the complex $\mathfrak{W}$ is called a subcomplex of $\mathfrak{V}$. In this case, the inclusion $\iota^{(i)} : W^{(i)} \to V^{(i)}$ is a cochain map from $\mathfrak{W}$ to $\mathfrak{V}$ and induces a natural map between their cohomologies. If, additionally, there exists a cochain projection map from $\mathfrak{V}$ to $\mathfrak{W}$, it induces a surjection of cohomologies. In particular, the dimensions of $H^i(\mathfrak{W})$ are then bounded from above by those of $H^i(\mathfrak{V})$ for all i.

Remark 2.1. In the following, to unburden the notation, we will drop the superscripts of all differentials as it will always be clear from the context which differential is being used.

2.3. The de Rham complex of differential forms

Given a (sufficiently) smooth 2-manifold $\overline{\Omega} \subset \mathbb{R}^{\mathfrak{d}}$, $\mathfrak{d} = 2, 3$, let $T_{\boldsymbol{y}}\overline{\Omega}$ denote the 2-dimensional tangent space at $\boldsymbol{y} \in \overline{\Omega}$. A smooth differential i-form f, $i = 0, 1, 2$, on $\overline{\Omega}$ is a smooth field such that $f_{\boldsymbol{y}}$ is a real-valued skew-symmetric i-linear form on $T_{\boldsymbol{y}}\overline{\Omega} \times \cdots \times T_{\boldsymbol{y}}\overline{\Omega}$. Let $\Lambda^{(i)}(\overline{\Omega})$ denote the space of all smooth i-forms, $i = 0, 1, 2$.

For $i = 0, 1, 2$, and $f \in \Lambda^{(i)}(\overline{\Omega})$, the exterior derivative is a linear map of degree +1, $d : \Lambda^{(i)}(\overline{\Omega}) \to \Lambda^{(i+1)}(\overline{\Omega})$, such that $d \circ d = 0$. In local (curvilinear) coordinates $\boldsymbol{x} = (x^1, x^2)$ on $\overline{\Omega}$ such that $\boldsymbol{y} = \boldsymbol{y}(\boldsymbol{x})$, the differential forms and the action of d are simply

$$\Lambda^{(0)}(\overline{\Omega}) \ni f \ : \ f(\boldsymbol{x}) \qquad \overset{d}{\mapsto} \quad \frac{\partial f}{\partial x^i}\, dx^i \ , \tag{5}$$

$$\Lambda^{(1)}(\overline{\Omega}) \ni f \ : \ f_i(\boldsymbol{x})\, dx^i \qquad \overset{d}{\mapsto} \quad \left(\frac{\partial f_2}{\partial x^1} - \frac{\partial f_1}{\partial x^2} \right) dx^1 \wedge dx^2 \ , \tag{6}$$

$$\Lambda^{(2)}(\overline{\Omega}) \ni f \ : \ f_{12}(\boldsymbol{x})\, dx^1 \wedge dx^2 \quad \overset{d}{\mapsto} \quad 0 \ . \tag{7}$$

where dx^1 and dx^2 are a covector basis that span the cotangent spaces of $\overline{\Omega}$. In the above and the following, we assume Einstein's summation convention unless indicated otherwise. Finally, $\wedge \ : \ \Lambda^{(i)}(\overline{\Omega}) \times \Lambda^{(j)}(\overline{\Omega}) \to \Lambda^{(i+j)}(\overline{\Omega})$ is the product operator for differential forms. It is antisymmetric, associative and anti-commutative and, in particular, in our 2-dimensional setting we have

$$dx^1 \wedge dx^2 = -dx^2 \wedge dx^1 \ . \tag{8}$$

An i-form, $f \in \Lambda^{(i)}(\overline{\Omega})$, can be naturally integrated on any i-dimensional sub-manifold $\tilde{\Omega}$ of $\overline{\Omega}$, i.e., without any need for a metric. Moreover, if f is exact, i.e., $f = dg$, $g \in \Lambda^{(i-1)}(\overline{\Omega})$, then the Stokes' theorem holds,

$$\int_{\overline{\Omega}} f = \int_{\partial\overline{\Omega}} g \ , \tag{9}$$

where ∂ denotes the boundary operator. In other words, the exterior derivative can be thought of as the dual of the boundary operator with respect to the natural duality pairing of i-forms with i-dimensional submanifolds.

With $L^2\Lambda^{(i)}(\overline{\Omega})$ denoting the completion of $\Lambda^{(i)}(\overline{\Omega})$ with respect to the L^2 inner product of i-forms $(\cdot,\cdot)_{L^2\Lambda^{(i)}(\overline{\Omega})}$, we define $H\Lambda^{(i)}(\overline{\Omega})$ as

$$H\Lambda^{(i)}(\overline{\Omega}) \coloneqq \left\{ f \in L^2\Lambda^{(i)}(\overline{\Omega}) \ : \ df \in L^2\Lambda^{(i+1)}(\overline{\Omega}) \right\} . \tag{10}$$

With $(\cdot,\cdot)_{\overline{\Omega}} \coloneqq (\cdot,\cdot)_{L^2\Lambda^{(i)}(\overline{\Omega})}$, we equip $H\Lambda^{(i)}(\overline{\Omega})$ with the following graph norm-induced inner-product,

$$(f,g)_{H\Lambda^{(i)}(\overline{\Omega})} \coloneqq (f,g)_{\overline{\Omega}} + (df,dg)_{\overline{\Omega}} . \tag{11}$$

Note that $H\Lambda^{(2)}(\overline{\Omega}) = L^2\Lambda^{(2)}(\overline{\Omega})$ from Eq. (7). Then, the L^2 de Rham complex on $\overline{\Omega}$ is the closed and bounded Hilbert complex defined as

$$\mathfrak{R} \ : \ H\Lambda^{(0)}(\overline{\Omega}) \xrightarrow{\ d\ } H\Lambda^{(1)}(\overline{\Omega}) \xrightarrow{\ d\ } H\Lambda^{(2)}(\overline{\Omega}) . \tag{12}$$

When $\overline{\Omega}$ is contractible and has a single-connected component, we have $H^0(\mathfrak{R}) = \mathbb{R}$ and $H^1(\mathfrak{R}) = 0$. Moreover, if $\overline{\Omega}$ is a closed manifold, then $H^2(\mathfrak{R}) = \mathbb{R}$; else, $H^2(\mathfrak{R}) = 0$.

3. The univariate spline complex

In this section we present preliminary concepts about smooth polynomial splines defined on a partition of an interval, $\Omega \coloneqq [a,b] \subset \mathbb{R}$. In particular, we will allow the spline pieces to have different polynomial degrees, thereby introducing the concept of multi-degree spline spaces. We also present a set of basis functions for such spaces called multi-degree B-splines (or MDB-splines) and list some of their properties. Classical B-splines are a special case of MDB-splines.

3.1. The polynomial complex

3.1.1. Definition of the complex

In this preliminary section, we recall the simplest univariate spline complex on Ω that we can consider. For $p \in \mathbb{N}$, let $\mathcal{P}_p$ be the vector space of polynomials of degree $\leq p$. Then, the simplest spline space on Ω consists only of global polynomials,

$$\mathcal{S}_p^{-1} \coloneqq \left\{ \Omega \xrightarrow{f} \mathbb{R} \ : \ f \in \mathcal{P}_p \right\} .$$

Choosing $\mathcal{S}_p^{-1}$ as the space of 0-forms and $\mathcal{S}_{p-1}^{-1}$ as the space of 1-forms,

$$\Lambda_P^{(0)} \coloneqq \mathcal{S}_p^{-1} , \quad \Lambda_P^{(1)} \coloneqq \left\{ f\, dx \ : \ f \in \mathcal{S}_{p-1}^{-1} \right\} ,$$

the univariate polynomial complex is defined as

$$\mathfrak{G} \ : \ \Lambda_P^{(0)} \longrightarrow \Lambda_P^{(1)} . \tag{13}$$

It can be easily verified that the exterior derivative is a surjection from $\Lambda_P^{(0)}$ onto $\Lambda_P^{(1)}$, thereby yielding $H^1(\mathfrak{G}) = 0$. On the other hand, $H^0(\mathfrak{G})$ or the nullspace of d is one dimensional and contains constants, i.e., $H^0(\mathfrak{G}) = \mathbb{R}$.

3.1.2. Basis for discrete differential forms

We choose the Bernstein–Bézier polynomials $B_{i,p}$, $i = 0,\ldots,p$, as the preferred basis for 0-forms; these are defined as

$$B_{i,p}(x) = \binom{p}{i} \left(\frac{x-a}{b-a}\right)^i \left(\frac{b-x}{b-a}\right)^{p-i} , \tag{14}$$

and they span $\mathcal{S}_p^{-1}$. Therefore, $f \in \Lambda_P^{(0)}$ can be represented as a linear combination of the $B_{i,p}$ with some coefficients $f_i \in \mathbb{R}$,

$$f = \sum_{i=0}^{p} f_i B_{i,p} .$$

Furthermore, if $f \in \Lambda^{(0)}_P$ is a 0-form, then the 1-form $g := df \in \Lambda^{(1)}_P$ has the representation

$$g = \sum_{i=0}^{p} f_i dB_{i,p} = \sum_{i=0}^{p-1} (f_{i+1} - f_i)\overline{B}_{i,p}\, dx =: \sum_{i=0}^{p-1} g_i \overline{B}_{i,p}\, dx\ , \tag{15}$$

where the $\overline{B}_i$, $i = 0, \ldots, p-1$, are scaled Bernstein–Bézier polynomials of degree $p-1$,

$$\overline{B}_{i,p} := \frac{p}{b-a} B_{i,p-1}\ . \tag{16}$$

These are chosen as the preferred basis for discrete 1-forms. Doing so helps us define a discrete representation of the exterior derivative d in the form of the sparse matrix $\boldsymbol{D}^{(0)}_k$ of size $k \times (k+1)$, $k \geq 2$,

$$\boldsymbol{D}^{(0)}_k := \begin{bmatrix} -1 & 1 & & & \\ & -1 & 1 & & \\ & & \ddots & \ddots & \\ & & & -1 & 1 \end{bmatrix}\ . \tag{17}$$

Indeed, following Eq. (15) and arranging the coefficients g_i and f_i in column vectors $\boldsymbol{g}$ and $\boldsymbol{f}$, respectively, we see that $\boldsymbol{D}^{(0)}_p$ acts on the coefficients of the 0-form (with respect to the 0-form basis $B_{i,p}$) and yields the coefficients of its exterior derivative (with respect to the 1-form basis $\overline{B}_{i,p}$),

$$\boldsymbol{g} = \boldsymbol{D}^{(0)}_p \boldsymbol{f}\ . \tag{18}$$

3.1.3. Degree of freedom interpretation

We can give a geometric interpretation to Eq. (18) using a particular one-dimensional mesh. Let $0 = \gamma_0 < \gamma_1 < \cdots < \gamma_p = 1$ partition the unit interval $[0, 1]$, and consider the corresponding one-dimensional cell complex with vertices γ_i, $i = 0, \ldots, p$, and edges $\tau_i = \gamma_i \gamma_{i+1}$, $i = 0, \ldots, p-1$. We orient this complex by choosing the oriented boundary of each edge τ_i to be $\partial(\tau_i) = \gamma_{i+1} - \gamma_i$.

Then, we can interpret $f \in \Lambda^{(0)}_P$ and $g \in \Lambda^{(1)}_P$ as *cochains*, i.e., linear functionals on the edges and vertices,

$$f\ :\ \gamma_i \mapsto f_i\ , \quad g\ :\ \tau_i \mapsto g_i\ . \tag{19}$$

Doing so, we see that the preferred 1- and 0-form basis functions $B_{i,p}$ and $\overline{B}_{i,p}$, respectively, are cochain interpolants. Moreover, we see that our discrete representations mimic the continuous version of the Stokes theorem. Indeed, extending the maps in Eq. (19) to formal sums of edges and vertices via linearity, we see that

$$\begin{aligned} df\left(\sum_{i=0}^{p-1} c_i \tau_i\right) &= \boldsymbol{c} \cdot \boldsymbol{D}^{(0)}_p \boldsymbol{f} = \left(\boldsymbol{D}^{(0)}_p\right)^T \boldsymbol{c} \cdot \boldsymbol{f}\ , \\ &= f\left(\partial \sum_{i=0}^{p-1} c_i \tau_i\right)\ , \end{aligned} \tag{20}$$

since our choice of orientation makes $\left(\boldsymbol{D}^{(0)}_p\right)^T$ the discrete representation of the boundary operator that maps edges to oriented sums of vertices. The correspondence with the Stokes theorem is now clear.

Thus, our choice of the preferred 1- and 0-form basis functions leads to a discrete version of the Stokes theorem. This not only makes it easy to compute the degrees of freedom of an exact 1-form using Eq. (18), but in higher dimensions it will also help us exactly enforce $d \circ d = 0$ at the discrete level by a judicious choice of the discrete exterior derivatives. Finally, we will graphically depict the action of the discrete exterior derivative on the degrees of freedom as in the figure below. That is, the 0-form degrees of freedom are associated to the oriented zero-dimensional cells of the mesh (i.e., vertices), and the action of $\boldsymbol{D}^{(0)}_p$ yields new degrees of freedom associated to the oriented one-dimensional cells of the mesh (i.e., edges) (see Fig. 1).

3.2. The multi-degree spline complex

3.2.1. Multi-degree splines

We start by partitioning the interval Ω into a finite number of points (called breakpoints) and subintervals (called elements); the space of polynomial splines on Ω will be defined with respect to this partition.

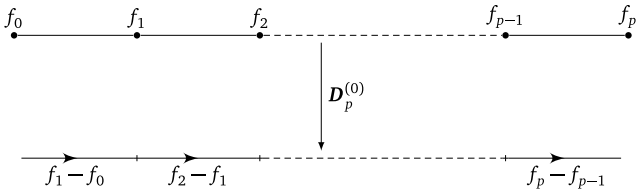

Fig. 1. We interpret the degrees of freedom of 0- and 1-forms in the polynomial complex $\mathfrak{G}$ as being associated to vertices and edges of a one-dimensional cell complex. Consequently, the discrete exterior derivative $\boldsymbol{D}_p^{(0)}$ corresponding to the choice of the preferred bases has a simple action as shown above.

Definition 3.1 (*Breakpoints and Elements*)**.** The $m+1$ strictly increasing real numbers x_i, such that $a =: x_0 < x_1 < \cdots < x_m := b$, will be called breakpoints that partition Ω. The breakpoints define the intervals Ω_i called elements,

$$\Omega_k = \begin{cases} [x_{k-1}, x_k) \,, & k = 1, \ldots, m-1 \,, \\ [x_{m-1}, x_m] \,, & k = m \,. \end{cases} \tag{21}$$

Next, we pick polynomial degrees $p_k \in \mathbb{N}$, $k = 1, \ldots, m$, associated to each element Ω_k. We also choose a non-negative order of smoothness $r_k \in \mathbb{Z}_{\geq 0}$, $k = 1, \ldots, m-1$, for each breakpoint of the partition, and $r_0 = r_m \in \mathbb{Z}_{\geq -1}$. We will distinguish between the following two cases,

$$\begin{aligned} &\text{Non-periodic setting:} \quad && r_0 = r_m = -1 \,, \\ &\text{Periodic setting:} && r_0 = r_m \geq 0 \,. \end{aligned} \tag{22}$$

All the p_k and r_k are arranged in vectors $\boldsymbol{p}$ and $\boldsymbol{r}$, respectively. Before proceeding, we place the following mild compatibility assumption on the chosen degrees and orders of smoothness.

Assumption 1

Each "Assumption" introduced will hold for the entirety of the document following it.

Assumption 2: Degree-smoothness compatibility

For all $1 \leq k \leq m-1$, we assume that

$$r_k \leq \begin{cases} \min\{p_m, p_1\} \,, & k = 0 \,, \\ \min\{p_k, p_{k+1}\} \,, & k = 1, \ldots, m-1 \,. \end{cases}$$

Definition 3.2 (*Multi-degree Spline Space*)**.** Given degree and smoothness distributions, we define a spline space on Ω as

$$\begin{aligned} \mathcal{S} := \mathcal{S}_{\boldsymbol{p}}^{\boldsymbol{r}} := \Big\{ \; \Omega \xrightarrow{f} \mathbb{R} \;:\; f\big|_{\Omega_k} \in \mathcal{P}_{p_k} \,,\; 0 < k \leq m \,, \\ D_-^r f(x_k) = D_+^r f(x_k) \,,\; 0 < k < m \,,\; 0 \leq r \leq r_k \Big\} \,. \end{aligned} \tag{23}$$

Moreover, when $r_0 = r_m \geq 0$, a periodic spline space on Ω is defined as

$$\mathcal{S}^{\text{per}} := \mathcal{S}_{\boldsymbol{p}}^{\boldsymbol{r},\text{per}} := \Big\{ \; f \in \mathcal{S} \;:\; D_-^r f(x_m) = D_+^r f(x_0) \,,\; 0 \leq r \leq r_0 \Big\} \,. \tag{24}$$

Remark 3.3. In Sections 3.2.2 and 3.2.3 , the non-periodic setting will be discussed, and the periodic setting will be discussed in Sections 3.2.5 and 3.2.5 .

The dimension formulas for $\mathcal{S}$ and $\mathcal{S}^{\text{per}}$ can be derived in a multitude of ways [30,31,44]. With n and n^{per} denoting their respective dimensions, we have

$$n = \boldsymbol{\theta}(m) - \boldsymbol{\phi}(m) \,, \quad n^{\text{per}} = n - r_0 - 1 \,, \tag{25}$$

$$\boldsymbol{\theta}(k) \coloneqq \sum_{j=1}^{k} (p_j + 1) \,, \quad \boldsymbol{\phi}(k) \coloneqq \sum_{j=1}^{k-1} (r_j + 1) \,. \tag{26}$$

where an empty-sum is taken to be zero.

Assumption 3: Periodic degree-smoothness compatibility

With n and n^{per} as defined in Eq. (25), when $r_0 \geq 0$ we assume that

$$n \geq \max_k p_k + r_0 + 2 \iff n^{\text{per}} \geq \max_k p_k + 1 \,.$$

3.2.2. The non-periodic setting: Definition of the complex

To build the multi-degree spline complex, we will use the multi-degree spline spaces $\mathcal{S}$ and $\mathcal{S}^- \coloneqq \mathcal{S}^{r^-}_{\boldsymbol{p}^-}$, where we define vectors $\boldsymbol{p}^-$ and $\boldsymbol{r}^-$ such that

$$p_k^- \coloneqq p_k - 1 \,, \quad r_k^- \coloneqq \max\{-1, r_k - 1\} \,. \tag{27}$$

Then, the spaces of 0- and 1-forms are respectively chosen as follows,

$$\Lambda_M^{(0)} \coloneqq \mathcal{S} \,, \quad \Lambda_M^{(1)} \coloneqq \left\{ f \, dx \;:\; f \in \mathcal{S}^- \right\} \,,$$

yielding the multi-degree spline complex

$$\mathfrak{M} \;:\; \Lambda_M^{(0)} \longrightarrow \Lambda_M^{(1)} \,. \tag{28}$$

It can once again be easily verified (e.g., using (23)) that the exterior derivative is a surjection from $\Lambda_M^{(0)}$ onto $\Lambda_M^{(1)}$, making $H^1(\mathfrak{M}) = 0$. Similarly to the polynomial complex, $H^0(\mathfrak{M})$ or the nullspace of d here is one dimensional and only contains constants, i.e., $H^0(\mathfrak{M}) = \mathbb{R}$.

3.2.3. The non-periodic setting: Basis for discrete differential forms

Here, we will choose the so-called *multi-degree B-splines* (MDB-splines) as the preferred basis for the 0-forms. MDB-splines are a multi-degree generalization of the classical B-splines and the properties of the former mirror those of the latter; e.g., see [30,44]. Let us denote the set of MDB-splines that span $\mathcal{S}$ with $\{N_i \;:\; i = 0, \ldots, n-1\}$. See Appendix A for a recursive definition of MDB-splines using integral relations. The following set of properties are relevant for us; proofs of the same and other properties can be found in [30,31,44], for instance.

Proposition 3.4 (*Select MDB-spline Properties*)**.** *With Assumption 2 in place, the following hold.*

(a) Non-negativity: $N_i(x) \geq 0$ for all $x \in \Omega$.
(b) Partition of unity: $\sum_{i=0}^{n-1} N_i(x) = 1$ for all $x \in \Omega$.
(c) Basis: $\{N_i : i = 0, \ldots, n-1\}$ are linearly independent and span the space $\mathcal{S}$.
(d) Local linear independence: Only $N_{\boldsymbol{\mu}(k)}, \ldots, N_{\boldsymbol{\mu}(k)+p_k}$ are supported on Ω_k, and they span $\mathcal{P}_{p_k}$, where

$$\boldsymbol{\mu}(k) \coloneqq \sum_{j=0}^{k-1} (p_{j+1} - r_j) - p_k + r_0 = \sum_{j=0}^{k-1} (p_{j+1} - r_j) - p_k - 1 \,. \tag{29}$$

(e) End-point interpolation: For any $0 \leq r \leq p_1$, only $N_0, \ldots, N_r$ have non-zero r-th derivatives at $x = a$. Similarly, for any $0 \leq r \leq p_m$, only $N_{n-r-1}, \ldots, N_{n-1}$ have non-zero r-th derivatives at $x = b$. In particular, $N_0(a) = N_{n-1}(b) = 1$.

Appendix B presents an algorithmic computation of MDB-splines that is much more efficient for computations than the recursive definitions from Appendix A. The algorithm computes a *multi-degree extraction* $\boldsymbol{H}$ [29,30] that helps express N_i on Ω_k as a linear combination of Bernstein–Bézier polynomials on Ω_k. We briefly explain this construction here.

For $k = 1, \ldots, m$, we denote by $B^{\Omega_k}_{j,p_k}$, $j = 0, \ldots, p_k$, the Bernstein–Bézier polynomials of degree p_k defined on Ω_k; see Eq. (14). Then, we extend them outside of Ω_k by 0 and relabel them as

$$B_{\boldsymbol{\theta}(k-1)+j} \coloneqq B^{\Omega_k}_{j,p_k} \ , \qquad j = 0, \ldots, p_k \ .$$

Next, arrange these relabelled basis functions in a single vector $\boldsymbol{B}$ of length $\boldsymbol{\theta}(m)$. Then, the multi-degree extraction $\boldsymbol{H}$ output by the algorithm in Appendix B [45] helps build the MDB-splines using the following expression [30],

$$\boldsymbol{N} = \boldsymbol{H}\boldsymbol{B} \ , \tag{30}$$

where $\boldsymbol{N}$ is the vector containing all MDB-splines N_i. In particular, for $k = 1, \ldots, m$, we call $\boldsymbol{H}^{\Omega_k}$ the *element extraction*; it is the square submatrix of $\boldsymbol{H}$ of size $(p_k + 1) \times (p_k + 1)$ such that

$$\begin{bmatrix} N_{\boldsymbol{\mu}(k)}(x) \\ N_{\boldsymbol{\mu}(k)+1}(x) \\ \vdots \\ N_{\boldsymbol{\mu}(k)+p_k}(x) \end{bmatrix} = \boldsymbol{H}^{\Omega_k} \begin{bmatrix} B^{\Omega_k}_{0,p_k}(x) \\ B^{\Omega_k}_{1,p_k}(x) \\ \vdots \\ B^{\Omega_k}_{p_k,p_k}(x) \end{bmatrix} , \quad x \in \Omega_k \ . \tag{31}$$

The matrices $\boldsymbol{H}$ and $\boldsymbol{H}^{\Omega_k}$ have properties that mirror those of MDB-splines as presented in Proposition 3.4; e.g., see [30].

Proposition 3.5 (*Extraction Properties*)**.** *With Assumption 2 in place, the following hold.*

(a) Non-negativity: All entries of $\boldsymbol{H}$ *and* $\boldsymbol{H}^{\Omega_k}$, $k = 1, \ldots, m$, *lie in* $[0, 1]$.
(b) Column stochasticity: All columns of $\boldsymbol{H}$ *and* $\boldsymbol{H}^{\Omega_k}$, $k = 1, \ldots, m$, *sum to* 1.
(c) Non-degeneracy: The matrix $\boldsymbol{H}$ *has full rank.*
(d) Local invertibility: The matrices $\boldsymbol{H}^{\Omega_k}$, $k = 1, \ldots, m$, *are non-singular.*

With the above choice of the 0-form basis, we now outline how a preferred basis for the space of 1-forms can be constructed. Note that, in general, this preferred basis will not be the same as the MDB-splines for the space $\mathcal{S}^-$. The following mimics the exposition from Section 3.1.2.

Let $\{\overline{N}_i \ : \ i = 0, \ldots, \overline{n} - 1\}$ denote the set of preferred basis functions that span $\mathcal{S}^-$; note that Eq. (25) implies that

$$\overline{n} = n - 1 \ .$$

Since this is the set of preferred basis functions, it means that for a 0-form $f \in \Lambda^{(0)}_M$,

$$f = \sum_{i=0}^{n-1} f_i N_i \ ,$$

the 1-form $g = df \in \Lambda^{(1)}_M$ can be expressed as

$$g = \sum_{i=0}^{n-1} f_i dN_i = \sum_{i=0}^{\overline{n}-1} (f_{i+1} - f_i)\overline{N}_i \, dx =: \sum_{i=0}^{\overline{n}-1} g_i \overline{N}_i \, dx \ , \tag{32}$$

The following shows how the basis functions $\overline{N}_i$ can be defined element-wise; its proof is presented in Appendix C.

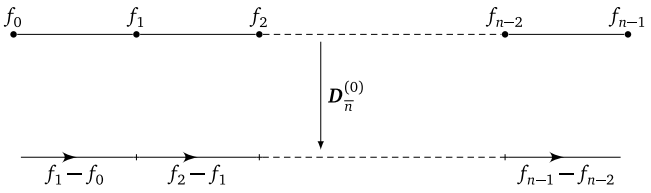

Fig. 2. A similar degree of freedom interpretation as in Section 3.1.3 can be performed for the multi-degree complex $\mathfrak{M}$. With the degrees of freedom of 0- and 1-forms associated to vertices and edges of a one-dimensional cell complex, the discrete exterior derivative $\boldsymbol{D}_{\overline{n}}^{(0)}$ corresponding to the choice of the preferred bases has a simple action as shown above.

Proposition 3.6. *For $k = 1, \ldots, m$,*

$$\begin{bmatrix} \overline{N}_{\boldsymbol{\mu}(k)}(x) \\ \overline{N}_{\boldsymbol{\mu}(k)+1}(x) \\ \vdots \\ \overline{N}_{\boldsymbol{\mu}(k)+p_k-1}(x) \end{bmatrix} = \overline{\boldsymbol{H}}^{\Omega_k} \begin{bmatrix} \overline{B}_{0,p_k}^{\Omega_k}(x) \\ \overline{B}_{1,p_k}^{\Omega_k}(x) \\ \vdots \\ \overline{B}_{p_k-1,p_k}^{\Omega_k}(x) \end{bmatrix} := \boldsymbol{C}\boldsymbol{H}^{\Omega_k} \left(\boldsymbol{D}_{p_k}^{(0)}\right)^T \begin{bmatrix} \overline{B}_{0,p_k}^{\Omega_k}(x) \\ \overline{B}_{1,p_k}^{\Omega_k}(x) \\ \vdots \\ \overline{B}_{p_k-1,p_k}^{\Omega_k}(x) \end{bmatrix}, \quad x \in \Omega_k \,, \tag{33}$$

where $\boldsymbol{C}$ is a lower-triangular matrix of size $p_k \times (p_k + 1)$ with all entries equal to -1. All $\overline{N}_i$, $i = 0, \ldots, \overline{n} - 1$, are, moreover, locally linearly independent and form a basis for $\mathcal{S}^-$.

3.2.4. The non-periodic setting: Degree of freedom interpretation

Similarly to the discussion in Section 3.1.3 focused on the polynomial complex, we can give a geometric interpretation to the non-periodic multi-degree spline complex using Eq. (32). Let $0 = \gamma_0 < \gamma_1 < \cdots < \gamma_{n-1} = 1$ partition the unit interval $[0, 1]$, and consider the corresponding one-dimensional cell complex with vertices γ_i, $i = 0, \ldots, n-1$, and edges $\tau_i = \gamma_i \gamma_{i+1}$, $i = 0, \ldots, \overline{n} - 1$. We again orient this complex by choosing the oriented boundary of each edge τ_i to be $\partial(\tau_i) = \gamma_{i+1} - \gamma_i$.

Once again, we interpret 0- and 1-forms as linear functionals on the cell complex, and this leads to a discrete representation of the Stokes theorem. The discussion is exactly as in Section 3.1.3, therefore we do not repeat here. Instead, we only present graphical representation showing the action of the discrete exterior derivative on the 0-form degrees of freedom (see Fig. 2).

3.2.5. The periodic setting: Definition of the complex

In the periodic setting, i.e., with $r_0 \geq 0$, we identify the right endpoint of Ω with its left endpoint, $a \equiv b$. We will denote this domain with Ω^{per} and note that the end-point identification makes it a topological circle. Let us now build the multi-degree spline complex on this periodic domain; the developments are very similar to the exposition thus far in Sections 3.2.2 and 3.2.3.

The multi-degree spline complex in the periodic setting is built by choosing the spaces of 0- and 1-forms as

$$\Lambda_M^{(0)} := \mathcal{S}^{\text{per}} \,, \quad \Lambda_M^{(1)} := \{ f \, dx \ : \ f \in \mathcal{S}^{-,\text{per}} \} \,,$$

where $\mathcal{S}^{-,\text{per}}$ is the periodic analogue of $\mathcal{S}^-$ with C^{r_0-1} smoothness enforced between the identified ends of Ω^{per}. Then, the periodic multi-degree spline complex is given by

$$\mathfrak{M}^{\text{per}} \ : \ \Lambda_M^{(0)} \longrightarrow \Lambda_M^{(1)} \,. \tag{34}$$

Once again, $H^0(\mathfrak{M}^{\text{per}})$ or the nullspace of the exterior derivative contains only constants in $\Lambda_M^{(0)}$. However, $H^1(\mathfrak{M}^{\text{per}})$ is non-trivial and one-dimensional here, mirroring the non-trivial topology of the periodic domain Ω^{per}. Indeed, constants are in $\Lambda_M^{(1)}$ but are not in the image of d. Thus, both $H^0(\mathfrak{M}^{\text{per}})$ and $H^1(\mathfrak{M}^{\text{per}})$ are isomorphic as vector spaces to $\mathbb{R}$.

3.2.6. The periodic setting: Basis for discrete differential forms

We choose periodic MDB-splines $\{N_i^{\text{per}} \ : \ i = 0, \ldots, n^{\text{per}} - 1\}$ as the basis for the 0-form space $\Lambda_M^{(0)}$. These can be computed starting from the MDB-splines for the non-periodic space $\mathcal{S}$ [45]. In particular, we can compute a matrix $\tilde{\boldsymbol{H}}$ using Algorithm 3 from Appendix D such that

$$\boldsymbol{N}^{\text{per}} = \tilde{\boldsymbol{H}}\boldsymbol{N} = \tilde{\boldsymbol{H}}\boldsymbol{H}\boldsymbol{B} =: \boldsymbol{H}^{\text{per}}\boldsymbol{B} \ . \tag{35}$$

Note that, when working in the periodic setting, all indices (of basis functions, elements, etc.) are treated in a circular fashion here. That is, if we write "N_i^{per}", the subscript is to be understood as below,

$$i \equiv i \mod n^{\text{per}} \ . \tag{36}$$

Periodic MDB-splines have the same set of properties (except end-point interpolation unless $r_0 = 0$) as their non-periodic counterparts, and these are summarized in the following result; these properties can be derived from the properties of $\boldsymbol{H}$ and the properties of $\tilde{\boldsymbol{H}}$ as shown in Proposition D.1.

Proposition 3.7 (*Select Periodic MDB-spline Properties*)**.** *With Assumptions 2 and 3 in place, the following hold.*

(a) Non-negativity: $N_i^{per}(x) \geq 0$ *for all* $x \in \Omega^{per}$.
(b) Partition of unity: $\sum_{i=0}^{n^{per}-1} N_i^{per}(x) = 1$ *for all* $x \in \Omega^{per}$.
(c) Basis: $\{N_i^{per} : i = 0, \ldots, n^{per} - 1\}$ *are linearly independent and span the space* $\mathcal{S}^{per}$.
(d) Local linear independence: Only $N_{\boldsymbol{\mu}(k)}^{per}, \ldots, N_{\boldsymbol{\mu}(k)+p_k}^{per}$ *are supported on* Ω_k*, and they span* $\mathcal{P}_{p_k}$*, where*

$$\boldsymbol{\mu}(k) := \sum_{j=0}^{k-1}(p_{j+1} - r_j) - p_k + r_0 \ . \tag{37}$$

In particular, combining Eqs. (30), (31) and (35), we can write element-local representations of the periodic MDB-splines using element extraction operators,

$$\begin{bmatrix} N_{\boldsymbol{\mu}(k)}^{\text{per}}(x) \\ N_{\boldsymbol{\mu}(k)+1}^{\text{per}}(x) \\ \vdots \\ N_{\boldsymbol{\mu}(k)+p_k}^{\text{per}}(x) \end{bmatrix} = \boldsymbol{H}^{\Omega_k,\text{per}} \begin{bmatrix} B_{0,p_k}^{\Omega_k}(x) \\ B_{1,p_k}^{\Omega_k}(x) \\ \vdots \\ B_{p_k,p_k}^{\Omega_k}(x) \end{bmatrix} , \quad x \in \Omega_k \ . \tag{38}$$

The extraction matrices $\boldsymbol{H}^{\text{per}}$ and $\boldsymbol{H}^{\Omega_k,\text{per}}$ have properties that again mirror those of the periodic MDB-splines; see Proposition D.1.

Proposition 3.8 (*Periodic Extraction Properties*)**.** *With Assumptions 2 and 3 in place, the following hold.*

(a) Non-negativity: All entries of $\boldsymbol{H}^{per}$ *and* $\boldsymbol{H}^{\Omega_k,per}$*,* $k = 1, \ldots, m$*, lie in* $[0, 1]$.
(b) Column stochasticity: All columns of $\boldsymbol{H}^{per}$ *and* $\boldsymbol{H}^{\Omega_k,per}$*,* $k = 1, \ldots, m$*, sum to* 1.
(c) Non-degeneracy: The matrix $\boldsymbol{H}^{per}$ *has full rank.*
(d) Local invertibility: The matrices $\boldsymbol{H}^{\Omega_k,per}$*,* $k = 1, \ldots, m$*, are non-singular.*

The periodic MDB-splines are chosen as the preferred basis for 0-forms, and all computations are performed on each element via Eq. (38). For 1-forms, let $\{\overline{N}_i^{\text{per}} \ : \ i = 0, \ldots, \overline{n}^{\text{per}} - 1\}$ denote the set of preferred basis functions that span $\mathcal{S}^{-,\text{per}}$; note that in the non-periodic setting, the dimension of $\mathcal{S}^{-,\text{per}}$ is the same as that of $\mathcal{S}^{\text{per}}$, i.e.,

$$\overline{n}^{\text{per}} = n^{\text{per}} \ .$$

Since this is the set of preferred basis functions, it means that for 0-form $f \in \Lambda_M^{(0)}$,

$$f = \sum_{i=0}^{n^{\text{per}}-1} f_i N_i^{\text{per}} \ ,$$

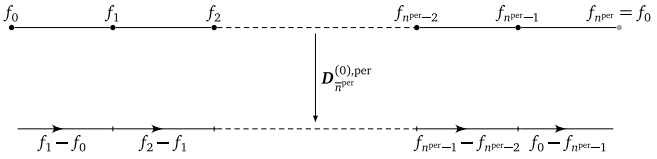

Fig. 3. The degree of freedom interpretation for the multi-degree complex can be extended to the periodic complex $\mathfrak{M}^{\text{per}}$. The discrete exterior derivative $\boldsymbol{D}^{(0),\text{per}}_{\overline{n}^{\text{per}}}$ corresponding to the choice of the periodic preferred bases has a simple action as shown above.

the 1-form $g := df \in \Lambda^{(1)}_M$ can be expressed as

$$g = \sum_{i=0}^{n^{\text{per}}-1} f_i dN_i^{\text{per}} = \sum_{i=0}^{\overline{n}^{\text{per}}-1} (f_{i+1} - f_i)\overline{N}_i^{\text{per}}\, dx =: \sum_{i=0}^{\overline{n}^{\text{per}}-1} g_i \overline{N}_i^{\text{per}}\, dx\ , \tag{39}$$

where the coefficients g_i are now obtained from f_i by the action of the periodic discrete exterior derivative $\boldsymbol{D}^{(0),\text{per}}_{\overline{n}^{\text{per}}}$, where $\boldsymbol{D}^{(0),\text{per}}_{k}$ is defined as the following matrix of size $k \times k$,

$$\boldsymbol{D}^{(0),\text{per}}_{k} := \begin{bmatrix} -1 & 1 & & \\ & -1 & 1 & \\ & & \ddots & \ddots \\ 1 & & & -1 \end{bmatrix}\ . \tag{40}$$

The following shows how the basis functions $\overline{N}_i^{\text{per}}$ can be defined element-wise; its proof can be found in Appendix E.

Proposition 3.9. *For $k = 1, \ldots, m$,*

$$\begin{bmatrix} \overline{N}^{per}_{\boldsymbol{\mu}(k)}(x) \\ \overline{N}^{per}_{\boldsymbol{\mu}(k)+1}(x) \\ \vdots \\ \overline{N}^{per}_{\boldsymbol{\mu}(k)+p_k-1}(x) \end{bmatrix} = \overline{\boldsymbol{H}}^{\Omega_k,per} \begin{bmatrix} \overline{B}^{\Omega_k}_{0,p_k}(x) \\ \overline{B}^{\Omega_k}_{1,p_k}(x) \\ \vdots \\ \overline{B}^{\Omega_k}_{p_k-1,p_k}(x) \end{bmatrix} := \boldsymbol{C}\boldsymbol{H}^{\Omega_k,per} \left(\boldsymbol{D}^{(0)}_{p_k}\right)^T \begin{bmatrix} \overline{B}^{\Omega_k}_{0,p_k}(x) \\ \overline{B}^{\Omega_k}_{1,p_k}(x) \\ \vdots \\ \overline{B}^{\Omega_k}_{p_k-1,p_k}(x) \end{bmatrix}, \quad x \in \Omega_k\ , \tag{41}$$

where $\boldsymbol{C}$ is a lower-triangular matrix of size $p_k \times (p_k+1)$ with all entries equal to -1. All $\overline{N}^{per}_i$, $i = 0, \ldots, \overline{n}^{per}-1$, are, moreover, locally linearly independent and form a basis for $\mathcal{S}^{-,per}$.

3.2.7. The periodic setting: Degree of freedom interpretation

Let us now give a geometric interpretation of the periodic multi-degree spline complex using Eq. (39). Let $0 = \gamma_0 < \gamma_1 < \cdots < \gamma_{n-1} = 1$ partition the unit interval $[0, 1]$, and consider the corresponding one-dimensional cell complex with vertices γ_i, $i = 0, \ldots, n^{\text{per}} - 1$, and edges $\tau_i = \gamma_i\gamma_{i+1}$, $i = 0, \ldots, \overline{n}^{\text{per}} - 1$. We again orient this complex by choosing the oriented boundary of each edge τ_i to be $\partial(\tau_i) = \gamma_{i+1} - \gamma_i$. Note that, due to periodicity, $\tau_{\overline{n}^{\text{per}}-1} = \gamma_{\overline{n}^{\text{per}}-1}\gamma_{\overline{n}^{\text{per}}} = \gamma_{n^{\text{per}}-1}\gamma_0$.

Once again, we interpret 0- and 1-forms as linear functionals on the cell complex, and this leads to a discrete representation of the Stokes theorem. The corresponding graphical representation showing the action of the discrete exterior derivative on the 0-form degrees of freedom is presented in Fig. 3.

4. The tensor-product spline complex and mapped geometries

Using the univariate multi-degree spline complexes, we can build multivariate spline complexes via tensor-products of the multi-degree spline spaces. Here, since we are mainly interested in surfaces in $\mathbb{R}^2$ or $\mathbb{R}^3$, we only focus on bivariate spline complexes. First, we detail how these are built on a rectangular parametric domain Ω,

$$\Omega := \Omega^1 \times \Omega^2 := [a^1, b^1] \times [a^2, b^2] \subset \mathbb{R}^2\ , \tag{42}$$

and then we show how they can be used to build spline complexes on mapped surfaces in $\mathbb{R}^2$ or $\mathbb{R}^3$.

4.1. Tensor-product splines

Let $\mathcal{S}^i$ be some univariate multi-degree spline spaces built on Ω^i and denote the corresponding sets of MDB-splines with $\{N_j^i \ : \ j = 0, \dots, n^i - 1\}$, $i = 1, 2$. Unless otherwise specified, spline spaces $\mathcal{S}^i$ are allowed to be non-periodic or periodic; we simply drop the superscript of "per" to simplify the notation whenever the context is unambiguous. Moreover, let $\{\overline{N}_j^i \ : \ j = 0, \dots, \overline{n}^i - 1\}$, $i = 1, 2$, denote the respective sets of preferred 1-form basis functions corresponding to $\mathcal{S}^1$ and $\mathcal{S}^2$; these span the spline spaces $\mathcal{S}^{1,-}$ and $\mathcal{S}^{2,-}$, respectively. Using the above univariate spline spaces, we define the following tensor-product bivariate spline spaces,

$$\mathcal{S}^{(0,0)} \coloneqq \text{span}\left\langle N_i^1(x^1) N_j^2(x^2) \ : \ i = 0, \dots, n^1 - 1 \ , \ j = 0, \dots, n^2 - 1 \right\rangle \ , \ n^{(0,0)} \coloneqq \dim\left(\mathcal{S}^{(0,0)}\right) = n^1 \times n^2 \ , \tag{43}$$

$$\mathcal{S}^{(1,0)} \coloneqq \text{span}\left\langle \overline{N}_i^1(x^1) N_j^2(x^2) \ : \ i = 0, \dots, \overline{n}^1 - 1 \ , \ j = 0, \dots, n^2 - 1 \right\rangle \ , \ n^{(1,0)} \coloneqq \dim\left(\mathcal{S}^{(1,0)}\right) = \overline{n}^1 \times n^2 \ , \tag{44}$$

$$\mathcal{S}^{(0,1)} \coloneqq \text{span}\left\langle N_i^1(x^1) \overline{N}_j^2(x^2) \ : \ i = 0, \dots, n^1 - 1 \ , \ j = 0, \dots, \overline{n}^2 - 1 \right\rangle \ , \ n^{(0,1)} \coloneqq \dim\left(\mathcal{S}^{(0,1)}\right) = n^1 \times \overline{n}^2 \ , \tag{45}$$

$$\mathcal{S}^{(1,1)} \coloneqq \text{span}\left\langle \overline{N}_i^1(x^1) \overline{N}_j^2(x^2) \ : \ i = 0, \dots, \overline{n}^1 - 1 \ , \ j = 0, \dots, \overline{n}^2 - 1 \right\rangle \ , \ n^{(1,1)} \coloneqq \dim\left(\mathcal{S}^{(1,1)}\right) = \overline{n}^1 \times \overline{n}^2 \ . \tag{46}$$

4.2. Definition of the complex

Using the above tensor-product spline spaces, we choose the spaces of 0-, 1- and 2-forms on Ω as follows,

$$\Lambda_T^{(0)} \coloneqq \mathcal{S}^{(0,0)} \ , \quad \Lambda_T^{(1)} \coloneqq \{f_i \, dx^i \ : \ f_1 \in \mathcal{S}^{(1,0)} \ , \ f_2 \in \mathcal{S}^{(0,1)}\} \ , \quad \Lambda_T^{(2)} \coloneqq \{f \, dx^1 \wedge dx^2 \ : \ f \in \mathcal{S}^{(1,1)}\} \ .$$

Then, the bivariate tensor-product spline complex on Ω is defined as

$$\mathfrak{T} \ : \ \Lambda_T^{(0)} \longrightarrow \Lambda_T^{(1)} \longrightarrow \Lambda_T^{(2)} \ . \tag{47}$$

Theorem 4.1. *The cohomology spaces of the complex $\mathfrak{T}$ satisfy:*

$$H^0(\mathfrak{T}) = \mathbb{R} \ ;$$

$$H^1(\mathfrak{T}) = \begin{cases} 0 \ , & \mathcal{S}^1 \text{ and } \mathcal{S}^2 \text{ are non-periodic} \ , \\ \mathbb{R} \ , & \text{either } \mathcal{S}^1 \text{ or } \mathcal{S}^2 \text{ is periodic} \ , \\ \mathbb{R}^2 \ , & \text{both } \mathcal{S}^1 \text{ and } \mathcal{S}^2 \text{ are periodic} \ ; \end{cases}$$

$$H^2(\mathfrak{T}) = \begin{cases} 0 \ , & \text{at least one of } \mathcal{S}^1 \text{ and } \mathcal{S}^2 \text{ is non-periodic} \ , \\ \mathbb{R} \ , & \text{both } \mathcal{S}^1 \text{ and } \mathcal{S}^2 \text{ are periodic} \ . \end{cases}$$

Proof. It is clear that only constants in $\Lambda_T^{(0)}$ are annihilated by the exterior derivative, thus showing that $H^0(\mathfrak{T}) = \mathbb{R}$. The proof for $H^1(\mathfrak{T})$ and $H^2(\mathfrak{T})$ for non-periodic spline spaces can be obtained by, for instance, following the proof of [12, Theorem 4.1]. The cases with periodic spline spaces make Ω a topological cylinder or torus, and the cohomology spaces can be verified to be,

$$H^1(\mathfrak{T}) = \begin{cases} \text{span}\left\langle \alpha \, dx^i \ : \ \alpha \in \mathbb{R} \right\rangle \ , & \text{if only } \mathcal{S}^i \text{ is periodic} \ , \\ \text{span}\left\langle \alpha_i \, dx^i \ : \ \alpha_i \in \mathbb{R} \ , \ i = 1, 2 \right\rangle \ , & \text{both } \mathcal{S}^1 \text{ and } \mathcal{S}^2 \text{ are periodic} \ ; \end{cases}$$

$$H^2(\mathfrak{T}) = \begin{cases} 0 \ , & \text{if only one of } \mathcal{S}^1 \text{ and } \mathcal{S}^2 \text{ is periodic} \ , \\ \text{span}\left\langle \alpha_{12} \, dx^1 \wedge dx^2 \ : \ \alpha_{12} \in \mathbb{R} \right\rangle \ , & \text{both } \mathcal{S}^1 \text{ and } \mathcal{S}^2 \text{ are periodic} \ . \end{cases}$$

■

4.3. Basis for discrete differential forms

We have already chosen the preferred basis for 0-, 1- and 2-forms in Eqs. (43)–(46). Since all basis functions are tensor-product, their element-wise computations are done by tensoring the respective element extraction matrices from Eqs. (31) and (38) for the splines N^i_j, $i = 1, 2$, and using Propositions 3.6 and 3.9 for the splines $\overline{N}^i_j$, $i = 1, 2$. Therefore, it only remains to derive the discrete representations of the exterior derivatives akin to the univariate setting. We do so in the following.

Let $f \in \Lambda^{(0)}_T$, then

$$f = \sum_{i=0}^{n^1-1} \sum_{j=0}^{n^2-1} f_{ij} N^1_i N^2_j = \boldsymbol{N}^{(0,0)} \cdot \boldsymbol{f} \ ,$$

where $\boldsymbol{f}$ and $\boldsymbol{N}^{(0,0)}$ are column vectors obtained by placing f_{ij} and $N^1_i N^2_j$ in the $(i + jn^1)$-th locations, respectively. Then, using the univariate relations, we can write

$$\begin{aligned} \Lambda^{(1)}_T \ni g := df &= \sum_{i=0}^{n^1-1} \sum_{j=0}^{n^2-1} f_{ij} \left(\frac{dN^1_i}{dx^1} N^2_j dx^1 + N^1_i \frac{dN^2_j}{dx^2} dx^2 \right) \ , \\ &= \boldsymbol{N}^{(1,0)} \cdot \boldsymbol{D}^{(1,0)} \boldsymbol{f} \ dx^1 + \boldsymbol{N}^{(0,1)} \cdot \boldsymbol{D}^{(0,1)} \boldsymbol{f} \ dx^2 \ , \end{aligned} \tag{48}$$

where $\boldsymbol{N}^{(1,0)}$ and $\boldsymbol{N}^{(0,1)}$ are column vectors obtained by placing $\overline{N}^1_i N^2_j$ and $N^1_i \overline{N}^2_j$ in the $(i + j\overline{n}^1)$-th and $(i + jn^1)$-th locations, respectively, and the discrete exterior derivatives are given by

$$\boldsymbol{D}^{(1,0)} = \boldsymbol{I}_{n^2} \otimes \boldsymbol{D}^{(0)}_{\overline{n}^1} \ , \quad \boldsymbol{D}^{(0,1)} = \boldsymbol{D}^{(0)}_{\overline{n}^2} \otimes \boldsymbol{I}_{n^1} \ . \tag{49}$$

Similarly, let $f \in \Lambda^{(1)}_T$, then

$$\begin{aligned} f &= \sum_{i=0}^{\overline{n}^1-1} \sum_{j=0}^{n^2-1} f^1_{ij} \overline{N}^1_i N^2_j \ dx^1 + \sum_{i=0}^{n^1-1} \sum_{j=0}^{\overline{n}^2-1} f^2_{ij} N^1_i \overline{N}^2_j \ dx^2 \ , \\ &= \boldsymbol{N}^{(1,0)} \cdot \boldsymbol{f}^1 \ dx^1 + \boldsymbol{N}^{(0,1)} \cdot \boldsymbol{f}^2 \ dx^2 \ , \end{aligned}$$

where $\boldsymbol{f}^1$ and $\boldsymbol{f}^2$ are column vectors obtained by placing f^1_{ij} and f^2_{ij} in the $(i + j\overline{n}^1)$-th and $(i + jn^1)$-th locations, respectively. Then, using the univariate relations, we can write

$$\begin{aligned} \Lambda^{(2)}_T \ni g := df &= \sum_{i=0}^{\overline{n}^1-1} \sum_{j=0}^{n^2-1} f^1_{ij} \overline{N}^1_i \frac{dN^2_j}{dx^2} \ dx^2 \wedge dx^1 + \sum_{i=0}^{n^1-1} \sum_{j=0}^{\overline{n}^2-1} f^2_{ij} \frac{dN^1_i}{dx^1} \overline{N}^2_j \ dx^1 \wedge dx^2 \ , \\ &= \boldsymbol{N}^{(1,1)} \cdot \left(-\boldsymbol{D}^{(2,0)} \boldsymbol{f}^1 + \boldsymbol{D}^{(0,2)} \boldsymbol{f}^2 \right) \ dx^1 \wedge dx^2 \ , \end{aligned} \tag{50}$$

where $\boldsymbol{N}^{(1,1)}$ is a column vector obtained by placing $\overline{N}^1_i \overline{N}^2_j$ in the $(i + j\overline{n}^1)$-th locations, and the discrete exterior derivatives can once again be derived to be the following sparse outer products,

$$\boldsymbol{D}^{(2,0)} = \boldsymbol{D}^{(0)}_{\overline{n}^2} \otimes \boldsymbol{I}_{\overline{n}^1} \ , \quad \boldsymbol{D}^{(0,2)} = \boldsymbol{I}_{\overline{n}^2} \otimes \boldsymbol{D}^{(0)}_{\overline{n}^1} \ . \tag{51}$$

4.3.1. Degree of freedom interpretation

The geometric interpretation of the tensor-product complex follows directly from those for the univariate multi-degree complexes; see Sections 3.2.4 and 3.2.7 . This time we consider a tensor-product partition of $[0, 1]^2$ into $n^1 \times n^2$ quadrilaterals. The zero-dimensional, horizontal and vertical one-dimensional, and two-dimensional cells of this partition will be denoted, respectively, as

$$\begin{aligned} &\gamma_{ij} \ , \quad i = 0, \dots, n^1 - 1 \ , \ j = 0, \dots, n^2 - 1 \ , \\ &\tau^1_{ij} \ , \quad i = 0, \dots, \overline{n}^1 - 1 \ , \ j = 0, \dots, n^2 - 1 \ , \\ &\tau^2_{ij} \ , \quad i = 0, \dots, n^1 - 1 \ , \ j = 0, \dots, \overline{n}^2 - 1 \ , \\ &\sigma_{ij} \ , \quad i = 0, \dots, \overline{n}^1 - 1 \ , \ j = 0, \dots, \overline{n}^2 - 1 \ . \end{aligned}$$

Then, the degrees of freedom of the 0-, 1- and 2-forms are associated to these geometric objects. We define the oriented boundaries of the edges and the faces as

$$\partial\tau^1_{ij} = \gamma_{(i+1)j} - \gamma_{ij} \ , \quad \partial\tau^2_{ij} = \gamma_{i(j+1)} - \gamma_{ij} \ ,$$
$$\partial\sigma_{ij} = \tau^1_{ij} + \tau^2_{(i+1)j} - \tau^1_{i(j+1)} - \tau^2_{ij} \ .$$

Then, the discrete exterior derivatives from Eqs. (49) and (51) help us establish discrete versions of the Stokes theorem. The action of these on the spline degrees of freedom is presented in Fig. 4. Furthermore, it can be readily checked that, for $f \in \Lambda^{(0)}_T$, Eqs. (49) and (51) imply that $d \circ df = 0$. Alternatively, this fact is implied by the duality of the discrete exterior derivatives with the boundary operator since

$$d \circ df \left(\sum_{i=0}^{n^1-1} \sum_{j=0}^{n^2-1} c_{ij}\sigma_{ij} \right) = df \left(\partial \sum_{i=0}^{n^1-1} \sum_{j=0}^{n^2-1} c_{ij}\sigma_{ij} \right) = f \left(\partial \circ \partial \sum_{i=0}^{n^1-1} \sum_{j=0}^{n^2-1} c_{ij}\sigma_{ij} \right) = 0 \ , \tag{52}$$

as the boundary of a boundary is always empty.

4.4. Mapped geometries

Let us now transfer the spaces of spline differential forms onto a domain $\hat{\Omega} \subset \mathbb{R}^{\mathfrak{d}}$, $\mathfrak{d} = 2$ or 3, obtained via a geometric mapping of Ω. In particular, sticking to the isogeometric concept, we will look at geometric mappings built using tensor-product splines in $\mathcal{S}^{(0,0)}$ and, moreover, assume that $\hat{\Omega}$ is a manifold.

For $i = 0, \dots, n^1 - 1$, $j = 0, \dots, n^2 - 1$, choose $\boldsymbol{G}_{ij} \in \mathbb{R}^{\mathfrak{d}}$. Then, consider a 2-manifold $\hat{\Omega}$ obtained as the image of Ω under the spline map $\boldsymbol{G}$ defined as

$$\begin{aligned} \mathbb{R}^2 \supset \Omega \ni \boldsymbol{x} = (x^1, x^2) \longmapsto \boldsymbol{G}(\boldsymbol{x}) &\coloneqq (G^1(\boldsymbol{x}), \dots, \ G^{\mathfrak{d}}(\boldsymbol{x})) \in \hat{\Omega} \subset \mathbb{R}^{\mathfrak{d}} \ , \\ &\coloneqq \sum_{i=0}^{n^1-1} \sum_{j=0}^{n^2-1} \boldsymbol{G}_{ij} N^1_i(x^1) N^2_j(x^2) \ . \end{aligned} \tag{53}$$

Then $\hat{\Omega}$ has local, curvilinear coordinates x^1, x^2, and global Cartesian coordinates $y^1, \dots, y^{\mathfrak{d}}$. Assuming that $\hat{\Omega}$ is a $C^{\geq 1}$ smooth manifold, the vectors $\partial^{\boldsymbol{x}}_i = \frac{\partial \boldsymbol{G}}{\partial x^i}(\boldsymbol{x})$, $i = 1, 2$, form a basis for vectors tangent to $\hat{\Omega}$ at $\boldsymbol{G}(\boldsymbol{x})$. The vectors dual to $\partial^{\boldsymbol{x}}_i$ are dx^i, $i = 1, 2$, and they form a basis for the covectors tangent to $\hat{\Omega}$ at $\boldsymbol{G}(\boldsymbol{x})$. The 0-, 1- and 2-forms on $\hat{\Omega}$ can thus be denoted as f, $f_i \, dx^i$ and $f \, dx^1 \wedge dx^2$, respectively.

Denote the associated metric tensor, its ij-th component and its matrix determinant with $\boldsymbol{g}$, g_{ij} and g, respectively, and let $\partial^{\boldsymbol{y}}_i$, $i = 1, \dots, \mathfrak{d}$, be the canonical basis vectors in $\mathbb{R}^{\mathfrak{d}}$. Then,

$$\partial^{\boldsymbol{x}}_i = \frac{\partial G^j}{\partial x^i} \partial^{\boldsymbol{y}}_j \ , \quad \boldsymbol{g} = g_{ij} dx^i \otimes dx^j \ , \quad g_{ij} = \partial^{\boldsymbol{x}}_i \cdot \partial^{\boldsymbol{x}}_j \ , \quad g \coloneqq \det[g_{ij}] \ . \tag{54}$$

The quantity $\sqrt{g}$ thus denotes the Jacobian determinant of the map $\boldsymbol{G}$.

If the map $\hat{\Omega}$ is locally invertible, then $\sqrt{g} > 0$ and the components of the inverse of the 2×2 matrix $[g_{ij}]$ are denoted as g^{ij}. Using the metric and its inverse, we can explicitly define the Hodge star $\star$ in the present setting,

$$\begin{aligned} \star f &= \sqrt{g} f \ dx^1 \wedge dx^2 \ , \\ \star f_i \ dx^i &= \sqrt{g} f_i g^{ij} \epsilon_{jk} \ dx^k \ , \\ \star f_{12} \ dx^1 \wedge dx^2 &= \frac{1}{\sqrt{g}} f \ , \end{aligned} \tag{55}$$

where ϵ_{ij} is equal to 1 for $(i, j) = (1, 2)$, equal to -1 for $(i, j) = (2, 1)$, and zero otherwise. In particular, the L^2 inner product of i-forms can be expressed as (also see Appendix F)

$$(f, g)_{\hat{\Omega}} = \int_{\hat{\Omega}} f \wedge \star g \ . \tag{56}$$

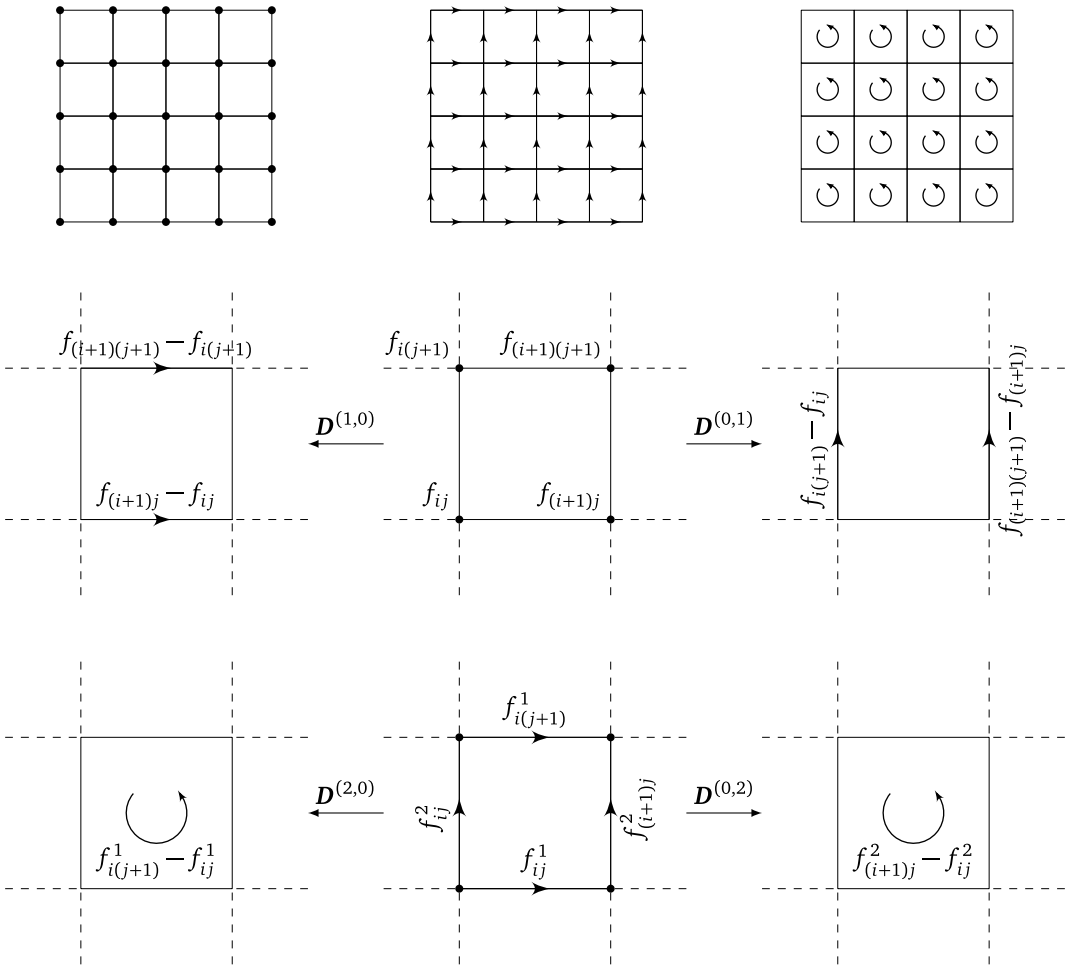

Fig. 4. The univariate degree of freedom interpretations for the multi-degree complexes directly lead to the same for the tensor-product complex $\mathfrak{T}$. The 0-, 1- and 2-forms are now associated to the vertices, edges and faces of a tensor-product cell complex, respectively; see the figures in the first row. These figures correspond to $n^1 = n^2 = 5$. Moreover, with respect to the preferred basis, the discrete exterior derivatives have $\boldsymbol{D}^{(1,0)}$, $\boldsymbol{D}^{(0,1)}$, $\boldsymbol{D}^{(2,0)}$ and $\boldsymbol{D}^{(0,2)}$ have a simple action as shown in the middle and bottom rows.

Finally, differential forms on $\hat{\Omega}$ in the canonical basis dy^i, $i = 1, \ldots, \mathfrak{d}$, can be pulled back to Ω using the map $\boldsymbol{G}^*$ as follows,

$$\begin{aligned} \boldsymbol{G}^*(f) &= f \circ \boldsymbol{G} \,, \\ \boldsymbol{G}^*\left(f_i \, dy^i\right) &= (f_i \circ \boldsymbol{G}) \, \frac{\partial G^i}{\partial x^j} \, dx^j \,, \\ \boldsymbol{G}^*\left(f_{ij} \, dy^i \wedge dy^j\right) &= \left(f_{ij} \circ \boldsymbol{G}\right) \frac{\partial G^i}{\partial x^k} \frac{\partial G^j}{\partial x^\ell} \, dx^k \wedge dx^\ell \,. \end{aligned} \tag{57}$$

The map $\boldsymbol{G}^*$ is called the pullback and it commutes with both the wedge product and the exterior derivative. Moreover, using it, we can perform integration of an i-form on an i-dimensional geometry $\boldsymbol{G}\left(\overline{\Omega}\right)$ as

$$\int_{\boldsymbol{G}(\overline{\Omega})} f = \int_{\overline{\Omega}} \boldsymbol{G}^*(f) \,. \tag{58}$$

(a) Type 1: Single polar singularity

(b) Type 2: Double polar singularity

Fig. 5. A single edge or a pair of opposite edges of a tensor-product spline patch can be collapsed for creating geometries with polar singularities. We will refer to the two modes of collapse as Type 1 and Type 2, respectively. The collapsed edges here are shown in red, and the black edges are identified with each other to enforce periodicity.

Using the pullback, we also define the spaces of spline differential forms on $\hat{\Omega}$ as

$$\hat{\Lambda}_T^{(i)} := \left\{ f \ : \ \boldsymbol{G}^*(f) \in \Lambda_T^{(i)} \right\} , \quad i = 0, 1, 2 , \tag{59}$$

and the corresponding spline complex on $\hat{\Omega}$ is defined as

$$\hat{\mathfrak{T}} \ : \ \hat{\Lambda}_T^{(0)} \longrightarrow \hat{\Lambda}_T^{(1)} \longrightarrow \hat{\Lambda}_T^{(2)} .$$

The pullback commutes with the exterior derivative and, thus, forms a cochain map from the complex $\hat{\mathfrak{T}}$ to $\mathfrak{T}$.

5. The polar spline complex

In this section, we build a spline complex on geometries $\hat{\Omega}$ that are obtained via a map $\boldsymbol{G}$ that collapses one or two edges of Ω to one or two points, respectively, in $\mathbb{R}^{\mathfrak{d}}$; see Fig. 5. These collapsed edges are called *polar singularities* or *poles*. Fig. 6 presents a topological representations of the tensor-product degree-of-freedom complexes following the introduction of polar singularities.

In general, the presence of poles means that $\hat{\Omega}$ will not be a $C^{\geq 1}$ smooth 2-manifold. However, by restricting each component of $\boldsymbol{G}$ to be a member of a suitable subspace of $\mathcal{S}^{(0,0)}$, we will be able to ensure smoothness of $\hat{\Omega}$. In Section 5.1, we build such a suitable subspace and use it to define smooth $\hat{\Omega}$; the splines in the former will be called *polar splines*. Thereafter, in Section 5.2, we build spaces of polar spline differential forms on $\hat{\Omega}$ and use them to define the polar spline complex in Section 5.3.

Assumption 4: Tensor-product configuration for building polar splines

With $\Omega = \Omega^1 \times \Omega^2$, the endpoints of Ω^1 have been identified. The univariate spline spaces $\mathcal{S}^1$ and $\mathcal{S}^2$ on Ω^1 and Ω^2 are periodic and non-periodic, respectively, and they are used to define all tensor-product spline spaces on Ω using Eqs. (43)–(46). Moreover,

- with $\boldsymbol{r}^i$ the smoothness vector used to define $\mathcal{S}^i$, $i = 1, 2$,

$$r_k^1 \geq 1 \ , \ k = 0, \dots, m^1 \ ,$$
$$r_k^2 \geq 1 \ , \ k = 1, \dots, m^2 - 1 \ ;$$

- the dimension $\mathcal{S}^2$ is at least 5, i.e., $n^2 \geq 5$.

5.1. C^1 smooth polar B-splines

Thanks to the end-point interpolation and partition of unity properties of MDB-splines (see Proposition 3.4(d)), the required edge collapse shown in Fig. 5 can be achieved by choosing in Eq. (53)

$$\boldsymbol{G}_{00} = \boldsymbol{G}_{10} = \cdots = \boldsymbol{G}_{(n^1-1)0} \iff \forall x^1 \in \Omega^1, \quad \boldsymbol{G}(x^1, a^2) = \boldsymbol{G}_{00} \ ; \tag{60}$$

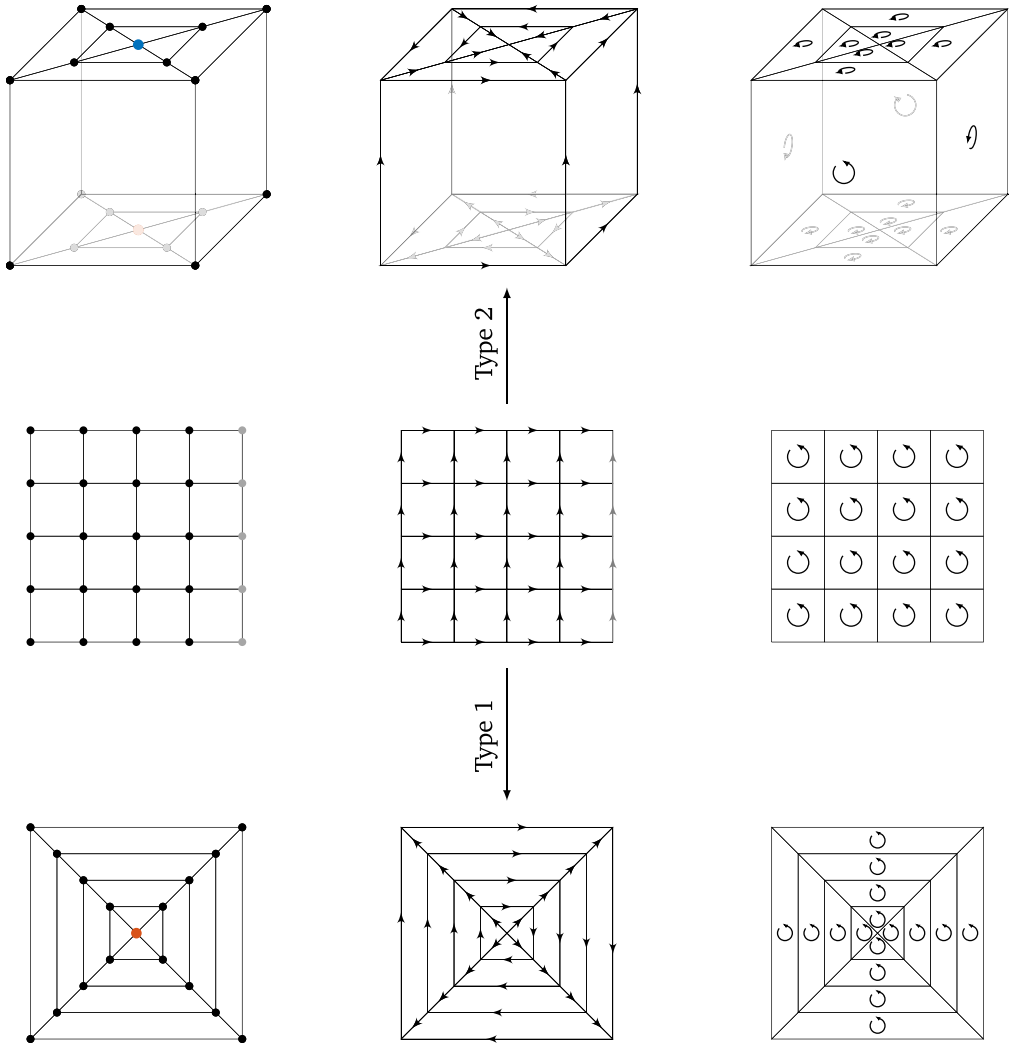

Fig. 6. This figure demonstrates how the tensor-product degree-of-freedom complex from Fig. 4 changes following Type 1 and Type 2 collapses from Fig. 5; also see Eqs. (60) and (61). The middle row shows the tensor-product complex for $(n^1, n^2) = (4, 5)$. The rightmost vertex and vertical edge degrees of freedom have been plotted in grey to indicate that periodicity in the first parametric direction has been imposed; see Assumption 4. The bottom row shows the tensor-product complex following Type 1 collapse, while the top row shows the tensor-product complex following Type 2 collapse.

$$\boldsymbol{G}_{0(n^2-1)} = \boldsymbol{G}_{1(n^2-1)} = \cdots = \boldsymbol{G}_{(n^1-1)(n^2-1)} \iff \forall x^1 \in \Omega^1, \quad \boldsymbol{G}(x^1, b^2) = \boldsymbol{G}_{0(n^2-1)} \,. \tag{61}$$

However, in general, this coefficient coalescing will introduce kinks at the poles and the surface representation will not be smooth. Nevertheless, it is possible to identify constraints on the remaining $\boldsymbol{G}_{ij}$ that ensure that $\hat{\Omega}$ is a C^1 smooth 2-manifold or, equivalently, such that it has a well-defined tangent plane at all points. Such constraints were identified in [29] for C^k smoothness, but for simplicity we restrict to the case of C^1 smoothness. In this section, we present the relevant constraints and their resolution. The discussion will be abbreviated and focused on practical considerations since the theory has already been elaborately addressed in [29] and, more recently, [32].

A polar surface will be smooth at a polar point if it can be locally (re)parametrized in a smooth way. Such parametrizations can be specified in a constructive manner and, for C^1 smoothness, they impose simple geometric constraints on the choice of the $\boldsymbol{G}_{ij}$ [29, Section 3.3]; these are presented in the following result.

Proposition 5.1 (C^1 *Smoothness at the Poles*)**.**

(a) For the edge-collapse in Eq. (60), $\hat{\Omega}$ has a well-defined tangent plane at $\boldsymbol{G}_{00}$ if

(i) the points $\boldsymbol{G}_{ij}$, $i = 0, \ldots, n^1 - 1$, $j = 0, 1$, are all coplanar;
(ii) the vectors $\boldsymbol{G}_{i1} - \boldsymbol{G}_{i0}$, $i = 0, \ldots, n^1 - 1$, are all distinct, non-zero, and form a clockwise or counter-clockwise fan around $\boldsymbol{G}_{00}$.

The tangent plane at $\boldsymbol{G}_{00}$ is then spanned by $\boldsymbol{G}_{01} - \boldsymbol{G}_{00}$ and $\boldsymbol{G}_{11} - \boldsymbol{G}_{10}$.

(b) For the edge-collapse in Eq. (61), $\hat{\Omega}$ has a well-defined tangent plane at $\boldsymbol{G}_{0(n^2-1)}$ if

(i) the points $\boldsymbol{G}_{ij}$, $i = 0, \ldots, n^1 - 1$, $j = n^2 - 2, n^2 - 1$, are all coplanar;
(ii) the vectors $\boldsymbol{G}_{i(n^2-1)} - \boldsymbol{G}_{i(n^2-2)}$, $i = 0, \ldots, n^1 - 1$, all distinct, non-zero, and form a clockwise or counter-clockwise fan around $\boldsymbol{G}_{0(n^2-1)}$.

The tangent plane at $\boldsymbol{G}_{0(n^2-1)}$ is then spanned by $\boldsymbol{G}_{0(n^2-1)} - \boldsymbol{G}_{0(n^2-2)}$ and $\boldsymbol{G}_{1(n^2-1)} - \boldsymbol{G}_{1(n^2-2)}$.

In particular, assigning Ω a counter-clockwise orientation, $\boldsymbol{G}$ preserves the orientation in a neighbourhood of the poles if the fans in (a) and (b) above are clockwise and counter-clockwise, respectively.

Proof. See [Section 3.3][29]. ■

Depending on Type 1 or Type 2 edge collapse (see Fig. 5), we would want the satisfaction of either the conditions in Proposition 5.1(a), or those in both Proposition 5.1(a) and (b), respectively. Then, [29] suggest the following simple way of satisfying the above smoothness constraints at the poles. Choose triangles $\triangle^1$ and $\triangle^2$ with vertices $\{\boldsymbol{v}_i^1 \in \mathbb{R}^\mathfrak{d}\}_{i=1}^3$ and $\{\boldsymbol{v}_i^2 \in \mathbb{R}^\mathfrak{d}\}_{i=1}^3$, respectively. Next, require the following relations to hold,

$$\text{Proposition 5.1(a)}: \quad \boldsymbol{G}_{ij} = \sum_{k=1}^{3} \chi_{ij}^{k,1} \boldsymbol{v}_k^1 , \quad \sum_{k=1}^{3} \chi_{ij}^{k,1} = 1 , \quad i = 0, \ldots, n^1 - 1 , \ j = 0, 1 , \tag{62}$$

$$\text{Proposition 5.1(b)}: \quad \boldsymbol{G}_{ij} = \sum_{k=1}^{3} \chi_{ij}^{k,2} \boldsymbol{v}_k^2 , \quad \sum_{k=1}^{3} \chi_{ij}^{k,2} = 1 , \quad i = 0, \ldots, n^1 - 1 , \ j = n^2 - 2, n^2 - 1 . \tag{63}$$

In other words, with regard to Proposition 5.1(a) (respectively, Proposition 5.1(b)), we force $\boldsymbol{G}_{ij}$ to lie in the plane of $\triangle^1$ (respectively, $\triangle^1$), and the numbers $\chi_{ij}^{k,1}$ (respectively, $\chi_{ij}^{k,2}$), $k = 1, 2, 3$, are its corresponding barycentric coordinates. We will call $\triangle^1$ and $\triangle^2$ the domain triangles for the above sets of $\boldsymbol{G}_{ij}$.

Next, conditions *(ii)* of both Proposition 5.1(a) and (b) can be satisfied equally easily by choosing the barycentric coordinates as follows. Define $\theta_i \in (0, 2\pi)$ as

$$\theta_i := 2\pi - \frac{(1 + 2i)\pi}{n^1} . \tag{64}$$

Next, compute the required barycentric coordinates using the following two equations for $i = 0, \ldots, n^1 - 1$,

$$\chi_{i0}^{j,1} = \chi_{i(n^2-1)}^{j,2} = \frac{1}{3} , \quad j = 1, 2, 3 , \tag{65}$$

$$\begin{bmatrix} \chi_{i1}^{1,1} \\ \chi_{i1}^{2,1} \\ \chi_{i1}^{3,1} \end{bmatrix} = \begin{bmatrix} \chi_{(n^1-1-i)(n^2-2)}^{1,2} \\ \chi_{(n^1-1-i)(n^2-2)}^{2,2} \\ \chi_{(n^1-1-i)(n^2-2)}^{3,2} \end{bmatrix} = \begin{bmatrix} \frac{1}{3} & 0 & \frac{1}{3} \\ -\frac{1}{6} & \frac{\sqrt{3}}{6} & \frac{1}{3} \\ -\frac{1}{6} & -\frac{\sqrt{3}}{6} & \frac{1}{3} \end{bmatrix} \begin{bmatrix} \cos(\theta_i) \\ \sin(\theta_i) \\ 1 \end{bmatrix} . \tag{66}$$

Lemma 5.2. *All $\chi_{ij}^{k,1}$ and $\chi_{ij}^{k,2}$, as specified by Eqs. (65) and (66), are non-negative. Moreover, the corresponding $\boldsymbol{G}_{ij}$ defined as in Eqs. (62) and (63) satisfy the conditions of Proposition 5.1(a) and (b), respectively.*

Proof. As explained in [29], Eqs. (65) and (66) implicitly impose that the $\boldsymbol{G}_{ij}$ are uniformly distributed on circles centred at the poles and, moreover, that these circles are contained within the domain triangles. Therefore, the barycentric coordinates are all non-negative. ■

Therefore, depending on Type K collapse, $K = 1, 2$, the number of coefficients needed to define the tensor-product coefficients is equal to n^{pol},

$$n^{\text{pol}} := n^{(0,0)} - K(2n^1 - 3) . \tag{67}$$

Doing so, and recalling Eq. (43), let us define the *polar extraction* $\boldsymbol{E}^{\text{pol}}$ of size $n^{\text{pol}} \times n^{(0,0)}$ as

$$\boldsymbol{E}^{\text{pol}} := \begin{bmatrix} \boldsymbol{E}^1 & & \\ & \boldsymbol{I}_{n^{\text{pol}}-6} & \\ & & \boldsymbol{E}^2 \end{bmatrix} , \tag{68}$$

where $\boldsymbol{E}^1$ and $\boldsymbol{E}^2$ are defined as

$$\boldsymbol{E}^k := \begin{cases} \begin{bmatrix} \chi_{0j}^{1,k} & \cdots & \chi_{(n^1-1)j}^{1,k} & \chi_{0(j+1)}^{1,k} & \cdots & \chi_{(n^1-1)(j+1)}^{1,k} \\ \chi_{0j}^{2,k} & \cdots & \chi_{(n^1-1)j}^{2,k} & \chi_{0(j+1)}^{2,k} & \cdots & \chi_{(n^1-1)(j+1)}^{2,k} \\ \chi_{0j}^{3,k} & \cdots & \chi_{(n^1-1)j}^{3,k} & \chi_{0(j+1)}^{3,k} & \cdots & \chi_{(n^1-1)(j+1)}^{3,k} \end{bmatrix} , & (j,k) = (0,1) \text{ and Type 1 or Type 2} \\ & \text{or} \\ & (j,k) \in \{(1,1), (n^2-2,2)\} \text{ and Type 2} \\ \boldsymbol{I}_3 , & \text{otherwise} . \end{cases} , \tag{69}$$

Proposition 5.3 (*Polar Extraction Properties*)**.**

(a) Non-negativity: All entries of $\boldsymbol{E}^{pol}$ *lie in* $[0, 1]$.
(b) Column stochasticity: All columns of $\boldsymbol{E}^{pol}$ *sum to* 1.
(c) Non-degeneracy: The matrix $\boldsymbol{E}^{pol}$ *has full rank.*

Proof. The properties follow from Lemma 5.2 and the definition of the extraction operator via Eqs. (68) and (69). ■

The properties of the polar extraction helps us define *polar B-splines*, N_i^{pol}, $i = 0, \ldots, n^{\text{pol}} - 1$, as linear combinations of tensor product B-splines that span $\mathcal{S}^{(0,0)}$. More precisely, we define

$$\boldsymbol{N}^{\text{pol}} := \boldsymbol{E}^{\text{pol}} \boldsymbol{N}^{(0,0)} , \tag{70}$$

where $\boldsymbol{N}^{\text{pol}}$ is a vector containing the polar B-splines N_i^{pol}. Consequently, we define $\mathcal{S}^{\text{pol}}$ as the space spanned by the polar B-splines,

$$\mathcal{S}^{\text{pol}} := \text{span}\left\langle N_i^{\text{pol}} \ : \ i = 0, \ldots, n^{\text{pol}} - 1 \right\rangle . \tag{71}$$

The following result summarizes their relevant properties; see [29, Proposition 3.1 and 3.2].

Corollary 5.4 (*Select Polar B-spline Properties*)**.**

(a) Non-negativity: $N_i^{pol}(\boldsymbol{x}) \geq 0$ *for all* $\boldsymbol{x} \in \Omega$.
(b) Partition of unity: $\sum_{i=0}^{n^{pol}-1} N_i^{pol}(\boldsymbol{x}) = 1$ *for all* $\boldsymbol{x} \in \Omega$.
(c) Basis: $\{N_i^{pol} : i = 0, \ldots, n^{pol} - 1\}$ *are linearly independent and thus form a basis for* $\mathcal{S}^{pol}$.

Proof. The properties are a direct consequence of Proposition 5.3. ■

With $\boldsymbol{G}_i^{\text{pol}} \in \mathbb{R}^{\mathfrak{d}}$, $i = 0, \ldots, n^{\text{pol}} - 1$, let $\hat{\Omega}$ be obtained via the geometric map $\boldsymbol{G}^{\text{pol}}$ defined as

$$\mathbb{R}^2 \supset \Omega \ni \boldsymbol{x} = (x^1, x^2) \longmapsto \boldsymbol{G}^{\text{pol}}(\boldsymbol{x}) := \sum_{i=0}^{n^{\text{pol}}-1} \boldsymbol{G}_i^{\text{pol}} N_i^{\text{pol}}(\boldsymbol{x}) \in \hat{\Omega} . \tag{72}$$

Then, the following result holds.

Proposition 5.5 (*Smoothness of Polar B-splines*)**.** *The image of* $\boldsymbol{G}^{pol}$, $\hat{\Omega}$, *is a smooth 2-manifold. Moreover, the functions* $\{\hat{N}_i^{pol} : \hat{N}_i^{pol} \circ \boldsymbol{G}^{pol} = N_i^{pol}\}$ *are* C^1 *smooth on* $\hat{\Omega}$.

Proof. The smoothness of $\hat{\Omega}$ is only suspect at the poles. However, the claim follows from Proposition 5.1, Eqs. (62), (63), (68) and (70). Indeed, for $\boldsymbol{G}_{ij}$, $i = 0, \ldots, n^1 - 1$, $j = 0, \ldots, n^2 - 1$, and $\ell = i + jn^1$, define $\boldsymbol{G}_{ij}$

as

$$\boldsymbol{G}_{ij} \coloneqq \sum_{k=0}^{n^{\text{pol}}-1} E^{\text{pol}}_{k\ell} \boldsymbol{G}^{\text{pol}}_{k} \,, \tag{73}$$

where $E^{\text{pol}}_{k\ell}$ is the $k\ell$-th entry of $\boldsymbol{E}^{\text{pol}}$. Then, it is clear that $\boldsymbol{G}_{ij}$ satisfy the constraints of Proposition 5.1. The smoothness of the pushforwards of polar B-spline functions was shown in [29] and we omit the proof here for brevity. ■

5.2. Basis for discrete differential forms

Let us now describe the construction of polar spline discrete differential forms that are built with $\mathcal{S}^{\text{pol}}$ chosen as the space of 0-forms. First, let us describe the motivation behind, and an overview of, our construction.

5.2.1. Motivation for the construction

The motivation for the construction presented herein is derived from the relations for mapped geometries presented in Section 4.4. In particular, the introduction of edge-collapses implies that $\sqrt{g} = 0$ at the poles. This implies that, in general, spline differential forms will not be bounded in a neighbourhood of the poles; e.g., see Eq. (55). Equipped with the C^1 smooth polar B-splines as 0-forms, we counteract this singular behaviour by imposing "local exactness" for all 1- and 2-forms in a neighbourhood of the poles. That is, in the vicinity of the poles, spline differential k-forms, $k = 1, 2$, will be restricted to be exact. Then, at the poles, C^1 smoothness of the 0-forms automatically translates to C^0 and C^{-1} smoothness of the 1- and 2-forms and, moreover, avoids the blowup. Note that, away from the poles, all differential forms are going to have the same smoothness as their tensor-product counterparts.

Following the above motivation, and by the construction of the 0-form polar splines as in Eq. (70), we now present polar analogues of the tensor-product cell complexes from Fig. 4. These are shown in Fig. 7; c.f. Fig. 6. Note the following about the polar degree-of-freedom complex in the top and bottom rows.

- There are three degrees of freedom for polar 0-forms near the poles.
- Imposing local exactness of polar 1-forms at the poles, there are two degrees of freedom for them near the poles.
- Imposing local exactness of polar 2-forms at the poles, and from the above bullet, there are no degrees of freedom for them near the poles.

Next, let us explain the different vertical and horizontal maps in Fig. 7. The left-most column of the figure corresponds to Eq. (73), i.e., the vertical maps in that column send degrees of freedom for polar 0-forms to those for tensor-product 0-forms. The horizontal maps in the middle row have been defined in Eqs. (49) and (51). It remains to define the remaining vertical (i.e., from polar degrees of freedom to tensor-product degrees of freedom) and horizontal maps (i.e., discrete exterior derivatives that act on polar degrees of freedom). The transposes of the vertical maps will help specify the basis functions for polar 1- and 2-forms as linear combinations of those for tensor-product 1- and 2-forms, respectively, similarly to Eq. (70) for polar 0-forms.

A concrete discussion in the following subsections requires a numbering of the degrees of freedom for 0-, 1- and 2-forms in the Type 1 and Type 2 polar complexes from Fig. 7; these numberings are then shared by the basis functions for polar 0-, 1- and 2-forms, respectively. The total number of degrees of freedom associated to 0-, 1- and 2-forms can be found using Eqs. (43)–(46). Observing that Assumption 4 implies $\overline{n}^1 = n^1$, the number of degrees of freedom are computed as below for Type K collapse, $K = 1, 2$,

$$n^{(0),\text{pol}} \coloneqq n^{\text{pol}} = n^{(0,0)} - K(2n^1 - 3) \,, \tag{74}$$

$$n^{(1),\text{pol}} \coloneqq n^{(1,0)} + n^{(0,1)} - K(3n^1 - 2) \,, \tag{75}$$

$$n^{(2),\text{pol}} \coloneqq n^{(1,1)} - Kn^1 \,. \tag{76}$$

The degrees of freedom are numbered using the scheme shown in Fig. 8.

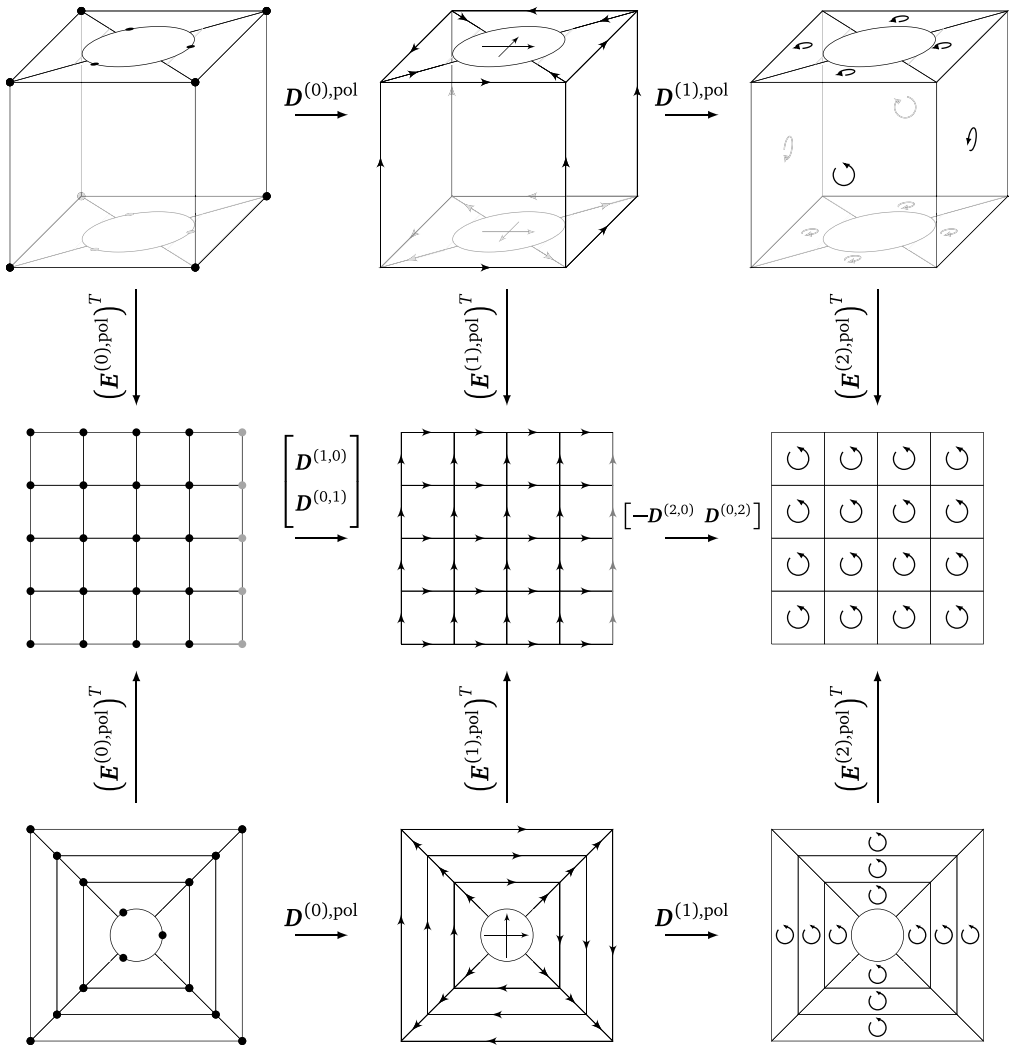

Fig. 7. This figure demonstrates the Type 1 (bottom row) and Type 2 (top row) polar degree-of-freedom complexes corresponding to the basis function construction in Section 5.2, and their relation to the tensor-product degree-of-freedom complex (middle row); all diagrams correspond to $(n^1, n^2) = (4, 5)$. With $\boldsymbol{E}^{(0,0),\text{pol}} := \boldsymbol{E}^{\text{pol}}$ from Eq. (68), the degrees of freedom for polar 0-forms can be related to the tensor-product degrees of freedom via Eq. (73), thus defining the left-most vertical maps in the above figure. Section 5.2 presents the construction of polar discrete exterior derivatives $\boldsymbol{D}^{(0),\text{pol}}$ and $\boldsymbol{D}^{(1),\text{pol}}$, and the corresponding polar extraction operators $\boldsymbol{E}^{(1),\text{pol}}$ and $\boldsymbol{E}^{(2),\text{pol}}$ such that both the top-two and bottom-two rows form commutative diagrams. The latter polar extraction operators specify the basis for polar 1- and 2-forms as suitable linear combinations of the tensor-product 1- and 2-form basis functions. (Note that, to simplify the notation, we use the same symbols to denote the extractions and discrete exterior derivatives for Type 1 and Type 2 polar complexes.).

5.2.2. *Polar* 0*-forms*

Define $\mathcal{S}^{(0),\text{pol}} := \mathcal{S}^{\text{pol}}$ and $\boldsymbol{E}^{(0),\text{pol}} := \boldsymbol{E}^{\text{pol}}$. Then, using Eq. (70) and for any $f \in \mathcal{S}^{(0),\text{pol}}$,

$$f = \sum_{i=0}^{n^{\text{pol}}-1} f_i N_i^{\text{pol}} = \boldsymbol{f} \cdot \boldsymbol{N}^{\text{pol}} = \boldsymbol{f} \cdot \boldsymbol{E}^{\text{pol}} \boldsymbol{N}^{(0,0)} \,.$$

where $\boldsymbol{f}$ is a vector containing all coefficients f_i.

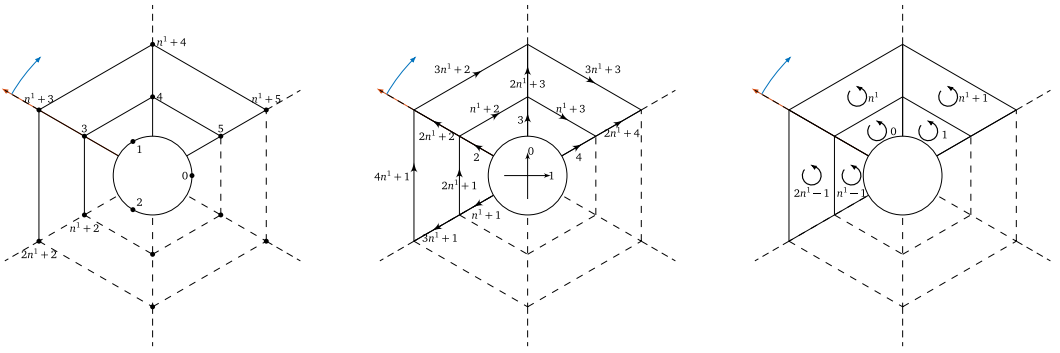

(a) Numbering near the bottom pole

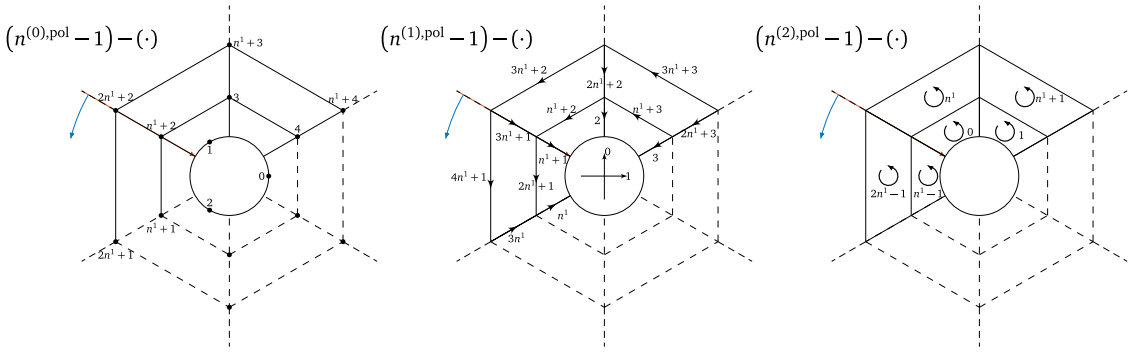

(b) Numbering near the top pole

Fig. 8. The above figures show the degree-of-freedom indexing scheme adopted near the bottom and top poles — figures (a) and (b), respectively. Except the degrees of freedom associated to the poles, the numbering increases first in the direction of the blue arrow, and then along the red arrow. Furthermore, note that the indices in figure (b) are obtained by subtracting the labels from $n^{(0),\text{pol}}-1$ for 0-forms, from $n^{(1),\text{pol}}-1$ for 1-forms, and from $n^{(2),\text{pol}}-1$ for 2-forms. Also, keeping Fig. 7 in mind, the numbering near the top pole (which is applicable only for Type 2 collapse) assumes that we are looking down at the pole from above the degree-of-freedom complex.

5.2.3. *Polar* 1*-forms*

Let $f \in \mathcal{S}^{(0),\text{pol}}$ and apply the exterior derivative to it. Then, using Eq. (48),

$$\begin{aligned} g \coloneqq df &= d\left(\boldsymbol{f}\cdot\boldsymbol{E}^{\text{pol}}\boldsymbol{N}^{(0,0)}\right) , \\ &= \boldsymbol{N}^{(1,0)}\cdot\boldsymbol{D}^{(1,0)}\left(\boldsymbol{E}^{\text{pol}}\right)^{T}\boldsymbol{f}\,dx^1 + \boldsymbol{N}^{(0,1)}\cdot\boldsymbol{D}^{(0,1)}\left(\boldsymbol{E}^{\text{pol}}\right)^{T}\boldsymbol{f}\,dx^2 . \end{aligned} \tag{77}$$

Then, with reference to Fig. 9, let us define two maps $\boldsymbol{D}^{(0),\text{pol}}$ and $\boldsymbol{E}^{(1),\text{pol}}$. We do so by defining their actions on the degrees of freedom, considering both regions away from the poles and near the poles.

- Fig. 9(a): Far away from the poles, the degree-of-freedom complexes locally look like their tensor-product counterparts, i.e., the topology is that of a structured quadrilateral grid; c.f. Figs. 4, 6, 7 and 8. This is the case shown in this figure where the degrees of freedom $f_{i_1},\ldots,f_{i_4}$ for a polar 0-form lie on the vertices of a quadrilateral. Eq. (73) maps these degrees of freedom to their tensor-product counterparts via the identity map. Then, we define the action of the maps $\boldsymbol{D}^{(0),\text{pol}}$ and the transpose of $\boldsymbol{E}^{(1),\text{pol}}$ via the following equations,

$$\underbrace{\begin{aligned} f_{k\ell} &= f_{i_1} , \\ f_{(k+1)\ell} &= f_{i_2} , \\ f_{k(\ell+1)} &= f_{i_3} , \\ f_{(k+1)(\ell+1)} &= f_{i_4} . \end{aligned}}_{\left(\boldsymbol{E}^{(0),\text{pol}}\right)^{T}} \Rightarrow \underbrace{\begin{aligned} g_{j_1} &\coloneqq f_{i_2} - f_{i_1} , \\ g_{j_2} &\coloneqq f_{i_4} - f_{i_3} , \\ g_{j_3} &\coloneqq f_{i_3} - f_{i_1} , \\ g_{j_4} &\coloneqq f_{i_4} - f_{i_2} ; \end{aligned}}_{\boldsymbol{D}^{(0),\text{pol}}} \quad \underbrace{\begin{aligned} g^1_{k\ell} &\coloneqq g_{j_1} , \\ g^2_{k\ell} &\coloneqq g_{j_3} , \\ g^1_{k(\ell+1)} &\coloneqq g_{j_2} , \\ g^2_{(k+1)\ell} &\coloneqq g_{j_4} . \end{aligned}}_{\left(\boldsymbol{E}^{(1),\text{pol}}\right)^{T}} \tag{78}$$

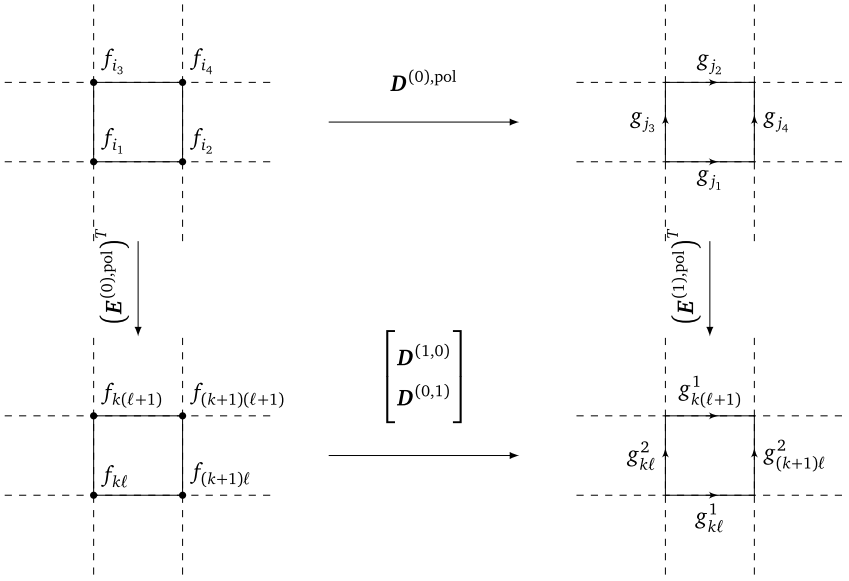

(a) Away from a pole

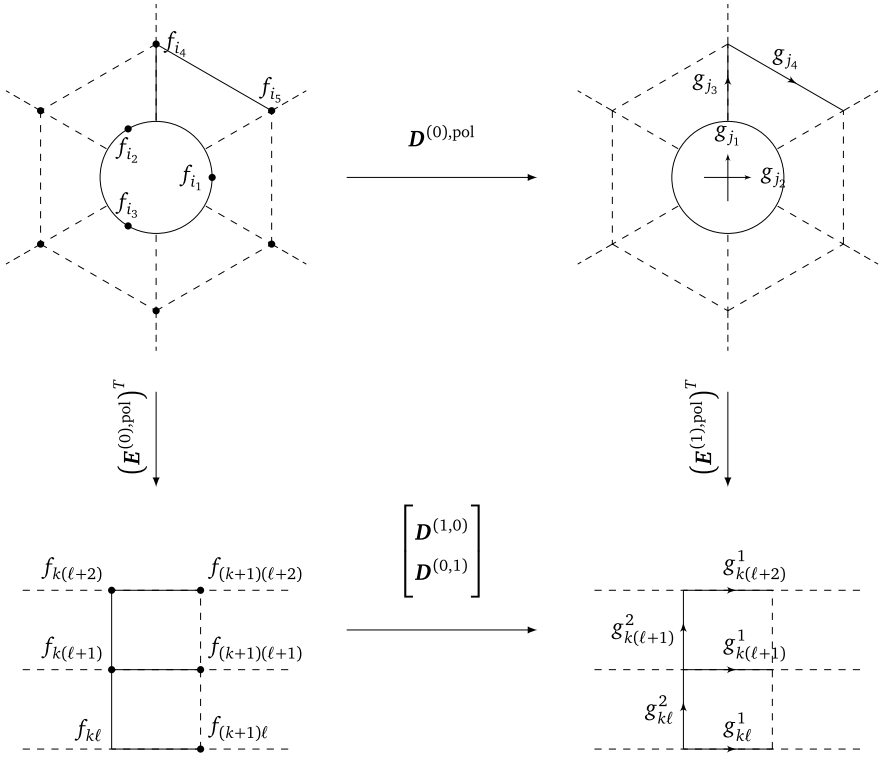

(b) In the vicinity of a pole

Fig. 9. Eqs. (78), (84) and (100), in conjunction with the above figures, help define the polar discrete exterior derivative $\boldsymbol{D}^{(0),\mathrm{pol}}$ and the polar extraction operator $\boldsymbol{E}^{(1),\mathrm{pol}}$. Figure (a) considers the case when the degrees of freedom are far away from a pole; in this case the polar degree of freedom complexes have the same topology as their tensor-product counterparts. Figure (b) instead considers the case when the degrees of freedom are in the vicinity of a pole. As Proposition 5.6 shows, the diagrams in (a) and (b) commute.

The relations between the different subscripts is easily deciphered from Eq. (73) and the degree-of-freedom numbering shown in Fig. 8. More precisely, fixing k, ℓ, Fig. 8 implies the following relations between them,

$$i_1 = k + \ell n^1 + 3\,, \quad i_2 = 3 + (\ell - 1)n^1 + [k+1 \mod n^1]\,, \quad i_3 = i_1 + n^1\,, \quad i_4 = i_2 + n^1\,, \tag{79}$$

$$j_1 = k + (2\ell - 3)\, n^1 + 2\,, \quad j_2 = j_1 + 2n^1\,, \quad j_3 = j_1 + n^1\,, \quad j_4 = j_3 + [k+1 \mod n^1] - [k \mod n^1]\,. \tag{80}$$

In the above, k, ℓ can be any values from the following ranges for Type K, $K = 1, 2$, collapse,

$$k \in \{0, 1, \ldots, n^1 - 1\}\,, \quad \ell \in \{2, \ldots, n^2 - 2K\}\,. \tag{81}$$

- Fig. 9(b): Consider the degrees of freedom $f_{i_1}, \ldots, f_{i_5}$ for a polar 0-form. Then, the relations between the indices depend on whether the pole is the bottom one or the top one.
Bottom pole: Assuming that the pole is the bottom one, let us define the actions of $\boldsymbol{D}^{(0),\mathrm{pol}}$ and the transpose of $\boldsymbol{E}^{(1),\mathrm{pol}}$. Given k, ℓ, the following relations between the different indices hold from Fig. 8(a),

$$i_1 = 0\,, \quad i_2 = 1\,, \quad i_3 = 2\,, \quad i_4 = k + 3\,, \quad i_5 = \big[k+1 \mod n^1\big] + 3\,, \tag{82}$$

$$j_1 = 0\,, \quad j_2 = 1\,, \quad j_3 = k + 2\,, \quad j_4 = j_3 + n^1\,. \tag{83}$$

Here, $\ell = 0$ and $k \in \{0, \ldots, n^1\}$. Recall Eq. (73) that helps map degrees of freedom for a polar 0-form onto those for a tensor-product 0-form. Using that map, we define the actions of $\boldsymbol{D}^{(0),\mathrm{pol}}$ and the transpose of $\boldsymbol{E}^{(1),\mathrm{pol}}$ as below,

$$\underbrace{\begin{aligned} &f_{k\ell} = f_{(k+1)\ell} = \textstyle\sum_{s=1}^{3} \frac{f_{i_s}}{3}\,, \\ &f_{k(\ell+1)} = \textstyle\sum_{s=1}^{3} \chi^{s,1}_{k(\ell+1)} f_{i_s}\,, \\ &f_{(k+1)(\ell+1)} = \textstyle\sum_{s=1}^{3} \chi^{s,1}_{(k+1)(\ell+1)} f_{i_s}\,, \\ &f_{k(\ell+2)} = f_{i_4}\,, \\ &f_{(k+1)(\ell+2)} = f_{i_5}\,. \end{aligned}}_{(\boldsymbol{E}^{(0),\mathrm{pol}})^T} \Rightarrow \underbrace{\begin{aligned} &g_{j_1} \coloneqq f_{i_2} - f_{i_1}\,, \\ &g_{j_2} \coloneqq f_{i_3} - f_{i_1}\,, \\ &g_{j_4} \coloneqq f_{i_5} - f_{i_4}\,, \\ &g_{j_3} \coloneqq f_{i_4} - \textstyle\sum_{s=1}^{3} \chi^{s,1}_{k(\ell+1)} f_{i_s}\,; \end{aligned}}_{\boldsymbol{D}^{(0),\mathrm{pol}}} \underbrace{\begin{aligned} &g^1_{k\ell} \coloneqq 0\,, \\ &g^2_{k\ell} \coloneqq \textstyle\sum_{s=1}^{2} (\chi^{s+1,1}_{k(\ell+1)} - \chi^{s+1,1}_{k\ell}) g_{j_s}\,, \\ &g^1_{k(\ell+1)} \coloneqq \textstyle\sum_{s=1}^{2} (\chi^{s+1,1}_{(k+1)(\ell+1)} - \chi^{s+1}_{k(\ell+1)}) g_{j_s}\,, \\ &g^2_{k(\ell+1)} \coloneqq g_{j_3}\,, \\ &g^1_{k(\ell+2)} \coloneqq g_{j_4}\,. \end{aligned}}_{(\boldsymbol{E}^{(1),\mathrm{pol}})^T} \tag{84}$$

Top pole: For the case of the top pole, the above relations can be analogously defined by suitable index-relabelling; we present them here for completeness. Firstly, the following relations between the indices hold from Fig. 8(b),

$$i_1 = n^{(0),\mathrm{pol}} - 3\,, \quad i_2 = i_1 + 1\,, \quad i_3 = i_2 + 1\,, \quad i_4 = i_1 + [k+1 \mod n^1] - n^1\,, \quad i_5 = i_1 + k - n^1\,, \tag{85}$$

$$j_1 = n^{(1),\mathrm{pol}} - 1\,, \quad j_2 = j_1 - 1\,, \quad j_3 = j_2 + [k+1 \mod n^1] - n^1\,, \quad j_4 = j_3 - n^1 - 1\,. \tag{86}$$

Here, $\ell = n^2 - 3$ and $k \in \{0, \ldots, n^1\}$. It is important to note here that, compared to Fig. 8(b), the edges associated to the degrees of freedom g_{j_3} and g_{j_4} are oppositely oriented. Since Fig. 8 provides a simple and global way of assigning orientations, with regards to the global operator definitions we are actually interested in the degrees of freedom $\overline{g}_{j_3}$ and $\overline{g}_{j_4}$,

$$\overline{g}_{j_3} \coloneqq -g_{j_3}\,, \quad \overline{g}_{j_4} \coloneqq -g_{j_4}\,. \tag{87}$$

Then, using Eq. (73), we define the actions of $\boldsymbol{D}^{(0),\text{pol}}$ and the transpose of $\boldsymbol{E}^{(1),\text{pol}}$ as below,

$$\underbrace{\begin{aligned} &f_{k(\ell+2)} = f_{(k+1)(\ell+2)} = \textstyle\sum_{s=1}^{3} \frac{f_{i_s}}{3} \ , \\ &f_{k(\ell+1)} = \textstyle\sum_{s=1}^{3} \chi^{s,2}_{k(\ell+1)} f_{i_s} \ , \\ &f_{(k+1)(\ell+1)} = \textstyle\sum_{s=1}^{3} \chi^{s,2}_{(k+1)(\ell+1)} f_{i_s} \ , \\ &f_{k\ell} = f_{i_5} \ , \\ &f_{(k+1)\ell} = f_{i_4} \ . \end{aligned}}_{(\boldsymbol{E}^{(0),\text{pol}})^T} \Rightarrow \underbrace{\begin{aligned} &g_{j_1} \coloneqq f_{i_2} - f_{i_1} \ , \\ &g_{j_2} \coloneqq f_{i_3} - f_{i_1} \ , \\ &\overline{g}_{j_4} \coloneqq f_{i_4} - f_{i_5} \ , \\ &\overline{g}_{j_3} \coloneqq \textstyle\sum_{s=1}^{3} \chi^{s,2}_{(k+1)(\ell+1)} f_{i_s} - f_{i_4} \ ; \end{aligned}}_{\boldsymbol{D}^{(0),\text{pol}}} \quad \underbrace{\begin{aligned} &g^1_{k(\ell+2)} \coloneqq 0 \ , \\ &g^2_{(k+1)(\ell+1)} \coloneqq \textstyle\sum_{s=1}^{2} (\chi^{s+1,2}_{k(\ell+2)} - \chi^{s+1,2}_{k(\ell+1)}) g_{j_s} \ , \\ &g^1_{k(\ell+1)} \coloneqq \textstyle\sum_{s=1}^{2} (\chi^{s+1,2}_{(k+1)(\ell+1)} - \chi^{s+2}_{k(\ell+1)}) g_{j_s} \ , \\ &g^2_{(k+1)\ell} \coloneqq \overline{g}_{j_3} \ , \\ &g^1_{k\ell} \coloneqq \overline{g}_{j_4} \ . \end{aligned}}_{(\boldsymbol{E}^{(1),\text{pol}})^T} \tag{88}$$

Proposition 5.6. *Eqs. (78), (84) and (88) imply that the diagrams in Fig. 9(a) and (b) commute.*

Proof. The claim can be immediately verified using the explicit relations. For Eq. (78), the verification is trivial, so let us look at Eq. (84). Consider the definitions of $f_{k\ell}$, $f_{k(\ell+1)}$ and $g^2_{k\ell}$. Then, we have

$$\begin{aligned} f_{k(\ell+1)} - f_{k\ell} &= \sum_{s=1}^{3} \chi^{s,1}_{k(\ell+1)} f_{i_s} - \sum_{s=1}^{3} \frac{f_{i_s}}{3} \ , \\ &= \sum_{s=1}^{3} \left(\chi^{s,1}_{k(\ell+1)} - \chi^{s,1}_{k\ell} \right) f_{i_s} \ , \\ &= \sum_{s=1}^{3} \left(\chi^{s,1}_{k(\ell+1)} - \chi^{s,1}_{k\ell} \right) f_{i_s} + \sum_{s=1}^{3} \left(\chi^{s,1}_{k(\ell+1)} - \chi^{s,1}_{k\ell} \right) f_{i_1} \ , \\ &= \sum_{s=1}^{2} \left(\chi^{s+1,1}_{k(\ell+1)} - \chi^{s+1,1}_{k\ell} \right) \left(f_{i_{s+1}} - f_{i_1} \right) \ , \\ &= \sum_{s=1}^{2} \left(\chi^{s+1,1}_{k(\ell+1)} - \chi^{s+1,1}_{k\ell} \right) g_{j_s} = g^2_{k\ell} \ . \end{aligned}$$

The other relations can be similarly verified. ■

Eqs. (79)–(83), (85) and (86) contain all the information for assembling the relations from Eqs. (78), (84) and (88) into matrices $\boldsymbol{E}^{(1),\text{pol}}$ and $\boldsymbol{D}^{(0),\text{pol}}$. These are matrices of size $n^{(1),\text{pol}} \times (n^{(1,0)} + n^{(0,1)})$ and $n^{(1),\text{pol}} \times n^{(0),\text{pol}}$, respectively.

For instance, with regards to Eq. (84), the j_3-th row of $\boldsymbol{D}^{(0),\text{pol}}$ contains a 1 in its i_4-th column, and $-\chi^{s,1}_{k(\ell+1)}$ in its i_s-th column, $s = 1, 2, 3$.

Then, following Proposition 5.6, Eq. (77) implies

$$\begin{aligned} g \coloneqq df &= \boldsymbol{N}^{(1,0)} \cdot \boldsymbol{D}^{(1,0)} \left(\boldsymbol{E}^{\text{pol}} \right)^T \boldsymbol{f} \, dx^1 + \boldsymbol{N}^{(0,1)} \cdot \boldsymbol{D}^{(0,1)} \left(\boldsymbol{E}^{\text{pol}} \right)^T \boldsymbol{f} \, dx^2 \ , \\ &= \boldsymbol{E}^{(1),\text{pol}} \begin{bmatrix} \boldsymbol{N}^{(1,0)} \, dx^1 \\ \boldsymbol{N}^{(0,1)} \, dx^2 \end{bmatrix} \cdot \boldsymbol{D}^{(0),\text{pol}} \boldsymbol{f} \ . \end{aligned} \tag{89}$$

Let $\boldsymbol{E}^{(1,0),\text{pol}}$ and $\boldsymbol{E}^{(0,1),\text{pol}}$ be matrices of size $n^{(1),\text{pol}} \times n^{(1,0)}$ and $n^{(1),\text{pol}} \times n^{(0,1)}$, respectively, so that

$$\boldsymbol{E}^{(1),\text{pol}} = \left[\boldsymbol{E}^{(1,0),\text{pol}} \ , \ \boldsymbol{E}^{(0,1),\text{pol}} \right] \ , \tag{90}$$

and define the polar B-splines ${N_i}^{(1,0),\text{pol}}$ and ${N_i}^{(0,1),\text{pol}}$, $i = 0, \ldots, n^{(1),\text{pol}} - 1$, as

$${N_i}^{(1,0),\text{pol}} \coloneqq \sum_{j=0}^{\overline{n}^1 - 1} \sum_{k=0}^{n^2 - 1} E^{(1,0),\text{pol}}_{i(j+kn^1)} \, \overline{N}^1_j N^2_k \ , \quad {N_i}^{(0,1),\text{pol}} \coloneqq \sum_{j=0}^{n^1 - 1} \sum_{k=0}^{\overline{n}^2 - 1} E^{(0,1),\text{pol}}_{i(j+kn^1)} \, N^1_j \overline{N}^2_k \ . \tag{91}$$

The space of polar 1-forms is defined as the span of these functions,

$$\mathcal{S}^{(1),\text{pol}} := \text{span}\left\langle {N_i}^{(1,0),\text{pol}}\, dx^1 + {N_i}^{(0,1),\text{pol}}\, dx^2 \;:\; i = 0, \ldots, n^{(1),\text{pol}} - 1 \right\rangle . \tag{92}$$

Proposition 5.7. *The one-form polar B-splines ${N_i}^{(1,0),pol}\, dx^1 + {N_i}^{(0,1),pol}\, dx^2$, $i = 0, \ldots, n^{(1),pol} - 1$, form a basis for $\mathcal{S}^{(1),pol}$. Moreover, with reference to Eq. (72), any 1-form f such that $\boldsymbol{G}^{*,pol}(f) \in \mathcal{S}^{(1),pol}$ is at least C^0 smooth on $\hat{\Omega}$.*

Proof. The linear-independence claim follows from the full rank of the extraction operator $\boldsymbol{E}^{(1),\text{pol}}$.

- Eq. (78) implies that, away from the poles, $\boldsymbol{E}^{(1),\text{pol}}$ is an identity map.
- Similarly, Eqs. (84) and (88) imply that, near the bottom and top poles, respectively, the non-zero parts of the first two rows of $\boldsymbol{E}^{(1),\text{pol}}$ are obtained by taking differences of the columns of the matrices from Eq. (69). The latter matrices have rank 3, and implies that the first and last two rows of $\boldsymbol{E}^{(1),\text{pol}}$ are also linearly independent.

The smoothness of the one-form polar B-splines is implied by their local exactness at the poles (see Section 5.2.1) and Proposition 5.5. ■

5.2.4. Polar 2-forms

Let $f \in \mathcal{S}^{(1),\text{pol}}$ and apply the exterior derivative to it. Then, using Eq. (50),

$$\begin{aligned} \Lambda^{(2)}_T \ni g := df &= \boldsymbol{N}^{(1,1)} \cdot \left(-\boldsymbol{D}^{(2,0)} \left(\boldsymbol{E}^{(1,0),\text{pol}}\right)^T + \boldsymbol{D}^{(0,2)} \left(\boldsymbol{E}^{(0,1),\text{pol}}\right)^T \right) \boldsymbol{f} \,, \\ &=: \sum_{i=0}^{\overline{n}^1-1} \sum_{j=0}^{\overline{n}^1-1} g_{ij} \overline{N}^1_i \overline{N}^2_j \,. \end{aligned} \tag{93}$$

However, by the local exactness of f at the poles (see Section 5.2.1), the above implies that $g_{ij} = 0$ if

$$\begin{aligned} &\text{Type 1 collapse} \;:\; j = 0 \,, \\ &\text{Type 2 collapse} \;:\; j = 0, \overline{n}^2 - 1 \,. \end{aligned}$$

Then, with reference to Fig. 10, let us define two maps $\boldsymbol{D}^{(1),\text{pol}}$ and $\boldsymbol{E}^{(2),\text{pol}}$. As in the previous section, we do so by defining their actions on the degrees of freedom, considering both regions away from the poles and near the poles.

- Fig. 10(a): Far away from the poles, the degree-of-freedom complexes locally look like their tensor-product counterparts, i.e., the topology is that of a structured quadrilateral grid; c.f. Figs. 4, 6, 7 and 8. This is the case shown in this figure where the degrees of freedom $f_{i_1}, \ldots, f_{i_4}$ for a polar 1-form lie on the vertices of a quadrilateral. Eq. (78) maps these degrees of freedom to their tensor-product counterparts via the identity map. Then, we define the action of the maps $\boldsymbol{D}^{(1),\text{pol}}$ and the transpose of $\boldsymbol{E}^{(2),\text{pol}}$ via the following equations,

$$\underbrace{\begin{aligned} f^1_{k\ell} &= f_{i_1} \,, \\ f^2_{k\ell} &= f_{i_3} \,, \\ f^1_{k(\ell+1)} &= f_{i_2} \,, \\ f^2_{(k+1)\ell} &= f_{i_4} \,. \end{aligned}}_{\left(\boldsymbol{E}^{(1),\text{pol}}\right)^T} \Rightarrow \underbrace{g_j := f_{i_1} + f_{i_4} - f_{i_2} - f_{i_3};}_{\boldsymbol{D}^{(1),\text{pol}}} \qquad \underbrace{g_{k\ell} := g_j \,.}_{\left(\boldsymbol{E}^{(2),\text{pol}}\right)^T} \tag{94}$$

  The relations between $i_1, \ldots, i_4$ and k, ℓ follows from Eqs. (79) and (81), and j is seen from Fig. 8 to be

$$j = k + (\ell - 1) n^1 \,. \tag{95}$$

- Fig. 10(b): Consider the degrees of freedom $f_{i_1}, \ldots, f_{i_5}$ for a polar 1-form. Then, the relations between the indices depend on whether the pole is the bottom one or the top one.
  Bottom pole: The relation between $i_1, \ldots, i_5$ and k, ℓ follows from Eq. (83); the relation of k, ℓ to j is simply

$$j = k \,. \tag{96}$$

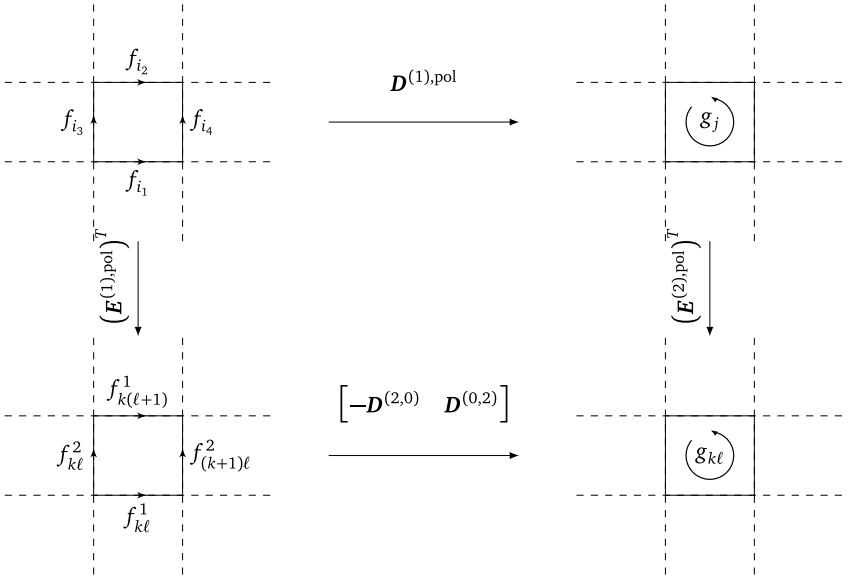

(a) Away from a pole

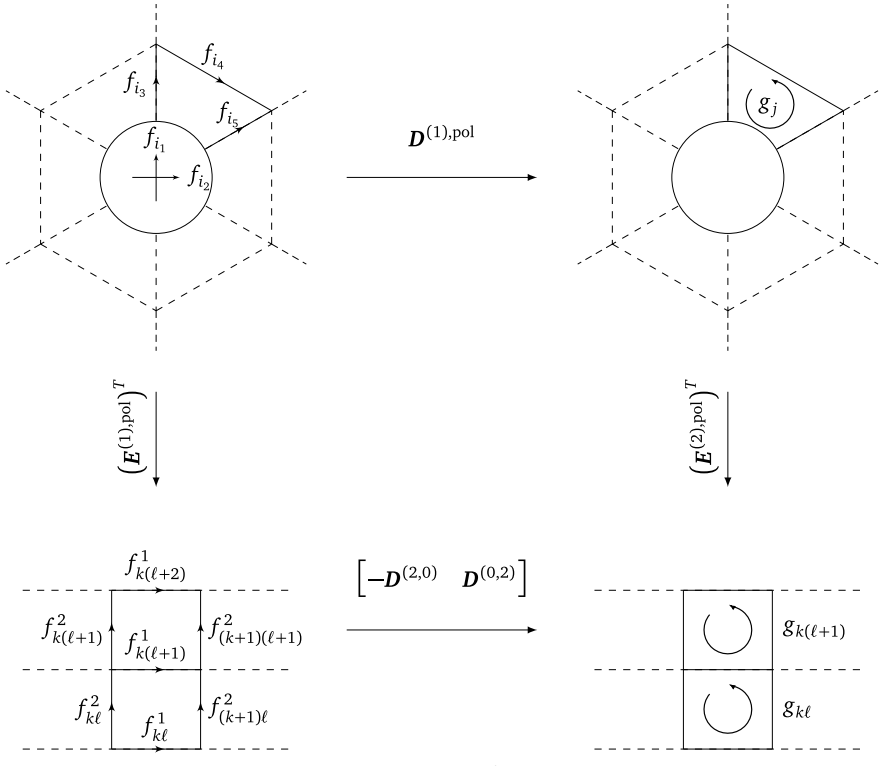

(b) In the vicinity of a pole

Fig. 10. Eqs. (94), (97) and (100), in conjunction with the above figures, help define the polar discrete exterior derivative $\boldsymbol{D}^{(1),\mathrm{pol}}$ and the polar extraction operator $\boldsymbol{E}^{(2),\mathrm{pol}}$. Figure (a) considers the case when the degrees of freedom are far away from a pole; in this case the polar degree of freedom complexes have the same topology as their tensor-product counterparts. Figure (b) instead considers the case when the degrees of freedom are in the vicinity of a pole. As Proposition 5.8 shows, the diagrams in (a) and (b) commute.

Eq. (84) maps the degrees of freedom for the polar 1-form onto those for a tensor-product 1-form; using that map, we define the actions of $\boldsymbol{D}^{(1),\mathrm{pol}}$ and the transpose of $\boldsymbol{E}^{(2),\mathrm{pol}}$ as below,

$$\underbrace{\begin{aligned} &f^1_{k\ell} \coloneqq 0\ , \\ &f^2_{k(\ell+1)} \coloneqq f_{i_3}\ , \\ &f^1_{k(\ell+2)} \coloneqq f_{i_4}\ , \\ &f^2_{(k+1)(\ell+1)} \coloneqq f_{i_5}\ , \\ &f^2_{k\ell} \coloneqq \textstyle\sum_{s=1}^{2}(\chi^{s+1,1}_{k(\ell+1)} - \chi^{s+1,1}_{k\ell})f_{i_s}\ , \\ &f^1_{k(\ell+1)} \coloneqq \textstyle\sum_{s=1}^{2}(\chi^{s+1,1}_{(k+1)(\ell+1)} - \chi^{s+1,1}_{k(\ell+1)})f_{i_s}\ , \\ &\underline{f^2_{(k+1)\ell} \coloneqq \textstyle\sum_{s=1}^{2}(\chi^{s+1,1}_{(k+1)(\ell+1)} - \chi^{s+1,1}_{(k+1)\ell})f_{i_s}\ ,} \end{aligned}}_{(\boldsymbol{E}^{(1),\mathrm{pol}})^T} \Rightarrow \underbrace{\begin{aligned} g_j \quad &\coloneqq f_{i_5} - f_{i_3} - f_{i_4} \\ &\quad + \textstyle\sum_{s=1}^{2}(\chi^{s+1,1}_{(k+1)(\ell+1)} - \chi^{s+1,1}_{k(\ell+1)})f_{i_s}\ ; \end{aligned}}_{\boldsymbol{D}^{(1),\mathrm{pol}}} \quad \underbrace{\begin{aligned} &g_{k\ell} \coloneqq 0\ , \\ &g_{k(\ell+1)} \coloneqq g_j\ . \end{aligned}}_{(\boldsymbol{E}^{(2),\mathrm{pol}})^T} \tag{97}$$

Top pole: The relation between $i_1, \ldots, i_5$ and k, ℓ follows from Eq. (86); the relation of k, ℓ to j is simply

$$j = n^{(2),\mathrm{pol}} + k - n^1\ . \tag{98}$$

Note that, as in Eq. (87), the edge associated to the degrees of freedom f_{i_3}, f_{i_4} and f_{i_5} are oppositely oriented to their specified global orientations in Fig. 8(b). Thus, we are actually interested in the degrees of freedom $\overline{f}_{i_3}$, $\overline{f}_{i_4}$ and $\overline{f}_{i_5}$,

$$\overline{f}_{i_3} = -f_{i_3}\ , \quad \overline{f}_{i_4} = -f_{i_4}\ , \quad \overline{f}_{i_5} = -f_{i_5}\ . \tag{99}$$

Eq. (88) maps the degrees of freedom for the polar 1-form onto those for a tensor-product 1-form; using that map, we define the actions of $\boldsymbol{D}^{(1),\mathrm{pol}}$ and the transpose of $\boldsymbol{E}^{(2),\mathrm{pol}}$ as below,

$$\underbrace{\begin{aligned} &f^1_{k(\ell+2)} \coloneqq 0\ , \\ &f^2_{k(\ell+1)} \coloneqq \overline{f}_{i_5}\ , \\ &f^1_{k\ell} \coloneqq \overline{f}_{i_4}\ , \\ &f^2_{(k+1)(\ell+1)} \coloneqq \overline{f}_{i_3}\ , \\ &f^2_{k(\ell+1)} \coloneqq \textstyle\sum_{s=1}^{2}(\chi^{s+1,2}_{k(\ell+2)} - \chi^{s+1,2}_{k(\ell+1)})f_{i_s}\ , \\ &f^1_{k(\ell+1)} \coloneqq \textstyle\sum_{s=1}^{2}(\chi^{s+1,2}_{(k+1)(\ell+1)} - \chi^{s+1,2}_{k(\ell+1)})f_{i_s}\ , \\ &\underline{f^2_{(k+1)(\ell+1)} \coloneqq \textstyle\sum_{s=1}^{2}(\chi^{s+1,2}_{(k+1)(\ell+2)} - \chi^{s+1,2}_{(k+1)(\ell+1)})f_{i_s}\ ,} \end{aligned}}_{(\boldsymbol{E}^{(1),\mathrm{pol}})^T} \Rightarrow \underbrace{\begin{aligned} g_j \quad &\coloneqq \overline{f}_{i_4} + \overline{f}_{i_3} - \overline{f}_{i_5} \\ &\quad - \textstyle\sum_{s=1}^{2}(\chi^{s+1,2}_{(k+1)(\ell+1)} - \chi^{s+1,2}_{k(\ell+1)})f_{i_s}\ ; \end{aligned}}_{\boldsymbol{D}^{(1),\mathrm{pol}}} \quad \underbrace{\begin{aligned} &g_{k(\ell+1)} \coloneqq 0\ , \\ &g_{k\ell} \coloneqq g_j\ . \end{aligned}}_{(\boldsymbol{E}^{(2),\mathrm{pol}})^T} \tag{100}$$

Proposition 5.8. *Eqs.* (94), (97) and (100)*imply that the diagrams in Fig.* 10*(a) and (b) commute.*

Proof. The proof is analogous to that for Proposition 5.6. Alternatively, it can be verified that $\boldsymbol{E}^{(2),\mathrm{pol}}\left(\boldsymbol{E}^{(2),\mathrm{pol}}\right)^T = \boldsymbol{I}_{n^{(2),\mathrm{pol}}}$, and that the definition of $\boldsymbol{D}^{(1),\mathrm{pol}}$ simply amounts to

$$\boldsymbol{D}^{(1),\mathrm{pol}} = \left(\boldsymbol{E}^{(2),\mathrm{pol}}\right)^T \left[-\boldsymbol{D}^{(2,0)} \quad \boldsymbol{D}^{(0,2)}\right] \left(\boldsymbol{E}^{(1),\mathrm{pol}}\right)^T\ . \quad \square$$

We can again assemble all the above relations from Eqs. (94), (97) and (100) into matrices $\boldsymbol{E}^{(2),\mathrm{pol}}$ and $\boldsymbol{D}^{(1),\mathrm{pol}}$. These are matrices of size $n^{(2),\mathrm{pol}} \times n^{(1,1)}$ and $n^{(2),\mathrm{pol}} \times n^{(1),\mathrm{pol}}$, respectively. Then, following Proposition 5.8, Eq. (93) implies

$$\begin{aligned} g \coloneqq df &= \boldsymbol{N}^{(1,1)} \cdot \left(-\boldsymbol{D}^{(2,0)}\left(\boldsymbol{E}^{(1,0),\mathrm{pol}}\right)^T + \boldsymbol{D}^{(0,2)}\left(\boldsymbol{E}^{(0,1),\mathrm{pol}}\right)^T\right)\boldsymbol{f}\ , \\ &= \boldsymbol{E}^{(2),\mathrm{pol}}\boldsymbol{N}^{(1,1)} \cdot \boldsymbol{D}^{(1),\mathrm{pol}}\boldsymbol{f}\ dx^1 \wedge dx^2\ . \end{aligned} \tag{101}$$

Then, define the polar B-splines $N_i^{(2),\text{pol}}$, $i = 0, \ldots, n^{(2),\text{pol}} - 1$, as

$$N_i^{(1),\text{pol}} := \sum_{j=0}^{\overline{n}^1-1} \sum_{k=0}^{\overline{n}^2-1} E^{(2),\text{pol}}_{i(j+kn^1)} \, \overline{N}^1_j \overline{N}^2_k \, . \tag{102}$$

The space of polar 2-forms is defined as the span of these functions,

$$\mathcal{S}^{(2),\text{pol}} := \text{span}\left\langle N_i^{(2),\text{pol}} \, dx^1 \wedge dx^2 \;\; : \;\; i = 0, \ldots, n^{(2),\text{pol}} - 1 \right\rangle \, . \tag{103}$$

Proposition 5.9. *The polar B-splines $N_i^{(2),pol}$, $i = 0, \ldots, n^{(2),pol} - 1$, form a basis for $\mathcal{S}^{(2),pol}$.*

Proof. The linear-independence claim follows from the full rank of the extraction operator $\boldsymbol{E}^{(2),\text{pol}}$. Indeed, Eqs. (94), (97) and (100) imply that $n^{(2),\text{pol}}$ columns of $\boldsymbol{E}^{(2),\text{pol}}$ are the distinct columns of the identity matrix $\boldsymbol{I}_{n^{(2),\text{pol}}}$; c.f. the proof of Proposition 5.8. ■

5.3. Definition of the complex

Using the above polar spline spaces, we choose the spaces of 0-, 1- and 2-forms on Ω as follows,

$$\Lambda_S^{(0)} := \mathcal{S}^{(0),\text{pol}} \, , \quad \Lambda_S^{(1)} := \mathcal{S}^{(1),\text{pol}} \, , \quad \Lambda_S^{(2)} := \mathcal{S}^{(2),\text{pol}} \, .$$

Then, the polar spline complex on Ω is defined as

$$\mathfrak{S} \; : \; \Lambda_S^{(0)} \longrightarrow \Lambda_S^{(1)} \longrightarrow \Lambda_S^{(2)} \, . \tag{104}$$

Theorem 5.10. *$\mathfrak{S}$ is a cochain complex, and its cohomology spaces satisfy*

$$H^0(\mathfrak{S}) = \mathbb{R} \, , \quad H^1(\mathfrak{S}) = 0 \, , \quad H^2(\mathfrak{S}) \cong \begin{cases} 0 \, , & \textit{Type 1 collapse} \, , \\ \mathbb{R} \, , & \textit{Type 2 collapse} \, . \end{cases} .$$

Proof. The fact that $\mathfrak{S}$ is a cochain complex is immediate from the construction of the polar spline spaces for 0-, 1- and 2-forms. We prove the claims for each cohomology space separately.

Zeroth cohomology. Let $f \in H^0(\mathfrak{S})$, i.e., $df = 0$. Then, Eqs. (78), (84) and (88) imply the following.

- Eq. (78): In Fig. 9(a), $f_{i_1} = \cdots = f_{i_4}$.
- Eqs. (84) and (88): In Fig. 9(b), $f_{i_1} = \cdots = f_{i_5}$.

As a consequence, $df = 0$ implies that all degrees of freedom f_i are equal to some $\alpha \in \mathbb{R}$. Then, by the partition of unity property of the 0-form polar B-splines,

$$f = \sum_{i=0}^{n^{(0),\text{pol}}-1} f_i N_i^{(0),\text{pol}} = \alpha \, .$$

First cohomology. For the cochain complex $\mathfrak{S}$, we have the following equivalence between alternating sums of the dimensions of the cohomologies and the dimensions of vector spaces that form the complex,

$$\dim\left(H^0(\mathfrak{S})\right) - \dim\left(H^1(\mathfrak{S})\right) + \dim\left(H^2(\mathfrak{S})\right) = \dim\left(\Lambda_S^{(0)}\right) - \dim\left(\Lambda_S^{(1)}\right) + \dim\left(\Lambda_S^{(2)}\right) \, .$$

The right hand-side follows from Eq. (74)–(76) and is equal to K for type K collapse. Then, since the first term on the left is equal to 1, to prove that $H^1(\mathfrak{S})$ is trivial, we only need to show that the last term on the left is equal to $K - 1$; this is proved in the following.

Second cohomology. Note that $df = 0$ for any $f \in \Lambda_S^{(2)}$. Then, let us build an $h \in \Lambda_S^{(1)}$ such that $dh = f$. This will always be possible for Type 1 collapse, while for Type 2 collapse we will need to place one constraint on f. The claim will thus follow. We define such an h by defining its degrees of freedom, and we start at the bottom pole; see Fig. 8(a). In the following, unless specified otherwise, the index i runs from 0 to $n^1 - 1$.

First, we set $h_0 = h_1 := 0$. Next, we set $h_{2+i} := 0$ and $h_{n^1+2+i} := -f_i$. Continuing on in this manner, we set $h_{2jn^1+2+i} := 0$ and $h_{(2j+1)n^1+2+i} := h_{(2j-1)n^1+2+i} - f_{jn^1+i}$, $j = 1, \ldots, n^2 - 2K - 1$, for Type K collapse. If $K = 1$, then we are done and it can be verified that $dh = f$.

On the other hand, if $K = 2$, then only $h_{n^{(1),\mathrm{pol}}-n^1-2}, \ldots, h_{n^{(1),\mathrm{pol}}-1}$ are undefined as yet. To be able to do so, we need an additional constraint on the f. Specifically, we need

$$\sum_{i=0}^{n^{(2),\mathrm{pol}}-1} f_i = 0 \,.$$

If this constraint is satisfied, then we can set $h_{n^{(1),\mathrm{pol}}-n^1-2} = h_{n^{(1),\mathrm{pol}}-2} = h_{n^{(1),\mathrm{pol}}-1} := 0$ and, moreover, for $i = 0, \ldots, n^1 - 2$,

$$h_{n^{(1),\mathrm{pol}}-n^1-1+i} := -h_{n^{(1),\mathrm{pol}}-2n^1-2+i} + h_{n^{(1),\mathrm{pol}}-n^1-2+i} + f_{n^{(2),\mathrm{pol}}-n^1+i} \,.$$

This completes the definition of h and it can be verified that $dh = f$. For Type 2 collapse, such an h can be found only when the above constraint is satisfied, implying that the cohomology space $H^2(\mathfrak{S})$ is one dimensional. ■

From the last part of the proof of Theorem 5.10, the polar 2-form $\sum_{i=0}^{n^{(2),\mathrm{pol}}-1} N_i^{(2),\mathrm{pol}}$ is not in the image of d for Type 2 collapse. This polar 2-form is thus a representative element of the one dimensional cohomology space $H^2(\mathfrak{S})$. In particular, this cohomology is isomorphic to the following vector space;

$$\mathfrak{h}^{(2)} := \left\{ \alpha \sum_{i=0}^{n^{(2),\mathrm{pol}}-1} N_i^{(2),\mathrm{pol}} \;:\; \alpha \in \mathbb{R} \right\} \,. \tag{105}$$

This vector space is closely related to the idea of "discrete harmonic forms" and it will play an important part in the numerical tests; see Section 6.3.

Finally, the polar spline complex on $\hat{\Omega}$ is defined as in Section 4.4. That is, we define $\hat{\Lambda}_S^{(i)}$ as below,

$$\hat{\Lambda}_S^{(i)} := \left\{ f \;:\; \boldsymbol{G}^{*,\mathrm{pol}}(f) \in \Lambda_S^{(i)} \right\} \,, \quad i = 0, 1, 2 \,, \tag{106}$$

and the corresponding spline complex on $\hat{\Omega}$ is built using them,

$$\hat{\mathfrak{S}} \;:\; \hat{\Lambda}_S^{(0)} \longrightarrow \hat{\Lambda}_S^{(1)} \longrightarrow \hat{\Lambda}_S^{(2)} \,,$$

with the pullback again acting as a cochain map from $\hat{\mathfrak{S}}$ to $\mathfrak{S}$.

6. Numerical tests

This section numerically investigates the approximation power and stability of the polar spline complexes by solving problems on smooth polar geometries in $\mathbb{R}^{\mathfrak{d}}$, $\mathfrak{d} = 2, 3$. In particular, we consider approximation of the Stokes flow on both fixed and deforming closed surfaces.

Our approach towards spline differential forms is well-suited for computations within the classical framework of finite element assembly loops. Indeed, starting from element-local representations of univariate splines (Section 3.2), tensor-product splines can be readily built. Subsequently, the tensor-product splines can themselves be combined using the polar extractions to build polar splines on each element of the two-dimensional parametric domain Ω. This approach is adopted for all computations presented here.

6.1. Spline spaces and geometries

For brevity, we only present numerical tests with the polar spline spaces as they already utilize the univariate and tensor-product splines defined in Sections 4 and 3.2 . Moreover, we only consider Type 2 collapse, i.e., closed polar manifolds. The numerical tests presented here show that the polar spline spaces demonstrate optimal approximation; similar results were obtained for the configurations not shown here (e.g., univariate and tensor-product spline spaces, Type 1 collapse).

Specifically, we consider three polar spline spaces built using Type 2 collapse. Each is built using tensor-product spline spaces of uniformly chosen bi-degree (p, p), $p = 2, 3, 4$. That is, the univariate spline spaces used to build

the tensor-product spline spaces are defined by choosing the polynomial degree on each element equal to p. The breakpoints and associated orders of smoothness are defined as below.

$$p = 2 : \begin{cases} \mathcal{S}^1 \ : \ (x_0, \ldots, x_3) = (0, 1, 2, 3) \ , \quad (r_0, \ldots, r_3) = (1, 1, 1, 1) \ , \\ \mathcal{S}^2 \ : \ (x_0, \ldots, x_3) = (0, 1, 2, 3) \ , \quad (r_0, \ldots, r_3) = (-1, 1, 1, -1) \ ; \end{cases} \tag{107}$$

$$p = 3 : \begin{cases} \mathcal{S}^1 \ : \ (x_0, \ldots, x_4) = (0, 1, 2, 3, 4) \ , \quad (r_0, \ldots, r_4) = (2, 2, 2, 2, 2) \ , \\ \mathcal{S}^2 \ : \ (x_0, x_1, x_2) = (0, 1, 2) \ , \quad (r_0, r_1, r_2) = (-1, 2, -1) \ ; \end{cases} \tag{108}$$

$$p = 4 : \begin{cases} \mathcal{S}^1 \ : \ (x_0, \ldots, x_5) = (0, 1, 2, 3, 4, 5) \ , \quad (r_0, \ldots, r_5) = (3, 3, 3, 3, 3, 3) \ , \\ \mathcal{S}^2 \ : \ (x_0, x_1) = (0, 1) \ , \quad (r_0, r_1) = (-1, -1) \ . \end{cases} \tag{109}$$

The polar manifolds built using the above spline spaces are shown in Fig. 11. The black lines delineate the Bézier elements of the mesh.

6.2. L^2 projection

As the most basic test of the approximation power of the individual spline spaces, we solve L^2 projection problems. Specifically, given $f_{\text{ex}} \in L^2\Lambda^{(i)}(\hat{\Omega})$, we find $f \in \hat{\Lambda}^{(i)}_S$ such that

$$\forall g \in \hat{\Lambda}^{(i)}_S \quad (g, f)_{\hat{\Omega}} = (g, f_{\text{ex}})_{\hat{\Omega}} \ . \tag{110}$$

The exact solutions are chosen to be

$$\begin{aligned} &L^2\Lambda^{(0)}(\hat{\Omega}) \ni f_{\text{ex}} = h \ , \\ &L^2\Lambda^{(1)}(\hat{\Omega}) \ni f_{\text{ex}} = h \ dy^1 + h \ dy^2 + h \ dy^3 \ , \\ &L^2\Lambda^{(2)}(\hat{\Omega}) \ni f_{\text{ex}} = h \ dy^2 \wedge dy^3 + h \ dy^3 \wedge dy^1 + h \ dy^1 \wedge dy^2 \ , \end{aligned} \tag{111}$$

where

$$h(y^1, y^2, y^3) = \sin\left(2\pi\left(y^1 + \frac{1}{3}\right)\right) \sin\left(2\pi\left(y^2 + \frac{1}{5}\right)\right) \sin\left(2\pi\left(y^3 + \frac{1}{7}\right)\right) \tag{112}$$

The L^2-projection problems project the pullbacks of the above exact solutions onto the appropriate polar spline spaces; c.f. Eq. (57). With the approximation error defined as $e := f_{\text{ex}} - f$, the L^2 norm of e and de displayed in Fig. 12. The error norms are plotted against the square root of the number of degrees of freedom. Note that the norm of de is omitted for 2-forms since the exterior derivative maps all 2-forms to zero. To the left of each error convergence plot, we also show the exact solutions for each polar geometry (see the online version of this article for high resolution pictures):

- for 0-forms, the surface is coloured by f_{ex} and the tangential vector field represents df_{ex};
- for 1-forms, the surface is coloured by values of df_{ex} and the tangential vector field represents f_{ex};
- for 2-forms, the surface is coloured by values of f_{ex}.

For optimal approximation, we expect the L^2 norm of e to decrease with order $p+1$ for 0-forms and p otherwise. The L^2 norm of de is expected to decrease with order p for both 0- and 1-forms. As can be observed in Fig. 12, the polar spline spaces demonstrate optimal approximation behaviour for all p.

6.3. Generalized Stokes flow

We now consider generalized Stokes flow on fixed and deforming polar manifolds $\hat{\Omega}$. This problem is important when studying, for instance, fluid flow on biological membranes such as lipid bilayers, and the problem formulation can be derived from first principles; e.g., see [34,46] for the derivation of Stokes flow[1]. We express the strong form

[1] Both [34,46] agree on the model for Stokes flow on surfaces. However, in the presence of inertial terms, the model derived in [34] contains a mistake that is rectified in [46].

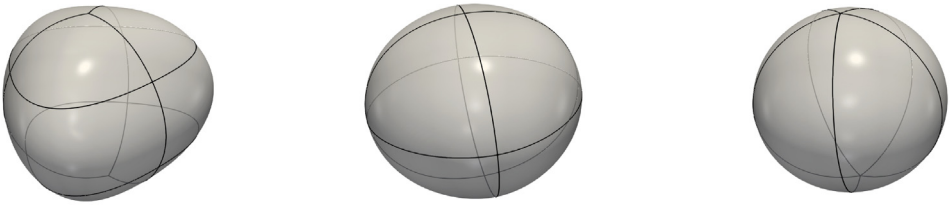

(a) $p = 2$ (b) $p = 3$ (c) $p = 4$

Fig. 11. The polar manifolds used in the numerical tests are shown above. The black lines delineate the Bézier elements at the coarsest refinement level. As can be seen, the coarsest meshes consist of 9, 8 and 5 elements for $p = 2$, 3 and 4, respectively. See Section 6.1 for details about the underlying polar spline spaces.

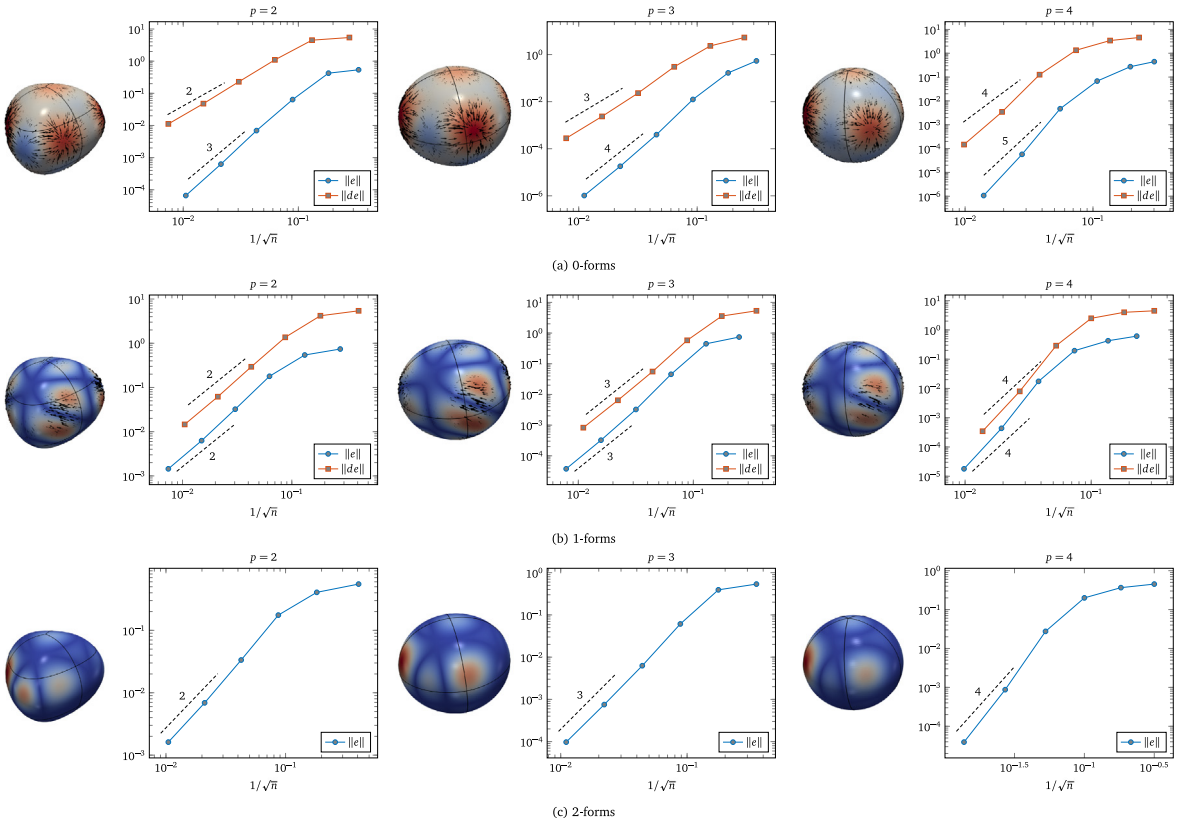

Fig. 12. L^2 projection problem: The convergence rates for L^2 projections of 0-, 1- and 2-forms on the polar manifolds in Fig. 11 are shown above; see Section 6.2.

of the generalized Stokes problem on $\hat{\Omega}$ as

$$\begin{aligned} d^\star q + \mu\left(2\kappa u - d d^\star u\right) - \alpha u &= f + \star\left(2\mu(\boldsymbol{k} - H\boldsymbol{g})\cdot d\star v\right) \ , \\ du &= h + Hv \ . \end{aligned} \tag{113}$$

The first equation pertains to momentum conservation on $\hat{\Omega}$ while the second one is the equation of mass conservation. Here, q is the pressure (2-form), u is the velocity (1-form) and v represents the (instantaneous) normal velocity field of the deforming domain $\hat{\Omega}$ (2-form). Moreover, f is an external force (1-form) on the system, h is a source of mass production (2-form), μ is the viscosity and α is a scalar constant. The remaining terms are related to $\hat{\Omega}$ — the metric tensor, $\boldsymbol{g}$; the second fundamental form, $\boldsymbol{k} = k_{ij} dx^i \otimes dx^j$; twice the mean curvature, H; and

the Gaussian curvature, κ. In particular, with $\boldsymbol{n}$ denoting the unit normal vector to $\hat{\Omega}$,

$$k_{ij} = \partial_i^{\boldsymbol{x}} \cdot \frac{\partial \boldsymbol{n}}{\partial x^j} \ , \quad H = k_{ij} g^{ij} \ , \quad \kappa = \frac{\det[k_{ij}]}{\det[g_{ij}]} \ . \tag{114}$$

Remark 6.1. The form of the generalized Stokes problem in Eq. (113) can be related to the usual vector calculus notation; see [34,46], for instance. In particular, we would like to mention that the velocity 1-form is related to the tangential fluid velocity on $\hat{\Omega}$, denoted $u^{\#} = u^{\#,i} \partial_i^{\boldsymbol{x}}$, as below,

$$u = -\sqrt{g} u^{\#,2} \, dx^1 + \sqrt{g} u^{\#,1} \, dx^2 \ . \tag{115}$$

From Appendix F, $u^{\#}$ is interpreted as a proxy field of $-\star u$. In particular, du is proportional to the surface divergence of $u^{\#}$, i.e.,

$$du = \sqrt{g} \mathrm{div}_{\hat{\Omega}} u^{\#} \, dx^1 \wedge dx^2 \ . \tag{116}$$

Remark 6.2. Interestingly, even in the absence of mass production ($h = 0$) and external forcing ($f = 0$), tangential flow on $\hat{\Omega}$ can be produced if the surface has non-zero normal velocity, v. This is directly related to the interpretation of the deforming surface $\hat{\Omega}$ as an inextensible material. An interesting example of such materials is lipid bilayers [34], which are envelopes for eukaryotic cell contents. These behave as in-plane fluids and out-of-plane solids. In particular, as in Eq. (113), the out-of-plane velocities of these surfaces, governed by solid mechanics, lead to in-plane flow. See Section 6.3.3 for examples of this phenomena.

6.3.1. Manufactured solution

In order to numerically verify optimal approximation of generalized Stokes flow, we create a smooth manufactured solution to the problem. Since $\hat{\Omega}$ is parametrically defined using piecewise polynomials, it does not have a simple implicit representation unlike other surfaces (e.g., spheres). This makes the derivation of a smooth manufactured solution a complicated task. For instance, fixing u and h, mass conservation implies $v = (du - h)/H$. The derivatives of v, needed for momentum conservation, therefore involve derivatives of the mean curvature H; note that these derivatives will clearly have a lower regularity than that of the surface $\hat{\Omega}$. Keeping these difficulties in mind, a smooth manufactured solution can nevertheless be derived by either

- assuming that $\hat{\Omega}$ is a Type 1, flat polar geometry so that, in particular, both $\boldsymbol{k}$ and H are trivial;
- or, by assuming that $v = 0$.

We adopt the second approach above so that we can demonstrate optimal approximation on arbitrarily curved polar geometries.

Therefore, choosing $v = 0$, the exact solutions for the different variables are chosen to be

$$\begin{aligned} u_{\mathrm{ex}} &= -\star (f_0 \, dx^1 + f_0 \, dx^2) \ , \\ q_{\mathrm{ex}} &= \sqrt{g} f_0 \, dx^1 \wedge dx^2 \ , \end{aligned}$$

where

$$f_0(x^1, x^2) = \left(\cos(2\pi x^1) - 1\right) \left(\cos(2\pi x^2) - 1\right)^2 \ . \tag{117}$$

Using the above u_{ex} and p_{ex}, we define $h_{\mathrm{ex}} = du_{\mathrm{ex}}$ and $f_{\mathrm{ex}} = d^\star q_{\mathrm{ex}} + \mu \left(2\kappa u_{\mathrm{ex}} - dd^\star u_{\mathrm{ex}}\right) - \alpha u_{\mathrm{ex}}$.

For the above choice of manufactured solution, we numerically solve the generalized Stokes problem in mixed form by introducing $w = d^\star u$, the vorticity (0-form). The corresponding weak form of the discrete problem is defined as follows. Given $(f_{\mathrm{ex}}, h_{\mathrm{ex}}) \in L^2\Lambda^{(1)}(\hat{\Omega}) \times L^2\Lambda^{(2)}(\hat{\Omega})$, we find $(w, u, q, v) \in \hat{\Lambda}_S^{(0)} \times \hat{\Lambda}_S^{(1)} \times \hat{\Lambda}_S^{(2)} \times \mathfrak{h}^{(2)}$ such that for all $(z_0, z_1, z_2, z_3) \in \hat{\Lambda}_S^{(0)} \times \hat{\Lambda}_S^{(1)} \times \hat{\Lambda}_S^{(2)} \times \mathfrak{h}^{(2)}$,

$$\begin{aligned} (z_0, w)_{\hat{\Omega}} - \left(dz_0, \sqrt{\mu} u\right)_{\hat{\Omega}} &= 0 \\ (dz_1, q)_{\hat{\Omega}} - \left(z_1, \sqrt{\mu} dw\right)_{\hat{\Omega}} + (z_1, (2\mu\kappa - \alpha) u)_{\hat{\Omega}} &= (z_1, f_{\mathrm{ex}})_{\hat{\Omega}} \ , \\ (z_2, du)_{\hat{\Omega}} + (z_2, v)_{\hat{\Omega}} &= (z_2, h_{\mathrm{ex}})_{\hat{\Omega}} \ , \\ (z_3, q)_{\hat{\Omega}} &= (z_3, q_{\mathrm{ex}})_{\hat{\Omega}} \ . \end{aligned} \tag{118}$$

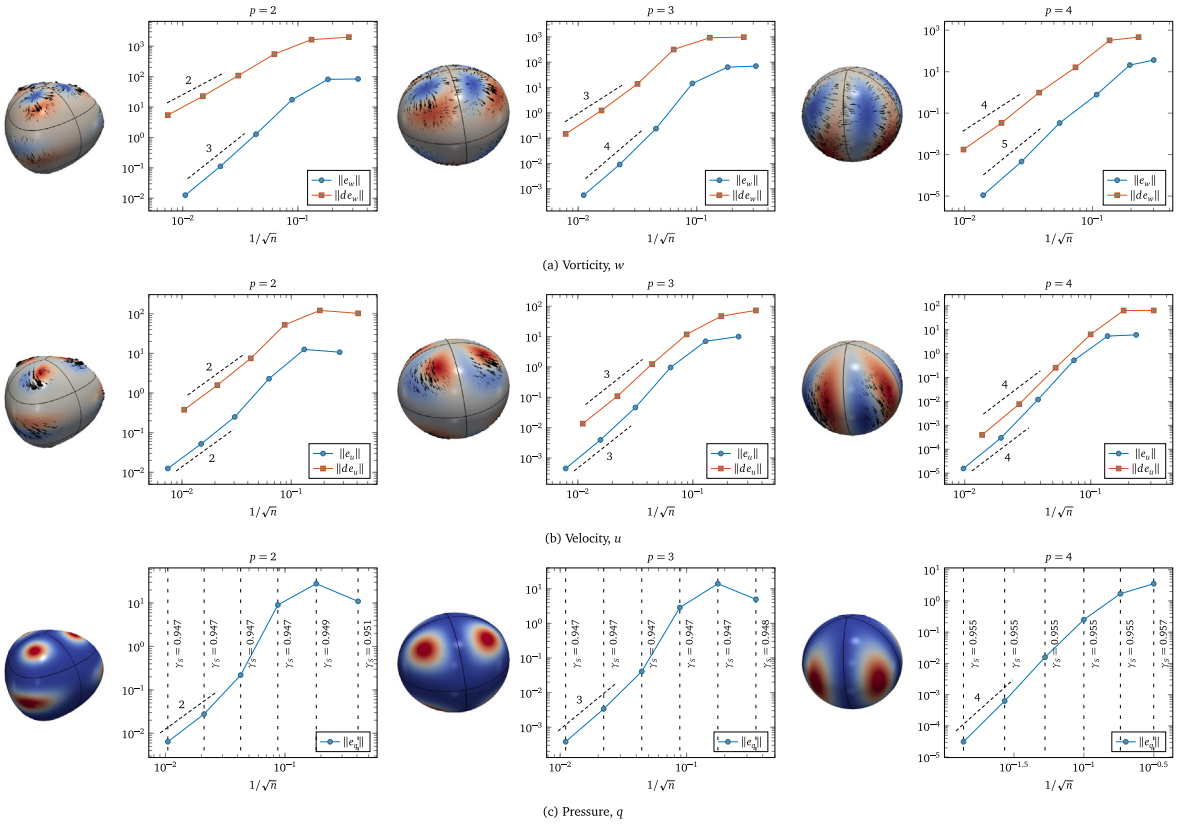

Fig. 13. Generalized Stokes flow w/ manufactured solution: The convergence rates for errors in vorticity, w, velocity, u, and pressure, q, are shown above; see Section 6.3.1.

For simplicity, we set $\mu = \alpha = 1$. For this mixed problem, we also numerically compute the inf–sup constant γ_S defined as

$$\gamma_S = \inf_{\overline{q} \in \hat{\Lambda}^{(2)}_S} \sup_{\overline{u} \in \hat{\Lambda}^{(1)}_S} \frac{(\overline{q}, d\overline{u})_\Omega}{\|\overline{u}\|_{\hat{\Lambda}^{(1)}_S} \|\overline{q}\|_{\hat{\Lambda}^{(2)}_S}} \,. \tag{119}$$

This constant can be numerical computed by solving a generalized eigenvalue problem [47]. In view of Theorem 5.10 and the fact that we are looking at Type 2 polar geometries, we expect to have $n^{(2),\text{pol}} - 1$ non-zero eigenvalues as the second cohomology space is one dimensional. The constant γ_S is the square-root of the smallest non-zero eigenvalue.

Fig. 13 show the results of the numerical approximation. The following information has been presented.

- The exact solutions for w_{ex}, dw_{ex}, u_{ex}, du_{ex}, q_{ex} and $d^\star q_{\text{ex}}$ have been plotted on the polar geometries. The values of 0- and 2-forms are used to colour the surfaces, and the 1-forms are displayed as tangential vector fields.
- With $e_\square := \square - \square_{\text{ex}}$, $\square \in \{w, u, q\}$, the L^2 norms of e_w, de_w, e_u, de_u and e_q have been plotted.
- Finally, the value of the inf–sup constant γ_S at each refinement level has been labelled in the plot where e_q has been shown.

For optimal approximation, and for polar splines built using tensor-product splines of bi-degree (p, p), we expect the errors for all 0-forms to reduce with order $p+1$ and for all 1- and 2-forms with order p. As shown in Fig. 13, all polar spline spaces demonstrate optimal approximation behaviour. Moreover, it can be seen that the spline spaces are inf–sup stable, i.e., the constant γ_S does not deteriorate with mesh refinements.

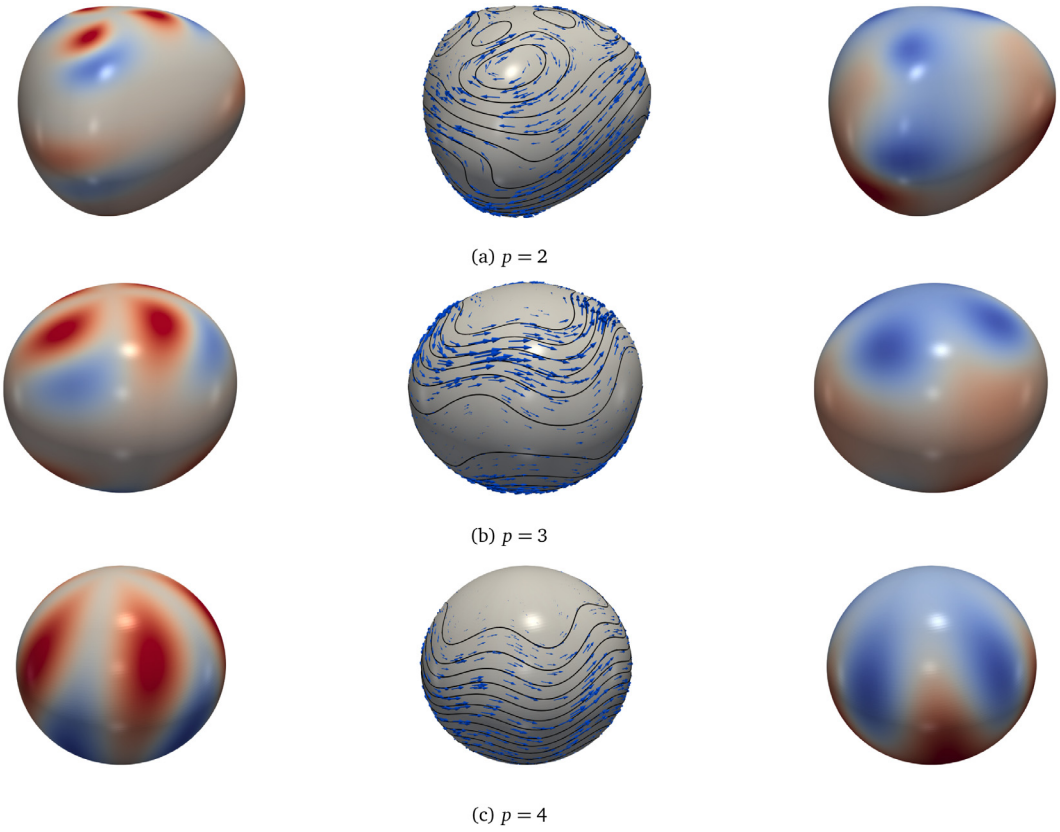

(a) $p = 2$

(b) $p = 3$

(c) $p = 4$

Fig. 14. Pointwise incompressible flows: The compatible spline spaces are built such that, if $h_{\text{ex}} = 0$ in Eq. (118), the discrete velocity satisfies $du = 0$ pointwise. Equivalently, with Remark 6.1 in mind, this implies that the associated tangential fluid velocity has zero surface divergence at each point of $\hat{\Omega}$. The above numerical tests show an example of such flow; all plots are for the discrete solutions of the generalized Stokes problem. The left plot in each row displays the vorticity, w; the middle plot shows streamfunction contours, ψ, and the tangential vector field, $u^{\#}$; and the right plot displays the pressure, q. The surface of the middle plot has been coloured by the value of du; this value is of the order of machine precision and thus the surface is uniformly coloured grey.

6.3.2. *Pointwise incompressibility*

Since $\hat{\mathfrak{S}}$ is a cochain complex, we know that d maps $\hat{\Lambda}_S^{(1)}$ into $\hat{\Lambda}_S^{(2)}$. (From Theorem 5.10, this map is a surjection only for Type 1 collapse as illustrated by the vanishing cohomology.) Then, if $h_{\text{ex}} \in \hat{\Lambda}_S^{(2)}$ in Eq. (118), then du is going to be pointwise equal to h_{ex}. In particular, if $h_{\text{ex}} = 0$, then the discrete velocity 1-form is going to be closed, i.e., $du = 0$ pointwise. Equivalently, the discrete tangential velocity $u^{\#}$ is going to have pointwise zero surface divergence; see Remark 6.1. Moreover, from Theorem 5.10, $du = 0$ implies that there exists a streamfunction ψ (0-form)such that $d\psi = u$.

We illustrate the above simple fact by solving the problem in Eq. (118) on the surfaces in Fig. 11 for the third refined level. It is important to note that pointwise incompressible solutions can be obtained for any refinement level, no matter how coarse or fine — the choice of the third refinement level is only to ensure accuracy of the discrete solutions. We choose $h_{\text{ex}} = 0 = \nu_{\text{ex}}$ and the forcing f_{ex} is chosen to be equal to the one in Eq. (118). The results are shown in Fig. 14. The left figures in each row correspond to the computed w; the middle figures to the tangential velocity vector field, $u^{\#}$, and contours of the streamfunction, ψ; and the right figures correspond to the pressures, q.

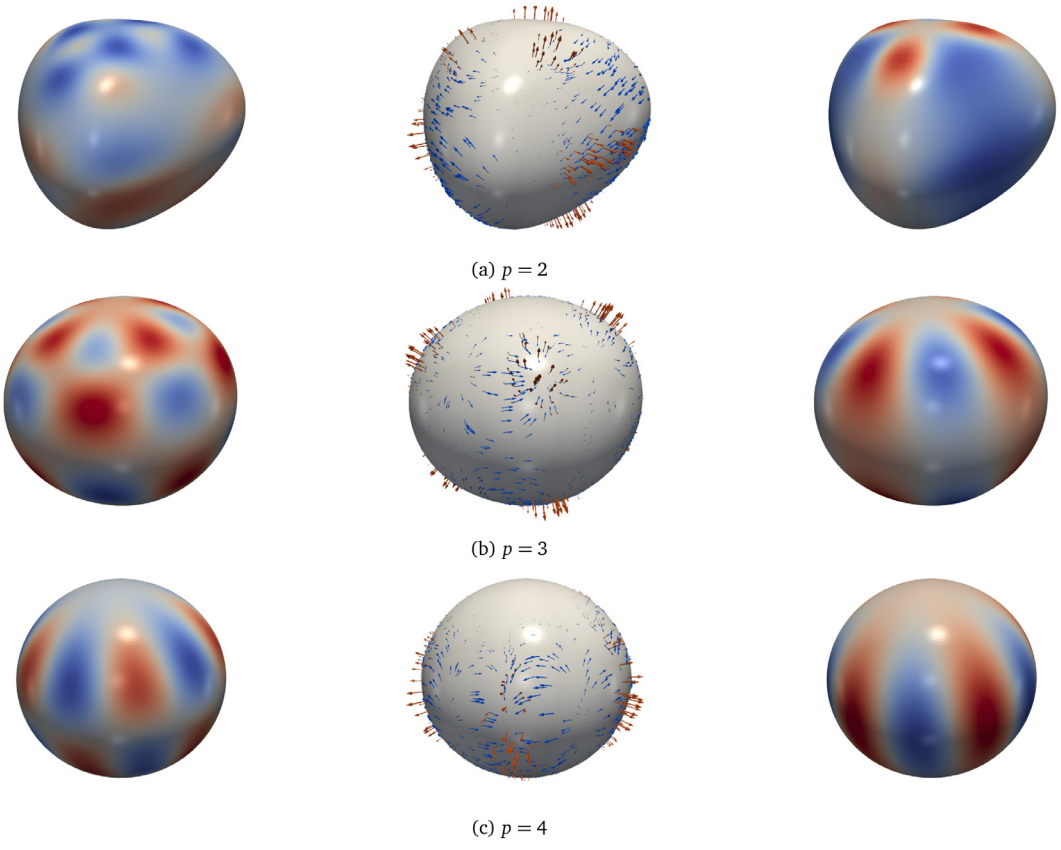

(a) $p = 2$

(b) $p = 3$

(c) $p = 4$

Fig. 15. Deforming domains: The above numerical tests show the discrete solutions to the generalized Stokes problem when $\hat{\Omega}$ is deforming with a prescribed normal velocity field; see Eq. (121). The left plot in each row displays the vorticity, w; the middle plot shows the tangential vector field, $u^{\#}$, in blue and the imposed normal velocity, $(\star v_{\text{ex}})\boldsymbol{n}$, in red; and the right plot displays the pressure, q. The relative scaling of the normal velocity arrows with respect to the tangential velocity arrows is 1.4 for $p = 2$ and 2.4 for $p = 3$ and 4.

6.3.3. Deforming domains

As a final numerical example, we consider the case where $v_{\text{ex}} \neq 0$. We choose $f_{\text{ex}} = 0 = h_{\text{ex}}$ and $v_{\text{ex}} = \sqrt{g} f_1 \, dx^1 \wedge dx^2$, where

$$f_1(x^1, x^2) = \cos(2\pi x^1) \left(\cos(2\pi x^2) - 1\right)^2 \ . \tag{120}$$

We also impose $q_{\text{ex}} \perp \mathfrak{h}^{(2)}$. The weak problem thus becomes to find $(w, u, q, v) \in \hat{\Lambda}^{(0)}_S \times \hat{\Lambda}^{(1)}_S \times \hat{\Lambda}^{(2)}_S \times \mathfrak{h}^{(2)}$ such that for all $(z_0, z_1, z_2, z_3) \in \hat{\Lambda}^{(0)}_S \times \hat{\Lambda}^{(1)}_S \times \hat{\Lambda}^{(2)}_S \times \mathfrak{h}^{(2)}$,

$$\begin{aligned} (z_0, w)_{\hat{\Omega}} - \left(dz_0, \sqrt{\mu} u\right)_{\hat{\Omega}} &= 0 \\ (dz_1, q)_{\hat{\Omega}} - \left(z_1, \sqrt{\mu} dw\right)_{\hat{\Omega}} + (z_1, (2\mu\kappa - \alpha)u)_{\hat{\Omega}} &= (z_1, \star 2\mu(\boldsymbol{k} - H\boldsymbol{g}) \cdot d \star v_{\text{ex}})_{\hat{\Omega}} \ , \\ (z_2, du)_{\hat{\Omega}} + (z_2, v)_{\hat{\Omega}} &= (z_2, H v_{\text{ex}})_{\hat{\Omega}} \ , \\ (z_3, q)_{\hat{\Omega}} &= 0 \ . \end{aligned} \tag{121}$$

Again, for simplicity we set $\mu = \alpha = 1$. Fig. 15 shows the results for the polar geometries in Fig. 11. The left figures in each row correspond to the computed w; the middle figures to the tangential fluid velocity, $u^{\#}$, and the normal velocity, $(\star v_{\text{ex}})\boldsymbol{n} = f_1 \boldsymbol{n}$; and the right figures correspond to the pressures, q.

7. Conclusions

We have investigated the development and applications of high-order accurate, spline differential forms in a variety of settings. In the univariate setting, we provide the construction of multi-degree spline differential forms, i.e., smooth, piecewise-polynomial differential forms that allow for local degree elevation; Section 3.2. The construction is presented within the paradigm of Bézier extractions, thus making our algorithms and approach easily implementable, particularly within element loop-based finite element software. In the bivariate setting, we first build spline differential forms using tensor-products of the univariate spline differential forms; Section 4. The properties of the univariate splines carry over to the tensor-product splines; this approach is easily extensible to higher dimensions. Next, in the bivariate setting, we focus on the case of singularly parametrized smooth surfaces (with and without boundary) called polar surfaces, and build spline differential forms on them; Section 5. Finally, the spline differential forms are used to solve L^2 projection problems and generalized Stokes flow on smooth polar surfaces in $\mathbb{R}^3$; Section 6. The results demonstrate optimal approximation and inf–sup stability of the spline spaces for the Stokes problem, simulations of pointwise incompressible flows, and simulations of flows on deforming inextensible surfaces.

Our approach here has been constructive. There are several extensions of the results and applications presented herein that are related to topics in computational mechanics as well as several areas of mathematics, such as algebraic topology, differential geometry and numerical analysis. As such, there are several opportunities for future research into theoretical and practical aspects of spline-based exterior calculus with the goal of solving PDEs on surfaces; a few of these are itemized below.

- For efficient computations, development of smooth polar differential forms using adaptively-refined splines, such as hierarchical B-splines [28] is important.
- Similarly, the 0-, 1- and 2-form spline spaces developed here are H^2, H^1 and L^2 conforming on polar surfaces. Extending this construction to higher orders of regularity [29] is interesting, for instance, for the variational multiscale framework for divergence-free flow simulations [48] where the 1- and 2-form spaces need to be H^2 and H^1 conforming, respectively.
- Another important research question is the development of commuting projection operators that help theoretically verify the stability of the spline spaces. Bounded cochain projections from the de Rham complex to spline complexes are needed for provable well-posedness at the discrete level. The theory on such cochain projections for adaptively refined and non-tensor-product splines is missing, even in the absence of singular parametrizations, and is beyond the scope of this paper. Instead, the examples in Section 6 provide numerical evidence of the well-posedness of the discrete problems.
- On the side of applications, we simulate flows on smoothly deforming surfaces with prescribed normal velocities. Incorporating mechanics into the equations to simulate the behaviour of fluid membranes, e.g., lipid bilayers, is a particularly interesting extension.

Declaration of competing interest

The authors declare that they have no known competing financial interests or personal relationships that could have appeared to influence the work reported in this paper.

Appendix A. Recursive definition of MDB-splines

Following [44,49], we define two MDB-spline knot vectors $\boldsymbol{u}$ and $\boldsymbol{v}$ as

$$\boldsymbol{u} \coloneqq [u_1,\ u_2,\ \ldots,\ u_n] \coloneqq [\underbrace{x_0,\ \ldots,\ x_0}_{p_1-r_0\ \text{times}},\ \underbrace{x_1,\ \ldots,\ x_1}_{p_2-r_1\ \text{times}},\ \ldots,\ \underbrace{x_{m-1},\ \ldots,\ x_{m-1}}_{p_m-r_{m-1}\ \text{times}}],$$

$$\boldsymbol{v} \coloneqq [v_1,\ v_2,\ \ldots,\ v_n] \coloneqq [\underbrace{x_1,\ \ldots,\ x_1}_{p_1-r_1\ \text{times}},\ \ldots,\ \underbrace{x_{m-1},\ \ldots,\ x_{m-1}}_{p_{m-1}-r_{m-1}\ \text{times}},\ \underbrace{x_m,\ \ldots,\ x_m}_{p_m-r_m\ \text{times}}].$$

With $p \coloneqq \max_i p_i$, the MDB-splines $N_i \coloneqq N_{i,p}$ are recursively defined. For $q = 0, \ldots, p$ and $i = p-q, \ldots, n-1$, the spline $N_{i,q}$ is supported on the interval $[u_i, v_{i-p+q}]$ and can be evaluated at $x \in [x_{j-1}, x_j) \subset [u_i, v_{i-p+q}]$ as

Algorithm 1 Computation of $\boldsymbol{H}$ (Appendix B)

$\boldsymbol{H} \leftarrow$ identity matrix (size : $\boldsymbol{\theta}(m) \times \boldsymbol{\theta}(m)$)
for $k = 1 : m - 1$ **do**
  $\boldsymbol{L} \leftarrow \boldsymbol{H}\boldsymbol{K}_k$
  for $j = 0 : r_k$ **do**
    $\overline{\boldsymbol{H}} \leftarrow$ sparse nullspace of j-th column of $\boldsymbol{L}$ (Algorithm 2)
    $\boldsymbol{H} \leftarrow \overline{\boldsymbol{H}}\boldsymbol{H}$
    $\boldsymbol{L} \leftarrow \overline{\boldsymbol{H}}\boldsymbol{L}$
return $\boldsymbol{H}$

Algorithm 2 nullspace of $\hat{\boldsymbol{c}}$ (Appendix B)

$\hat{\boldsymbol{H}} \leftarrow \boldsymbol{0}$ (size: $(q-1) \times q$)
$\hat{\boldsymbol{H}}(0,0) \leftarrow 1$
for $i = 0 : q - 3$ **do**
  $\hat{\boldsymbol{H}}(i, i+1) \leftarrow -\dfrac{\hat{c}_i \hat{\boldsymbol{H}}_1(i,i)}{\hat{c}_{i+1}}$
  $\hat{\boldsymbol{H}}(i+1, i+1) \leftarrow 1 - \hat{\boldsymbol{H}}(i, i+1)$
$\hat{\boldsymbol{H}}(q-2, q-1) = 1$
return $\hat{\boldsymbol{H}}$

follows:

$$N_{i,q}(x) \coloneqq \begin{cases} 1\,, & q = p - p_j\,, \\ \int_{-\infty}^{x} \left[\dfrac{N_{i,q-1}(y)}{M_{i,q-1}} - \dfrac{N_{i+1,q-1}(y)}{M_{i+1,q-1}} \right] dy\,, & q > p - p_j\,, \\ 0\,, & \text{otherwise}\,, \end{cases}$$

where

$$M_{k,q-1} \coloneqq \int_{-\infty}^{\infty} N_{k,q-1}(y)\, dy\,.$$

In the above it is assumed that any undefined $N_{k,q-1}$ with $k < p - q + 2$ or $k > n$ is equal to the zero function, and that if $M_{k,q-1} = 0$ then

$$\int_{-\infty}^{x} \frac{N_{k,q-1}(y)}{M_{k,q-1}}\, dy \coloneqq \begin{cases} 1\,, & x \geq u_k \text{ and } k \leq n\,, \\ 0\,, & \text{otherwise}\,. \end{cases}$$

Appendix B. Algorithmic definition of MDB-splines

For $1 \leq k \leq m-1$ let $\boldsymbol{K}_{k,-}$ be a matrix of size $(p_k + 1) \times (r_k + 1)$, whose j-th column, $j = 0, \ldots, r_k$, is given by,

$$\begin{bmatrix} 0 & \cdots & 0 & D_-^j B_{\boldsymbol{\theta}(k)-j-1}(x_k) & \cdots & D_-^j B_{\boldsymbol{\theta}(k)-1}(x_k) \end{bmatrix}^T\,, \tag{122}$$

and let $\boldsymbol{K}_{k,+}$ be a matrix of size $(p_{k+1} + 1) \times (r_k + 1)$, whose j-th column, $j = 0, \ldots, r_k$, is given by,

$$\begin{bmatrix} -D_+^j B_{\boldsymbol{\theta}(k)}(x_k) & \cdots & -D_+^j B_{\boldsymbol{\theta}(k)+j}(x_k) & 0 & \cdots & 0 \end{bmatrix}^T\,. \tag{123}$$

Using these matrices, we can build the matrix $\boldsymbol{K}_k$ of size $\boldsymbol{\theta}(m) \times (r_k + 1)$ which contains all constraints required to enforce C^{r_k} smoothness at x_k. This matrix is defined row-wise in the following manner:

1. the $(\boldsymbol{\theta}(k-1)+j)$-th row of $\boldsymbol{K}_k$ is equal to the j-th row of $\boldsymbol{K}_{k,-}$ for $j = 0, \ldots, p_k$,
2. the $(\boldsymbol{\theta}(k)+j)$-th row of $\boldsymbol{K}_k$ is equal to the j-th row of $\boldsymbol{K}_{k,+}$ for $k = 0, \ldots, p_{k+1}$, and,
3. all other rows of $\boldsymbol{K}_k$ are identically zero.

The multi-degree extraction $\boldsymbol{H}$ is a full-rank matrix built using Algorithm 1 and its rows span the collective left-nullspace of the matrices $\boldsymbol{K}_k$. This algorithm is a more efficient implementation of the one proposed in [29] and has been reproduced from [45].

Appendix C. Proof of Proposition 3.6

Proof. Observe that $\boldsymbol{C}$ is the left inverse of $\left(\boldsymbol{D}^{(0)}_{p_k}\right)^T$. Furthermore, since $\boldsymbol{H}^{\Omega_k}$ is column stochastic (Proposition 3.8) and the one dimensional nullspace of $\boldsymbol{D}^{(0)}_{p_k}$ is spanned by constant vectors of the form $\boldsymbol{v} = [\alpha, \ldots, \alpha]^T$, $\alpha \in \mathbb{R}$. Then, $(\boldsymbol{H}^{\Omega_k})^T \boldsymbol{v} = \boldsymbol{v}$ is in the nullspace of $\boldsymbol{D}^{(0)}_{p_k}$. Therefore, using Lemma C.1, and choosing

$$\boldsymbol{A}_1 = \boldsymbol{C}\ , \quad \boldsymbol{A}_2 = \boldsymbol{A}_4^T = \left(\boldsymbol{D}^{(0)}_{p_k}\right)^T\ , \quad \boldsymbol{A}_3^T = \boldsymbol{H}^{\Omega_k}\ ,$$

we see that

$$\left(\boldsymbol{D}^{(0)}_{p_k}\right)^T \boldsymbol{C}\boldsymbol{H}^{\Omega_k} \left(\boldsymbol{D}^{(0)}_{p_k}\right)^T = \boldsymbol{H}^{\Omega_k} \left(\boldsymbol{D}^{(0)}_{p_k}\right)^T$$

since $\boldsymbol{A}_2\boldsymbol{A}_1\boldsymbol{A}_3^T\boldsymbol{A}_4^T = \boldsymbol{A}_3^T\boldsymbol{A}_4^T$.

Then, for $f \in \Lambda^{(0)}_M$ and using Eq. (31), we see that

$$f|_{\Omega_k} = \begin{bmatrix} f_{\boldsymbol{\mu}(k)} & f_{\boldsymbol{\mu}(k)+1} & \cdots & f_{\boldsymbol{\mu}(k)+p_k} \end{bmatrix} \boldsymbol{H}^{\Omega_k} \begin{bmatrix} {B_{0,p_k}}^{\Omega_k} \\ \vdots \\ {B_{p_k,p_k}}^{\Omega_k} \end{bmatrix}$$

From Eq. (15),

$$\begin{aligned} df|_{\Omega_k} &= \begin{bmatrix} f_{\boldsymbol{\mu}(k)} & f_{\boldsymbol{\mu}(k)+1} & \cdots & f_{\boldsymbol{\mu}(k)+p_k} \end{bmatrix} \boldsymbol{H}^{\Omega_k} \left(\boldsymbol{D}^{(0)}_{p_k}\right)^T \begin{bmatrix} \overline{B}^{\Omega_k}_{0,p_k} \\ \vdots \\ \overline{B}^{\Omega_k}_{p_k-1,p_k} \end{bmatrix}, \\ &= \begin{bmatrix} f_{\boldsymbol{\mu}(k)} & f_{\boldsymbol{\mu}(k)+1} & \cdots & f_{\boldsymbol{\mu}(k)+p_k} \end{bmatrix} \left(\boldsymbol{D}^{(0)}_{p_k}\right)^T \boldsymbol{C}\boldsymbol{H}^{\Omega_k} \left(\boldsymbol{D}^{(0)}_{p_k}\right)^T \begin{bmatrix} \overline{B}^{\Omega_k}_{0,p_k} \\ \vdots \\ \overline{B}^{\Omega_k}_{p_k-1,p_k} \end{bmatrix}, \\ &= \begin{bmatrix} g_{\boldsymbol{\mu}(k)} & g_{\boldsymbol{\mu}(k)+1} & \cdots & g_{\boldsymbol{\mu}(k)+p_k-1} \end{bmatrix} \boldsymbol{C}\boldsymbol{H}^{\Omega_k} \left(\boldsymbol{D}^{(0)}_{p_k}\right)^T \begin{bmatrix} \overline{B}^{\Omega_k}_{0,p_k} \\ \vdots \\ \overline{B}^{\Omega_k}_{p_k-1,p_k} \end{bmatrix}, \\ &= \begin{bmatrix} g_{\boldsymbol{\mu}(k)} & g_{\boldsymbol{\mu}(k)+1} & \cdots & g_{\boldsymbol{\mu}(k)+p_k-1} \end{bmatrix} \begin{bmatrix} \overline{N}_{\boldsymbol{\mu}(k)} \\ \vdots \\ \overline{N}_{\boldsymbol{\mu}(k)+p_k-1} \end{bmatrix}. \end{aligned}$$

The i-th row of $\boldsymbol{C}$ takes the sum of the first i entries of the vector it acts upon (up to a minus sign). Thus, the spline $\overline{N}_{\boldsymbol{\mu}(k)+i}$ is defined, up to a minus sign, as the sum of the derivatives of $N_{\boldsymbol{\mu}(k)}, \ldots, N_{\boldsymbol{\mu}(k)+i}$. These sums are linearly independent; e.g., see [30]. ■

Lemma C.1. *Let $\boldsymbol{A}_i$ be matrices of sizes $j_i \times k_i$, $i = 1, \ldots, 4$, such that*

- $j_1 = k_2 \leq j_2 = k_1$ *and* $\boldsymbol{A}_1$ *is a left-inverse of* $\boldsymbol{A}_2$,

$$\boldsymbol{A}_1\boldsymbol{A}_2 = \boldsymbol{I}_{j_1} \ ;$$

- $k_3 = k_1,\ j_3 = k_4$ *and* $\boldsymbol{A}_3$ *maps the nullspace of* $\boldsymbol{A}_2^T$ *to that of* $\boldsymbol{A}_4$,

$$\boldsymbol{A}_2^T\boldsymbol{v} = \boldsymbol{0} \Rightarrow \boldsymbol{A}_4\boldsymbol{A}_3\boldsymbol{v} = \boldsymbol{0} \ .$$

Then, $\boldsymbol{A}_4\boldsymbol{A}_3\boldsymbol{A}_1^T\boldsymbol{A}_2^T = \boldsymbol{A}_4\boldsymbol{A}_3$.

Proof. Let $\boldsymbol{A}_1^T\boldsymbol{A}_2^T = \boldsymbol{I}_{k_1} + \boldsymbol{A}_5$. Then, each column of $\boldsymbol{A}_5$ must be in the nullspace of $\boldsymbol{A}_2^T$ since

$$\boldsymbol{A}_2^T(\boldsymbol{I}_{k_1} + \boldsymbol{A}_5) = \boldsymbol{A}_2^T\boldsymbol{A}_1^T\boldsymbol{A}_2^T = \boldsymbol{I}_{j_1}^T\boldsymbol{A}_2^T = \boldsymbol{A}_2^T \ .$$

Then, using the nullspace-preserving property of $\boldsymbol{A}_3$, the claim follows,

$$\boldsymbol{A}_4\boldsymbol{A}_3\boldsymbol{A}_1^T\boldsymbol{A}_2^T = \boldsymbol{A}_4\boldsymbol{A}_3(\boldsymbol{I}_{k_1} + \boldsymbol{A}_5) = \boldsymbol{A}_4\boldsymbol{A}_3 \ . \quad \square$$

Appendix D. Algorithmic definition of periodic MDB-splines

The periodic version of MDB-splines is built by starting from the non-periodic version. First, referring to Eqs. (122) and (123), build the matrices $K_{m,-}$ and $K_{0,+}$. These are matrices of sizes $(p_m + 1) \times (r_0 + 1)$ and $(p_0 + 1) \times (r_0 + 1)$, respectively. Using these matrices, we build the matrix $\boldsymbol{K}_m$ of size $\boldsymbol{\theta}(m) \times (r_0 + 1)$ which contains all constraints required to enforce C^{r_0} smoothness at $x_0 \equiv x_m$,

$$\boldsymbol{K}_m \coloneqq \begin{bmatrix} \boldsymbol{K}_{0,+} \\ \boldsymbol{0} \\ \boldsymbol{K}_{m,-} \end{bmatrix} \ .$$

With $\boldsymbol{H}$ the multi-degree extraction corresponding to the non-periodic spline space, let $\boldsymbol{P}$ be any row permutation matrix such that

$$\boldsymbol{P}\boldsymbol{H}\boldsymbol{K}_m = \begin{bmatrix} \boldsymbol{0}_1 \\ \hat{\boldsymbol{K}} \\ \boldsymbol{0}_2 \end{bmatrix} \ ,$$

such that

- $\boldsymbol{0}_i$ are zero matrices with the number of rows equal to $j_i \geq 0$, $i = 1, 2$ (i.e., $j_i = 0$ implies an empty matrix with no rows);
- $\hat{\boldsymbol{K}}$ has $2(r_0 + 1)$ rows.

We can always find such a $\boldsymbol{P}$ thanks to end-point derivative property of MDB-splines [30, Proposition 2.11(c)] and Eq. (25). Then, Algorithm 3 helps compute a matrix $\tilde{\boldsymbol{H}}$ of size n^{per} whose rows are in the left-nullspace of $\boldsymbol{P}\boldsymbol{H}\boldsymbol{K}_m$. In addition to the above definitions, the algorithm uses the row permutation matrix $\boldsymbol{Q}$ defined as

$$\boldsymbol{Q} = \begin{bmatrix} & & 1 & & \\ & & & \ddots & \\ & & & & 1 \\ 1 & & & & \\ & \ddots & & & \\ & & 1 & & \end{bmatrix} \ .$$

The highlighted entry of $\boldsymbol{Q}$ lies in its j_1-th column (with the first column having the index 0). This permutation matrix ensures that the $p_k + 1$ splines supported on Ω_k have indices $\boldsymbol{\mu}(k), \ldots, \boldsymbol{\mu}(k) + p_k$; recall the interpretation of indices in this periodic setting from Eq. (36).

Proposition D.1. *With Assumptions 2 and 3 in place, the matrix* $\tilde{\boldsymbol{H}}$ *has full rank.*

Algorithm 3 Computation of $\tilde{\boldsymbol{H}}$ (Appendix D)

$\tilde{\boldsymbol{H}} \leftarrow$ identity matrix (size : $n \times n$)
$\boldsymbol{L} \leftarrow \boldsymbol{P}\boldsymbol{H}\boldsymbol{K}_m$
for $j = 0 : r_m$ **do**
  $\overline{\boldsymbol{H}} \leftarrow$ sparse nullspace of j-th column of $\boldsymbol{L}$ (Algorithm 2)
  $\tilde{\boldsymbol{H}} \leftarrow \overline{\boldsymbol{H}}\tilde{\boldsymbol{H}}$
  $\boldsymbol{L} \leftarrow \overline{\boldsymbol{H}}\boldsymbol{L}$
$\tilde{\boldsymbol{H}} \leftarrow \boldsymbol{Q}\tilde{\boldsymbol{H}}$
return $\tilde{\boldsymbol{H}}$

Proof. The claim can be established by considering the spline space on a $2m$-element partition of $[a, 2b-a]$ that is built by duplicating the original partition on Ω at its right endpoint; the degree and smoothness distributions are also duplicated. For such a spline space, $\boldsymbol{P}\boldsymbol{H}\boldsymbol{K}_m$ is effectively an inner constraint matrix for imposition of C^{r_0} smoothness, and [30, Theorem 4.3] says that Algorithm 3 will build a full-rank nullspace of $\boldsymbol{P}\boldsymbol{H}\boldsymbol{K}_m$ as the product of bi-diagonal matrices built using Algorithm 2. In particular, this means that $\tilde{\boldsymbol{H}}$ will have the following block-diagonal structure up to a circular permutation of its rows,

$$\begin{bmatrix} \boldsymbol{I} & & \\ & \boldsymbol{A} & \\ & & \boldsymbol{I} \end{bmatrix},$$

where $\boldsymbol{I}$ are identity matrices and $\boldsymbol{A}$ is a $(r_0+1) \times (2r_0+2)$ matrix with the following sparsity structure,

$$\boldsymbol{A} = \begin{bmatrix} a_1^1 & a_2^1 & \cdots & a_{r_0+1}^1 & a_{r_0+2}^1 & & \\ & a_1^2 & a_2^2 & \cdots & a_{r_0+1}^2 & a_{r_0+2}^2 & \\ & & \ddots & \ddots & \cdots & \ddots & \ddots \\ & & & a_1^{r_0+1} & a_2^{r_0+1} & \cdots & a_{r_0+1}^{r_0+1} & a_{r_0+2}^{r_0+1} \end{bmatrix}$$

Here all a_i^j are non-negative, each column of $\boldsymbol{A}$ (and thus of $\tilde{\boldsymbol{H}}$) sums to 1 and $a_{r_0+2-j}^j = a_{r_0+3-j}^j$, $j = 1, \ldots, r_0+1$; the last equality corresponds to the imposition of C^0 smoothness at x_0. ■

Appendix E. Proof of Proposition 3.9

Proof. From Eq. (38), for a zero form $f \in \Lambda_M^{(0)}$,

$$f|_{\Omega_k} = \begin{bmatrix} f_{\boldsymbol{\mu}(k)} & f_{\boldsymbol{\mu}(k)+1} & \cdots & f_{\boldsymbol{\mu}(k)+p_k} \end{bmatrix} \boldsymbol{H}^{\Omega_k,\text{per}} \begin{bmatrix} B_{0,p_k}^{\Omega_k} \\ \vdots \\ B_{p_k,p_k}^{\Omega_k} \end{bmatrix}$$

From the definition of $\boldsymbol{\mu}(k)$ and Eqs. (17), (36) and (40), it is clear that

$$\begin{bmatrix} g_{\boldsymbol{\mu}(k)} & g_{\boldsymbol{\mu}(k)+1} & \cdots & g_{\boldsymbol{\mu}(k)+p_k-1} \end{bmatrix} = \begin{bmatrix} f_{\boldsymbol{\mu}(k)} & f_{\boldsymbol{\mu}(k)+1} & \cdots & f_{\boldsymbol{\mu}(k)+p_k} \end{bmatrix} \left(\boldsymbol{D}_{p_k}^{(0)}\right)^T.$$

Then, the claims follow immediately following the proof of Proposition 3.6 as presented in Appendix C. ■

Appendix F. Integration and proxy fields of differential forms

In this appendix we provide some relations that may help make sense of how differential forms can be manipulated or interpreted. We focus on the integration of 2-forms and proxy fields for i-forms, $i = 0, 1, 2$. In the following, $\overline{\Omega}$ is an i-dimensional subset of $\mathbb{R}^2$, and $\boldsymbol{G}$ maps $\overline{\Omega}$ to $\mathbb{R}^3$.

Integration. When implementing the approach presented herein, L^2 inner products of differential forms need to be evaluated. As in Eq. (56), the L^2 inner product of two i-forms f and g, $i = 0, 1, 2$, can be expressed as the integral of the 2-form $f \wedge \star g$. Thus, it is sufficient to describe how integrals of 2-forms can be computed.

Let $\overline{\Omega}$ be a 2-dimensional subset of $\mathbb{R}^2$, and let $f = f_{12}\, dx^1 \wedge dx^2$ be a 2-form in R^2. We will assume that the orientation function o is equal to $+1$ for domains with a counter-clockwise orientation and -1 for domains with a clockwise orientation; this is just convention and the opposite can be chosen as well. Choose one of the two orientations for $\overline{\Omega}$. The integral of f on $\overline{\Omega}$ is then computed as

$$\int_{\overline{\Omega}} f := o(\overline{\Omega}) \int_{\overline{\Omega}} f_{12}\, dx^1 dx^2 \,, \tag{124}$$

where the right hand side is the usual two-dimensional integral of a function f_{12} and $o(\overline{\Omega})$ is ± 1 dependent on the chosen orientation of $\overline{\Omega}$. Note that changing the orientation of $\overline{\Omega}$ reverses the sign of the right hand side; this is different from when the orientation-agnostic, two-dimensional integral $\int_{\overline{\Omega}} f_{12}\, dx^1 dx^2$ is computed.

When $\boldsymbol{G}(\overline{\Omega})$ is a two-dimensional subset of $\mathbb{R}^3$, any 2-form in R^3 can be integrated on $\boldsymbol{G}(\overline{\Omega})$ using the above and Eq. (58).

Scalar and vector proxies. On 2-manifolds, we can also relate 0-, 1- and 2-forms to proxy scalar, vector and scalar fields, respectively, using the metric tensor. In particular, let $\boldsymbol{G}(\overline{\Omega})$ be such a 2-manifold. Then, the following relations are used to map differential forms to their proxy fields,

$$\begin{aligned} f(\boldsymbol{x}) &\mapsto f(\boldsymbol{x}) \,, \\ f_i(\boldsymbol{x})\, dx^i &\mapsto g^{ij} f_j(\boldsymbol{x})\, \partial_i^{\boldsymbol{x}} \,, \\ f_{12}(\boldsymbol{x})\, dx^1 \wedge dx^2 &\mapsto \frac{1}{\sqrt{g}} f_{12}(\boldsymbol{x}) \,. \end{aligned} \tag{125}$$

Here we use the same notation as in Eq. (54). The above relations in combination with the pullback, see Eq. (57), can be used to associate i-forms in $\mathbb{R}^3$, $i = 0, 1, 2$, to proxy fields on 2-manifolds in $\mathbb{R}^3$. This can be seen as a link between our approach and the approach of, for instance, [41]; the latter approach solves for proxy fields of our differential forms.

References

[1] F. Brezzi, K. Lipnikov, V. Simoncini, A family of mimetic finite difference methods on polygonal and polyhedral meshes, Math. Models Methods Appl. Sci. 15 (10) (2005) 1533–1551.

[2] K. Lipnikov, G. Manzini, M. Shashkov, Mimetic finite difference method, J. Comput. Phys. 257 (2014) 1163–1227.

[3] J. Kreeft, M. Gerritsma, Mixed mimetic spectral element method for Stokes flow: A pointwise divergence-free solution, J. Comput. Phys. 240 (2013) 284–309.

[4] M. Gerritsma, R. Hiemstra, J. Kreeft, A. Palha, P. Rebelo, D. Toshniwal, The geometric basis of numerical methods, in: Spectral and High Order Methods for Partial Differential Equations, ICOSAHOM 2012, Springer, 2014, pp. 17–35.

[5] A.N. Hirani, Discrete Exterior Calculus (Ph.D. thesis), California Institute of Technology, 2003.

[6] M. Desbrun, A.N. Hirani, J.E. Marsden, Discrete exterior calculus for variational problems in computer vision and graphics, in: 42nd IEEE International Conference on Decision and Control (IEEE Cat. No. 03CH37475), Vol. 5, IEEE, 2003, pp. 4902–4907.

[7] D.N. Arnold, R.S. Falk, R. Winther, Finite element exterior calculus, homological techniques, and applications, Acta Numer. 15 (2006) 1.

[8] D. Arnold, R. Falk, R. Winther, Finite element exterior calculus: from Hodge theory to numerical stability, Bull. Amer. Math. Soc. 47 (2) (2010) 281–354.

[9] A. Buffa, G. Sangalli, R. Vázquez, Isogeometric analysis in electromagnetics: B-splines approximation, 199 (17) (2010) 1143–1152.

[10] A. Buffa, J. Rivas, G. Sangalli, R. Vázquez, Isogeometric discrete differential forms in three dimensions, SIAM J. Numer. Anal. 49 (2011) 818–844.

[11] J.A. Evans, T.J. Hughes, Isogeometric divergence-conforming B-splines for the steady Navier–Stokes equations, Math. Models Methods Appl. Sci. 23 (08) (2013) 1421–1478.

[12] A. Buffa, G. Sangalli, R. Vázquez, Isogeometric methods for computational electromagnetics: B-spline and T-spline discretizations, J. Comput. Phys. 257 (2014) 1291–1320.

[13] T. Frankel, The Geometry of Physics: An Introduction, Cambridge University Press, 2011.

[14] T. Hughes, J. Cottrell, Y. Bazilevs, Isogeometric analysis: CAD, finite elements, NURBS, exact geometry and mesh refinement, Comput. Methods Appl. Mech. Engrg. 194 (2005) 4135–4195.

[15] M.-C. Hsu, I. Akkerman, Y. Bazilevs, High-performance computing of wind turbine aerodynamics using isogeometric analysis, Comput. & Fluids 49 (1) (2011) 93–100.

[16] D. Kamensky, M.-C. Hsu, Y. Yu, J.A. Evans, M.S. Sacks, T.J.R. Hughes, Immersogeometric cardiovascular fluid–structure interaction analysis with divergence-conforming B-splines, Comput. Methods Appl. Mech. Engrg. 314 (2017) 408–472.
[17] H. Gómez, V.M. Calo, Y. Bazilevs, T.J.R. Hughes, Isogeometric analysis of the Cahn–Hilliard phase-field model, 197 (49) (2008) 4333–4352.
[18] J. Liu, C.M. Landis, H. Gomez, T.J.R. Hughes, Liquid-vapor phase transition: Thermomechanical theory, entropy stable numerical formulation, and boiling simulations, 297 (2015) 476–553.
[19] C. Zimmermann, D. Toshniwal, C.M. Landis, T.J. Hughes, K.K. Mandadapu, R.A. Sauer, An isogeometric finite element formulation for phase transitions on deforming surfaces, Comput. Methods Appl. Mech. Engrg. 351 (2019) 441–477.
[20] M.J. Borden, T.J.R. Hughes, C.M. Landis, C.V. Verhoosel, A higher-order phase-field model for brittle fracture: Formulation and analysis within the isogeometric analysis framework, Comput. Methods Appl. Mech. Engrg. 273 (2014) 100–118.
[21] M. Ambati, L. De Lorenzis, Phase-field modeling of brittle and ductile fracture in shells with isogeometric NURBS-based solid-shell elements, Comput. Methods Appl. Mech. Engrg. 312 (2016) 351–373.
[22] S. Takacs, T. Takacs, Approximation error estimates and inverse inequalities for B-splines of maximum smoothness, Math. Models Methods Appl. Sci. 26 (07) (2016) 1411–1445.
[23] A. Bressan, E. Sande, Approximation in FEM, DG and IGA: a theoretical comparison, Numer. Math. 143 (4) (2019) 923–942.
[24] E. Sande, C. Manni, H. Speleers, Explicit error estimates for spline approximation of arbitrary smoothness in isogeometric analysis, Numer. Math. (2020) 1–41.
[25] J.A. Evans, T.J.R. Hughes, Isogeometric divergence-conforming B-splines for the unsteady Navier–Stokes equations, 241 (2013) 141–167.
[26] R. Hiemstra, D. Toshniwal, R.H.M. Huijsmans, M.I. Gerritsma, High order geometric methods with exact conservation properties, J. Comput. Phys. 257 (2014) 1444–1471.
[27] K.A. Johannessen, M. Kumar, T. Kvamsdal, Divergence-conforming discretization for Stokes problem on locally refined meshes using LR B-splines, Comput. Methods Appl. Mech. Engrg. 293 (2015) 38–70.
[28] J.A. Evans, M.A. Scott, K.M. Shepherd, D.C. Thomas, R. Vázquez Hernández, Hierarchical B-spline complexes of discrete differential forms, IMA J. Numer. Anal. 40 (1) (2020) 422–473.
[29] D. Toshniwal, H. Speleers, R.R. Hiemstra, T.J. Hughes, Multi-degree smooth polar splines: A framework for geometric modeling and isogeometric analysis, Comput. Methods Appl. Mech. Engrg. 316 (2017) 1005–1061.
[30] D. Toshniwal, H. Speleers, R.R. Hiemstra, C. Manni, T.J.R. Hughes, Multi-degree B-splines: Algorithmic computation and properties, Comput. Aided Geom. Design 76 (2020).
[31] R.R. Hiemstra, T.J.R. Hughes, C. Manni, H. Speleers, D. Toshniwal, A tchebycheffian extension of multi-degree B-splines: Algorithmic computation and properties, SIAM J. Numer. Anal. 58 (2020) 1138–1163.
[32] H. Speleers, D. Toshniwal, A general class of C^1 smooth rational splines: Application to construction of exact ellipses and ellipsoids, Comput. Aided Design 132 (2021).
[33] C.J. Cotter, A.T. McRae, Compatible finite element methods for numerical weather prediction, 2014, arXiv preprint arXiv:1401.0616.
[34] M. Arroyo, A. DeSimone, Relaxation dynamics of fluid membranes, Phys. Rev. E 79 (3) (2009) 031915.
[35] A. Torres-Sánchez, D. Millán, M. Arroyo, Modelling fluid deformable surfaces with an emphasis on biological interfaces, J. Fluid Mech. 872 (2019) 218–271.
[36] A. Sahu, Y.A. Omar, R.A. Sauer, K.K. Mandadapu, Arbitrary Lagrangian–Eulerian finite element method for curved and deforming surfaces: I. General theory and application to fluid interfaces, J. Comput. Phys. 407 (2020) 109253.
[37] I. Nitschke, S. Reuther, A. Voigt, Discrete exterior calculus (DEC) for the surface Navier-Stokes equation, in: Transport Processes at Fluidic Interfaces, Springer, 2017, pp. 177–197.
[38] M.A. Olshanskii, A. Reusken, Trace finite element methods for PDEs on surfaces, in: Geometrically Unfitted Finite Element Methods and Applications, Springer, 2017, pp. 211–258.
[39] M.A. Olshanskii, A. Quaini, A. Reusken, V. Yushutin, A finite element method for the surface Stokes problem, SIAM J. Sci. Comput. 40 (4) (2018) A2492–A2518.
[40] G. Dziuk, C.M. Elliott, Finite element methods for surface PDEs, Acta Numer. 22 (2013) 289.
[41] T.-P. Fries, Higher-order surface FEM for incompressible Navier-Stokes flows on manifolds, Int. J. Numer. Methods Fluids 88 (2) (2018) 55–78.
[42] S. Reuther, A. Voigt, Solving the incompressible surface Navier-Stokes equation by surface finite elements, Phys. Fluids 30 (1) (2018) 012107.
[43] S. Reuther, I. Nitschke, A. Voigt, A numerical approach for fluid deformable surfaces, 2020, arXiv preprint arXiv:2003.10264.
[44] C.V. Beccari, G. Casciola, S. Morigi, On multi-degree splines, Comput. Aided Geom. Design 58 (2017) 8–23.
[45] H. Speleers, Algorithm 999: Computation of multi-degree B-splines, ACM Trans. Math. Software 45 (2019) Article No. 43.
[46] A. Yavari, A. Ozakin, S. Sadik, Nonlinear elasticity in a deforming ambient space, J. Nonlinear Sci. 26 (6) (2016) 1651–1692.
[47] D. Chapelle, K.-J. Bathe, The inf-sup test, Comput. Struct. 47 (1993) 537–545.
[48] J.A. Evans, D. Kamensky, Y. Bazilevs, Variational multiscale modeling with discretely divergence-free subscales, Comput. Math. Appl. (2020).
[49] B. Buchwald, G. Mühlbach, Construction of B-splines for generalized spline spaces generated from local ECT-systems, J. Comput. Appl. Math. 159 (2003) 249–267.